RHONALD BURGOS ATENCIA

Electronic transport properties of graphene sheets under strain

Niterói

2016

RHONALD BURGOS ATENCIA

Electronic transport properties of graphene sheets under strain

Tese apresentada ao Curso de Pós-Graduação em Física da Universidade Federal Fluminense, como requisito parcial para obtenção do Título de Doutor em Física.

Orientador:
Prof. Dr. CAIO HENRIQUE LEWENKOPF

Universidade Federal Fluminense
Instituto de Física

Niterói

2016

B957 Burgos Atencia, Rhonald.
Electronic transport properties of graphene sheets under strain / Rhonald Burgos Atencia ; orientador: Caio Henrique Lewenkopf. -- Niterói, 2016.
99 p. : il.

Tese (Doutorado) – Universidade Federal Fluminense, Instituto de Física, Niterói, 2016.
Bibliografia: p.82-88.

1.GRAFENO. 2.TRANSPORTE ELETRÔNICO. 3.DEFORMAÇÃO. 4.BÓSON. I. Lewenkopf, Caio Henrique, Orientador. II.Universidade Federal Fluminense. Instituto de Física, Instituição responsável. III.Título.

CDD 620.11

Agradecimentos

Agradezco a Caio por las enseñazas y en general a todos los profesores del instituto con los que tuve la oportunidad de discutir. Son muchos para mencionar, por lo que resalto a Marcos Moriconi y a Antonio Costa.

Mis mayores agradecimientos son para las agencia CNPq y DAAD por obvios motivos.

Abstract

In this thesis we address three theoretical problems related to electronic transport properties of graphene and one related to interacting Bosonic systems with disorder in one dimension.

Concerning graphene, we have studied some effects of strain. First, we calculated the effect of random gauge fields due to out off plane deformation in the Boltzmann conductivity. We have found that strain plays an important role as a disorder source that limits the conductivity.

We have also studied Weiss oscillation in graphene due to uniaxial strain. We have used a quantum Boltzmann approach and first order perturbution theory to this end. We found measurable values to the conductivity in this system.

The effect of weak localization is still a work in progress. Although the pseudo magnetic field in graphene does not break time reversal symmetry in the two valleys, we believe that the channel responsable for intravalley scattering must be sensitive to dephasing due to strain. This dephasing time has been calculated.

Concerning the Bosonic system, this is also a work in progress. We have identified some difficulties in the standard procedure of perturbation theory when applied to this system and a possible way to face them.

Resumo

Nesta tese estudamos três problemas teóricos relacionados ao grafeno e um problema relacionado a um sistema bosônico interagente e desordenado em uma dimensão.

Sobre o grafeno, estudamos alguns efeitos das deformações. Primeiro, calculamos o efeito de campos magnéticos aleatórios devido às deformações fora do plano em uma folha de grafeno na condutividade de Boltzmann. Encontramos que essas deformações são uma fonte importante de desordem para condutividade.

Também estudamos as oscilações de Weiss no grafeno devido a deformações unidimensionais. Usamos uma equação de Boltzmann quântica e teoria de perturbações até primeira ordem para resolver esse problema. Encontramos valores acessíveis experimentalmente para a condutividade.

O efeito de localização fraca na conductividade é ainda um problema em andamento. Mesmo sabendo que o pseudo-campo magnético devido a deformações não quebra a simetria de inversão temporal quando considerados os dois valleys, acreditamos que a parte responsável pelo espalhamento intra-valleys deve sentir o efeito desse pseudo-campo. O tempo de desfasagem devido a esse campo foi calculado.

O problema de sistemas bosônicos também está ainda em andamento. Identificamos algumas dificuldades na teoria de perturbações usada normalmente para sistemas fermiônicos e uma possivel forma de resolver esse problema.

List of Figures

Contents

1 Introduction

Graphene is a single layer of carbon atoms in a honeycomb structure. Since its synthesis [2, 3], there has been a lot of interest in this material: first, because of its potential technological applications as the first truly two-dimensional material and second, because of its unusual mechanical and electronic properties like linear dispersion relation and chiral nature of low energy excitations. These two properties make graphene very different from the conventional two dimensional electron gas (2DEG). Among these differences, we mention the possibility of controlling the Fermi energy by a gate voltage [2, 3] and the spectrum of the quantum Hall effect [4]. The linear dispersion relation and chiral nature suggests an analogy with Dirac-like particles and allow us to use methods already developed for quantum electrodynamics to study the behaviour of electrons in graphene [5].

At room temperature, graphene has a mobility of the order of $\mu \approx 15,000$ cm^{2}V^{-1}s^{-1}, which is larger than any other semiconductor. However, at very low temperatures this mobility increases only to $\mu \approx 200,000$ cm^{2}V^{-1}s^{-1} [2, 3], in contrast to mobilities of the order of $\mu \approx 10^6$ cm^{2}V^{-1}s^{-1} found in GaAs [6, 7]. This suggests that the mobility is limited by impurities. For potential applications of graphene, in electronics for instance, [8, 9, 10, 11, 12, 13, 14] and spintronics [9, 15, 16, 17, 18, 19, 20], a better understanding of the mechanism responsible for this limitation is of paramount importance. There are many studies in this line both numerical [21, 22, 23] and analytical [24, 25].

Many types of disorder have been considered as scattering mechanism in graphene. One type of disorder that has been extensively studied is disorder due to charged particles. In references [26, 27, 28, 29, 30], for instance, one can find some studies from a semiclassical point of view (Boltzmann's equation).

Another important type of disorder are lattice deformations [31, 32, 33, 34, 35]. There are studies that support that deformations give raise to random pseudo-electric and psedo-magnetic fields [36, 37]. This kind of disorder is anisotropic and must be studied in

a different way [38] than the presented in standard books [39]. This thesis is mainly concerned with these deformations.

In chapter 2 we give a brief description of the low effective Hamiltonian that governs the dynamics of electrons in graphene. The lattice structure of graphene consists of carbon atoms in a honeycomb-like crystalline structure or two inequivalent triangular sub-lattices, usually called A and B. Powerful electronic structure calculations, like density functional theory and ARPES experiments [40] indicates that the electronic properties close to the charge neutrality point are nicely captured by a tight-binding Hamiltonian with nearest-neighbor hopping. Its continumm limit is the Dirac Hamiltonian for massless fermions [40]. These are the effective models we use in this thesis. Next, we discuss the influence of lattice deformation, ubiquitous in graphene since it is a membrane, in its electronic properties [40]. We show that lattice deformation and strain ca be expressed in terms of a pseudo-magnetic field in the Dirac Hamiltonian [40].

In chapter 3 we introduce a disorder model for deformation. We discuss how ripples in the graphene sheet can give raise to random magnetic fields [33]. Those can be either intrinsic, due to strain, or extrinsic originated, for instance, by an external applied parallel magnetic field.

In chapter 4 we present the correction to the Drude-Boltzmann conductivity due to random magnetic field disorder discussed in chapter 3. This analysis is motivated by an experimental work [41]. We show that intrinsic and extrinsic magnetic fields disorder contribute differently to the conductivity tensor anisotropy and qualitatively explain the experimental data.

In chapter 5 we present the calculations of Weiss oscillations due to uniaxial strain and an external in-plane magnetic field. It has been theoretically predicted that this phenomena is quite different in graphene from that in 2DEG. We propose an experimental set up for Weiss oscillations. Moreover, we show that such experiment can provide further evidence of the existence of pseudo-magnetic fields in deformed graphene.

In chapter 6 we study the weak localization correction to the Drude-Boltzmann conductivity due to random magnetic fields. These quantum corrections complement the semiclassical analysis presented in chapter 4 and allow to fully discuss the experiment in Ref. [41].

Finally, in chapter 7 we address a problem of very different nature, namely, obtaining the N-particle density of state with disorder for fermions in two dimensions. We also

show some technical difficulties related to bosonic systems. This chapter corresponds to a work (still in progress) that I started during my Ph.D. under the supervison of Prof. Klaus Richter in Regensburg, Germany.

2 Low energy description of electrons in graphene: Basic theory

2.1 Elementary electronic structure of graphene

The tight-binding Hamiltonian for the the π-band of graphene in second quantization reads [40]

$$\mathcal{H} = -\sum_{<i,j>} t_{ij} a_i^\dagger b_j + H.c. \tag{2.1}$$

where $a_i^\dagger$ ($b_i^\dagger$) creates (annihilates) an electron in site A (B), t_{ij} is the electron hopping integral between neighbor atoms and the sum is taken over nearest neighbors sites only. In reciprocal space the Hamiltonian (2.1) reads

$$\mathcal{H} = -\sum_{\boldsymbol{k},n} t_n e^{-i\boldsymbol{k}\cdot\boldsymbol{\delta}_n} a_{\boldsymbol{k}}^\dagger b_{\boldsymbol{k}} + H.c. \tag{2.2}$$

In the above relations we assumed uniform strain, that is, in all sites the strain depends only on the neighbor direction corresponding to the index n, where the entries correspond to the sublattices A(B) and $\boldsymbol{\delta}_n$ are the nearest neighbor vectors (see Fig. 2). In matrix form (2.2) becomes

$$H = -\sum_n t_n \begin{pmatrix} 0 & e^{-i\boldsymbol{k}\cdot\boldsymbol{\delta}_n} \\ e^{i\boldsymbol{k}\cdot\boldsymbol{\delta}_n} & 0 \end{pmatrix}. \tag{2.3}$$

Diagonalization, gives the dispersion relation

$$E(\boldsymbol{k}) = \pm|\sum_n t_n e^{-i\boldsymbol{k}\cdot\boldsymbol{\delta}_n}|. \tag{2.4}$$

As illustrated in Fig. 1 the two bands touch each other at six points(which turn out to be high symmetry points in the Brillouin zone, see below). At $E = 0$ this energy correspond to the Fermi energy of the undopped system. Among these six points only two of them

are non equivalent, defining the valley $\boldsymbol{K}$ and $\boldsymbol{K}'$. The low energy properties of graphene can be accounted for by the study of electrons behaviour around these points [40]. Hence,

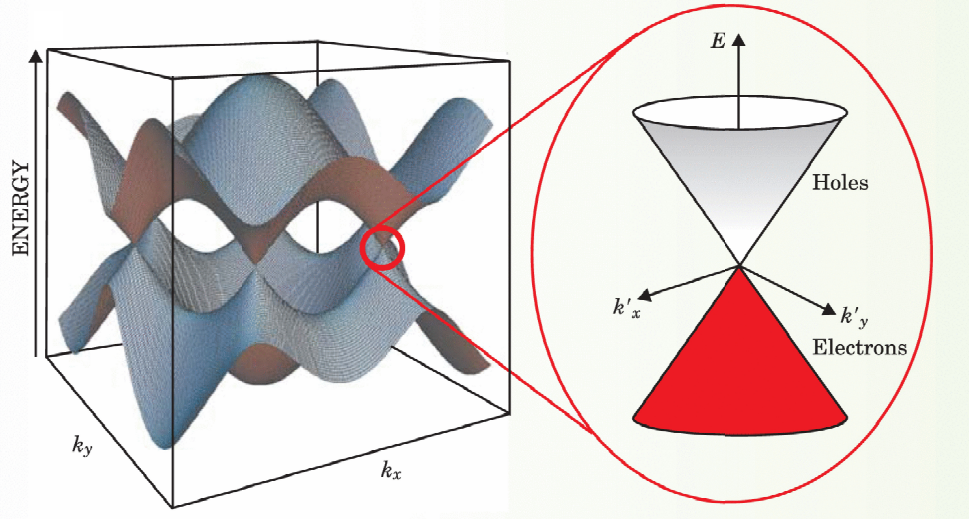

Figure 1: Dispersion relation for graphene. Taken from [1].

we expand the momentum around the $\boldsymbol{K}$-symmetry points. To this end, we introduce the substitution $\boldsymbol{k} \to \boldsymbol{K} + \boldsymbol{k}$ and write

$$H = -\sum_n t_n \begin{pmatrix} 0 & e^{-i\boldsymbol{K}\cdot\boldsymbol{\delta}_n} \\ e^{i\boldsymbol{K}\cdot\boldsymbol{\delta}_n} & 0 \end{pmatrix} [\cos(\boldsymbol{k}\cdot\boldsymbol{\delta}_n) + i\sigma_z \sin(\boldsymbol{k}\cdot\boldsymbol{\delta}_n)]. \tag{2.5}$$

Expanding up to second order in $\boldsymbol{k}$

$$H \approx -\sum_n t_n \begin{pmatrix} 0 & e^{-i\boldsymbol{K}\cdot\boldsymbol{\delta}_n} \\ e^{i\boldsymbol{K}\cdot\boldsymbol{\delta}_n} & 0 \end{pmatrix} \left[1 - \frac{(\boldsymbol{k}\cdot\boldsymbol{\delta}_n)^2}{2} + i\sigma_z(\boldsymbol{k}\cdot\boldsymbol{\delta}_n)\right]. \tag{2.6}$$

It has been shown [42] that the effect of strain in graphene is to modify the hopping integral as follows

$$t_n \approx t\left(1 - \frac{\beta}{a^2}\boldsymbol{\delta}_n \cdot \boldsymbol{u} \cdot \boldsymbol{\delta}_n\right), \tag{2.7}$$

where $a \approx 1.42$ Å is the carbon-carbon distance, $t \approx 2.7$ eV is the nearest neighbor π-orbitals hopping matrix element, and $\beta = -\partial \log t/\partial \log a \approx 2 - 3.37$ [42, 43] is the Grüneisen parameter, a dimensionless material dependent parameter that characterizes the coupling between the Dirac electrons and the lattice deformations and $\boldsymbol{u}$ is the strain

tensor whose expression is [42]

$$\begin{aligned} u_{xx}(\boldsymbol{r}) &= \frac{\partial u_x(\boldsymbol{r})}{\partial x} + \frac{1}{2}\left[\frac{\partial h(\boldsymbol{r})}{\partial x}\right]^2, \\ u_{yy}(\boldsymbol{r}) &= \frac{\partial u_y(\boldsymbol{r})}{\partial y} + \frac{1}{2}\left[\frac{\partial h(\boldsymbol{r})}{\partial y}\right]^2, \\ u_{xy}(\boldsymbol{r}) &= \frac{1}{2}\left(\frac{\partial u_x(\boldsymbol{r})}{\partial y} + \frac{\partial u_y(\boldsymbol{r})}{\partial x}\right) + \frac{1}{2}\frac{\partial h(\boldsymbol{r})}{\partial x}\frac{\partial h(\boldsymbol{r})}{\partial y}. \end{aligned} \tag{2.8}$$

where $h(\boldsymbol{r})$ gives the out of plane deformation of the graphene sheet and $\boldsymbol{u}_i$ is the displacement vector that can be calculated, for instance, by minimization of the elastic energy [42]

$$\mathcal{H}_{\text{elastic}} = \int d\mathbf{r} \left\{ \frac{\lambda}{2}\left[\sum_i u_{ii}(\mathbf{r})\right]^2 + \mu \sum_{ij} \left[u_{ij}(\mathbf{r})\right]^2 \right\}, \tag{2.9}$$

by fixing $h(\boldsymbol{r})$ and varying the in-plane contribution. λ and μ are in-plane elastic constants. Using the expression for the modified hopping integral in (2.6), we get

$$H \approx -t \sum_n \begin{pmatrix} 0 & e^{-i\boldsymbol{K}\cdot\boldsymbol{\delta}_n} \\ e^{i\boldsymbol{K}\cdot\boldsymbol{\delta}_n} & 0 \end{pmatrix} \left[1 - \frac{\beta}{a^2}\boldsymbol{\delta}_n \cdot \boldsymbol{u} \cdot \boldsymbol{\delta}_n\right] \left[1 - \frac{(\boldsymbol{k}\cdot\boldsymbol{\delta}_n)^2}{2} + i\sigma_z(\boldsymbol{k}\cdot\boldsymbol{\delta}_n)\right]. \tag{2.10}$$

The above equation can be separated in three terms, namely

$$H = H_0 + H_w + H_{\text{s}} \tag{2.11}$$

where H_0 gives the standard low energy Dirac Hamiltonian,

$$H_0 = -t \sum_n \begin{pmatrix} 0 & e^{-i\boldsymbol{K}\cdot\boldsymbol{\delta}_n} \\ e^{i\boldsymbol{K}\cdot\boldsymbol{\delta}_n} & 0 \end{pmatrix} \left[i\sigma_z \boldsymbol{k}\cdot\boldsymbol{\delta}_n\right], \tag{2.12}$$

H_w corresponds to a term called trigonal warping, and is given by

$$H_w = t \sum_n \begin{pmatrix} 0 & e^{-i\boldsymbol{K}\cdot\boldsymbol{\delta}_n} \\ e^{i\boldsymbol{K}\cdot\boldsymbol{\delta}_n} & 0 \end{pmatrix} \left[\frac{(\boldsymbol{k}\cdot\boldsymbol{\delta}_n)^2}{2}\right], \tag{2.13}$$

while H_{s} corresponds to the contribution of strain (in linear order) and is given by

$$H_{\text{s}} = t \sum_n \begin{pmatrix} 0 & e^{-i\boldsymbol{K}\cdot\boldsymbol{\delta}_n} \\ e^{i\boldsymbol{K}\cdot\boldsymbol{\delta}_n} & 0 \end{pmatrix} \left(\frac{\beta}{a^2}\boldsymbol{\delta}_n \cdot \boldsymbol{u} \cdot \boldsymbol{\delta}_n\right). \tag{2.14}$$

In the following sections we will explore in more detail each one of these contributions.

2.2 Dirac Hamiltonian and trigonal warping

Let us analyze here H_0 and H_w corresponding to Eq. 2.12 and Eq. 2.13. Let us assume a zigzag type lattice orientation along the x-axis, as shown in Fig. 2. In this case, the nearest neighbors vectors are

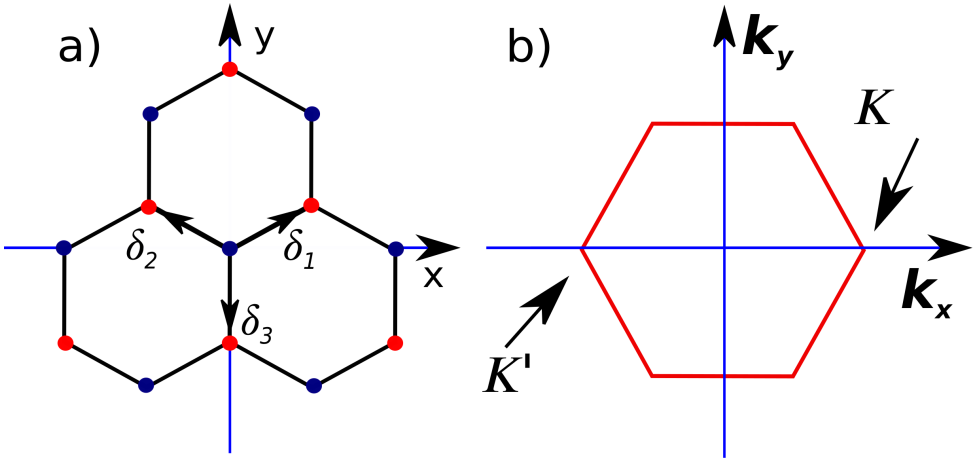

Figure 2: Sketch of a graphene lattice a) zigzag orientation in the x-direction and b) Corresponding Brillouin zone.

$$\boldsymbol{\delta}_1 = \frac{a}{2}\begin{pmatrix}\sqrt{3}\\1\end{pmatrix}, \quad \boldsymbol{\delta}_2 = \frac{a}{2}\begin{pmatrix}-\sqrt{3}\\1\end{pmatrix}, \qquad \text{and} \quad \boldsymbol{\delta}_3 = a\begin{pmatrix}0\\-1\end{pmatrix}. \tag{2.15}$$

while the two inequivalent high symmetry points are

$$\boldsymbol{K} = \frac{4\pi}{3a}\begin{pmatrix}\sqrt{3}/3\\0\end{pmatrix} \quad \text{and} \quad \boldsymbol{K}' = \frac{4\pi}{3a}\begin{pmatrix}-\sqrt{3}/3\\0\end{pmatrix}. \tag{2.16}$$

Using the $\boldsymbol{K}$-symmetry point for the expansion we arrive at the identity

$$\begin{pmatrix}0 & e^{-i\boldsymbol{K}\cdot\boldsymbol{\delta}_n}\\ e^{i\boldsymbol{K}\cdot\boldsymbol{\delta}_n} & 0\end{pmatrix} = i\frac{\boldsymbol{\sigma}\cdot\boldsymbol{\delta}_n}{a}\sigma_z, \tag{2.17}$$

Hence

$$H_0^{\boldsymbol{K}} = t\sum_n \frac{\boldsymbol{\sigma}\cdot\boldsymbol{\delta}_n}{a}\left(\boldsymbol{k}\cdot\boldsymbol{\delta}_n\right). \tag{2.18}$$

Finally, using the identity

$$\sum_{n=1}^{3}(\mathbf{v}_1\cdot\boldsymbol{\delta}_n)(\mathbf{v}_2\cdot\boldsymbol{\delta}_n) = \frac{3a^2}{3}\mathbf{v}_1\cdot\mathbf{v}_2 \tag{2.19}$$

where $\mathbf{v}_1$ and $\mathbf{v}_2$ are any arbitrary vectors in the 2D lattice, we write

$$H_0^{\boldsymbol{K}} = v_F \boldsymbol{\sigma} \cdot \boldsymbol{p} \tag{2.20}$$

where $v_F = 3at/(2\hbar)$ is usually called Fermi velocity and $\mathbf{p} = \hbar\mathbf{k}$. The eigenvalues of equation (2.20) are

$$E(\boldsymbol{k}) = \pm v_F \hbar |\boldsymbol{k}|. \tag{2.21}$$

We can interpret $E(\boldsymbol{k}) = +v_F\hbar|\boldsymbol{k}|$ as a dispersion relation for electrons (or conduction band) and $E(\boldsymbol{k}) = -v_F\hbar|\boldsymbol{k}|$ as a dispersion relation for holes (or valence band). The corresponding eigenvectors are:

$$|\boldsymbol{k}+\rangle = \frac{1}{\sqrt{2}} \begin{pmatrix} 1 \\ e^{i\theta} \end{pmatrix} \quad \text{and} \quad |\boldsymbol{k}-\rangle = \frac{1}{\sqrt{2}} \begin{pmatrix} 1 \\ -e^{i\theta} \end{pmatrix}, \tag{2.22}$$

with $\theta = \arctan(k_y/k_x)$.

Trigonal warping is a deviation from the liner dispersion relation. The calculation of this term around the $\boldsymbol{K}$-point is straightforward. Using again the identity (2.17), it is

$$H_w^{\boldsymbol{K}} = -\mu \begin{pmatrix} 0 & (p_x + ip_y)^2 \\ (p_x - ip_y)^2 & 0 \end{pmatrix}, \tag{2.23}$$

with $\mu = 3a^2t/8\hbar^2$. The importance of this contribution will be addressed in Chapter(6).

The Dirac Hamiltonian in the $\boldsymbol{K}'$ valley can be obtained as follows. Since $\mathbf{K}' = -\mathbf{K}$, using (2.17) one writes

$$\begin{pmatrix} 0 & e^{-i\boldsymbol{K}'\cdot\boldsymbol{\delta}_n} \\ e^{i\boldsymbol{K}'\cdot\boldsymbol{\delta}_n} & 0 \end{pmatrix} = \begin{pmatrix} 0 & e^{-i\boldsymbol{K}\cdot\boldsymbol{\delta}_n} \\ e^{i\boldsymbol{K}\cdot\boldsymbol{\delta}_n} & 0 \end{pmatrix}^* = -i\frac{\boldsymbol{\sigma}^* \cdot \boldsymbol{\delta}_n}{a}\sigma_z. \tag{2.24}$$

Hence

$$H_0^{\boldsymbol{K}'} = -v_F\hbar\boldsymbol{\sigma}^* \cdot \boldsymbol{k}. \tag{2.25}$$

For cases where both valley components mix, it is necessary to consider the full Hamiltonian. This more general case will be considered in chapter 6.

2.2.1 Density of states

The electronic density of states is defined as

$$\rho(E) = \frac{4}{\mathcal{A}} \sum_{\boldsymbol{k}} \delta(E - E(\boldsymbol{k})) \tag{2.26}$$

where the 4 factor takes into account the valley and spin degeneracy and $\mathcal{A}$ is the area of the graphene sheet. By inserting Eq.(2.21) into Eq. (2.26), we get

$$\rho(E) = \frac{2}{\pi}\frac{|E|}{(\hbar v_F)^2}. \tag{2.27}$$

This is different from the usual 2DEG where the density of states is constant, independent of the energy. The electronic density is calculated as

$$n = \int_0^{E_F} \rho(E)dE = \frac{k_F^2}{\pi} \tag{2.28}$$

and we have the relation $k_F = \sqrt{\pi|n|}$ between the Fermi wavelength and the electronic density. Again this expression is different from the one of a 2DEG ($k_F^{(2DEG)} = \sqrt{2\pi|n|}$). This difference between graphene and 2DEG in the density of states and the electronic densiy as a function of the Fermi wave length can be ascribed to the linear dispersion relation in graphene.

2.2.2 Helicity and chirality

The helicity is defined as the spin projection along the direction of the momentum. For graphene one defines the helicity by replacing the actual electronic spin by the pseudospin degree of freedom correspinding to the A and B sublattices. It reads[44]

$$\hat{h} = \frac{\boldsymbol{\sigma}\cdot\boldsymbol{p}}{|\boldsymbol{p}|} = \frac{1}{v_F|\boldsymbol{p}|}H_{\boldsymbol{K}}. \tag{2.29}$$

When the linear term in the Hamiltonian is *dominant*, the helicity is conserved in each valley (a symmetry of the system). This means that $[\hat{H}, \hat{h}] = 0$. For the valley $\boldsymbol{K}$ the helicity is positive(negative) for conduction(valence) electrons respectively, namely

$$\begin{aligned} \hat{h}|\boldsymbol{k}+\rangle &= |\boldsymbol{k}+\rangle \\ \hat{h}|\boldsymbol{k}-\rangle &= -|\boldsymbol{k}-\rangle, \end{aligned} \tag{2.30}$$

In the valley $\boldsymbol{K}'$

$$\begin{aligned} \hat{h}|\boldsymbol{k}'+\rangle &= -|\boldsymbol{k}'+\rangle \\ \hat{h}|\boldsymbol{k}'-\rangle &= |\boldsymbol{k}'-\rangle. \end{aligned} \tag{2.31}$$

This means that if we have a a long range scalar potential as the dominant source of disorder, backscattering is prohibited. In order to have backscattering it is needed the potential to be short-range in nature, this is, we need intervalley scattering.

Note that if we increase the energy (doping) this symmetry is broken and backscattering is allowed. This fact can be observed if we consider the linear term in the low energy Hamiltonian plus the trigonal warping. We explore this issue at length in Chapter(6), where we discuss the inter and intra-valley contribution to weak localization, namely a coherent backscattering correction to the Drude-Boltzmann conductivity.

2.3 Strain contribution and lattice orientation

The derivation of an effective low energy correction due to strain is very transparent and straightforward for the zigzag orientation, while for the armchair is a little more tricky. Here we put forward a simple derivation that works for any lattice orientation, as shown in Fig. (3). For convenience, let us assume that the zigzag lattice orientation is rotated with respect to the strain direction by θ. The strain contribution to the Hamiltonian

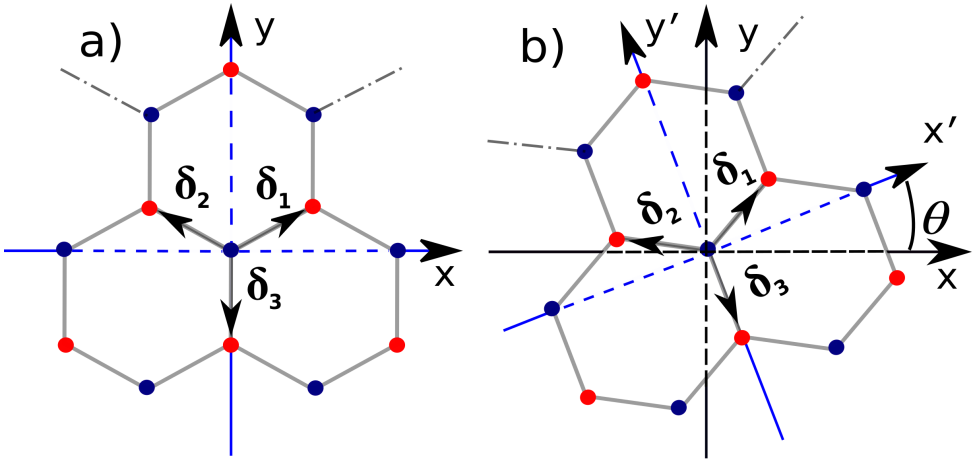

Figure 3: Honeycomb lattice orientation with respect to the strain tensor $x-y$ coordinates axis (a) x-axis aligned with the crystal zigzag direction (b) x-axis is rotated with respect to the zigzag crystal direction, defined by x'.

reads

$$H_{\rm s}^K = t\sum_n i\frac{\boldsymbol{\sigma}\cdot\boldsymbol{\delta}_n}{a}\sigma_z\left(\frac{\beta}{a^2}\boldsymbol{\delta}_n^T\cdot\boldsymbol{u}\cdot\boldsymbol{\delta}_n\right). \tag{2.32}$$

By construction $\boldsymbol{\delta}_n = R(\theta)\boldsymbol{\delta}_n^{\rm zz}$, hence [1]

$$H_{\rm s}^K = t\sum_{n=1}^{3} i\frac{\boldsymbol{\sigma}\cdot R(\theta)\boldsymbol{\delta}_n^{\rm zz}}{a}\sigma_z\left(\frac{\beta}{a^2}(\boldsymbol{\delta}_n^{\rm zz})^T\cdot\left[R^T(\theta)\boldsymbol{u}\,R(\theta)\right]\cdot\boldsymbol{\delta}_n^{\rm zz}\right) \tag{2.33}$$

[1] Here $\boldsymbol{\delta}_n^{\rm zz}$ represent the nearest-neighbor vectors of the honeycomb lattice with the zigzag crystallographic direction oriented along the x-axis of the strain tensor.

where the (active) rotation matrix is

$$R(\theta) = \begin{pmatrix} \cos\theta & -\sin\theta \\ \sin\theta & \cos\theta \end{pmatrix} \tag{2.34}$$

Let us introduce $\overline{\boldsymbol{u}} \equiv R^T(\theta)\boldsymbol{u}\,R(\theta)$, where calculated

$$\overline{u}_{xx} = \frac{u_{xx}+u_{yy}}{2} + \frac{u_{xx}-u_{yy}}{2}\cos 2\theta + u_{xy}\sin 2\theta \tag{2.35}$$

$$\overline{u}_{yy} = \frac{u_{xx}+u_{yy}}{2} - \frac{u_{xx}-u_{yy}}{2}\cos 2\theta - u_{xy}\sin 2\theta \tag{2.36}$$

$$\overline{u}_{xy} = -\frac{u_{xx}-u_{yy}}{2}\sin 2\theta + u_{xy}\cos 2\theta \tag{2.37}$$

To obtain $(\boldsymbol{\delta}_n^{\text{zz}})^T \cdot \overline{\boldsymbol{u}} \cdot \boldsymbol{\delta}_n^{\text{zz}}$ we copy the brute force results obtained for $\boldsymbol{\delta}_n \cdot \boldsymbol{u} \cdot \boldsymbol{\delta}_n$ in the zigzag case (see appendix (B)), namely,

$$\frac{1}{a^2}(\boldsymbol{\delta}_1^{\text{zz}})^T \cdot \overline{\boldsymbol{u}} \cdot \boldsymbol{\delta}_1^{\text{zz}} = \frac{1}{4}(3\overline{u}_{xx} + 2\sqrt{3}\overline{u}_{xy} + \overline{u}_{yy}) \tag{2.38}$$

$$\frac{1}{a^2}(\boldsymbol{\delta}_2^{\text{zz}})^T \cdot \overline{\boldsymbol{u}} \cdot \boldsymbol{\delta}_2^{\text{zz}} = \frac{1}{4}(3\overline{u}_{xx} - 2\sqrt{3}\overline{u}_{xy} + \overline{u}_{yy}) \tag{2.39}$$

$$\frac{1}{a^2}(\boldsymbol{\delta}_3^{\text{zz}})^T \cdot \overline{\boldsymbol{u}} \cdot \boldsymbol{\delta}_3^{\text{zz}} = \overline{u}_{yy} \tag{2.40}$$

Now we calculate $\boldsymbol{\delta}_n = R(\theta)\boldsymbol{\delta}_n^{\text{zz}}$

$$\boldsymbol{\delta}_1 = \frac{a}{2}\begin{pmatrix} \sqrt{3}\cos\theta - \sin\theta \\ \sqrt{3}\sin\theta + \cos\theta \end{pmatrix} \tag{2.41}$$

$$\boldsymbol{\delta}_2 = \frac{a}{2}\begin{pmatrix} -\sqrt{3}\cos\theta - \sin\theta \\ -\sqrt{3}\sin\theta + \cos\theta \end{pmatrix} \tag{2.42}$$

$$\boldsymbol{\delta}_3 = a\begin{pmatrix} \sin\theta \\ -\cos\theta \end{pmatrix} \tag{2.43}$$

Collecting all results we arrive at the final strain Hamiltonian term,

$$H_s = \frac{3ta}{2\hbar}\left[-\sigma_x\frac{\beta\hbar}{a}\left(\frac{u_{xx}-u_{yy}}{2}\cos 3\theta + u_{xy}\sin 3\theta\right) + \sigma_y\frac{\beta\hbar}{a}\left(-\frac{u_{xx}-u_{yy}}{2}\sin 3\theta + u_{xy}\cos 3\theta\right)\right] \tag{2.44}$$

Hence, we identify the vector

$$\mathbf{A}(\theta) = \frac{\beta\hbar}{ae}\begin{pmatrix} \frac{u_{xx}-u_{yy}}{2}\cos 3\theta + u_{xy}\sin 3\theta \\ \frac{u_{xx}-u_{yy}}{2}\sin 3\theta - u_{xy}\cos 3\theta \end{pmatrix}. \tag{2.45}$$

Using the vector potencial $\mathbf{A}$ obtained from the strain analysis in the zigzag case, Eq. (A.6), it is easy to verify that

$$\mathbf{A}(\theta) = \frac{\beta\hbar}{ae} \begin{pmatrix} \cos 3\theta & -\sin 3\theta \\ \sin 3\theta & \cos 3\theta \end{pmatrix} \begin{pmatrix} \frac{u_{xx}-u_{yy}}{2} \\ -u_{xy} \end{pmatrix}. \tag{2.46}$$

Or in a compact form

$$\mathbf{A}(\theta) = \mathbf{R}(3\theta) \cdot \mathbf{A}. \tag{2.47}$$

3 Random magnetic fields in graphene

In this chapter we present a model to study the effect of extrinsic and intrinsic sources of a random magnetic fields in the dynamics of electrons in corrugated graphene monolayer samples.

As discused in the introduction, close to the charge neutrality point, the electronic dispersion relation of pristine graphene monolayers is linear and has two degenerate components, with corresponding K and K' valley indices[44]. In the presence of a magnetic field, the effective electronic Hamiltonian for the K-valley reads

$$H^K = v_F \boldsymbol{\sigma} \cdot [\boldsymbol{p} + e\boldsymbol{A}(\boldsymbol{r})] = H_0^K + V(\boldsymbol{r}), \tag{3.1}$$

where the vector potential $\boldsymbol{A}(\boldsymbol{r})$ has been included in H^K by minimal coupling. Here $v_F \approx 10^6$m/s, $\boldsymbol{\sigma}$ are the Pauli matrices acting on the sublattice space, and $\boldsymbol{p}$ is the electron momentum operator. The Hamiltonian for the K' valley has a similar structure [44].

In the long wave length description, a generic long-ranged disorder potential $V(\boldsymbol{r})$ is represented in both K and K' valleys by

$$V(\boldsymbol{r}) = \sum_i \sigma_i V^{(i)}(\boldsymbol{r}), \tag{3.2}$$

where $i = 0$ stands for scalar disorder (with $\sigma_0 = I_2$) and $i = 1, 2$ for vector potential disorder, while $i = 3$ represents a mass term. The focus of our study are (intrinsic and extrinsic) disordered gauge fields, associated with $V^{(1)}$ and $V^{(2)}$. In this chapter we do not explicitly consider scalar disorder.

Let us introduce

$$\langle \boldsymbol{k}' s'|V|\boldsymbol{k}s\rangle = \frac{1}{2}\left[1 + ss' e^{i(\theta-\theta')}\right] V^{(0)}_{\boldsymbol{k}-\boldsymbol{k}'} + \frac{se^{i\theta}}{2}\left(V^{(1)}_{\boldsymbol{k}-\boldsymbol{k}'} - iV^{(2)}_{\boldsymbol{k}-\boldsymbol{k}'}\right) + \frac{s'e^{-i\theta'}}{2}\left(V^{(1)}_{\boldsymbol{k}-\boldsymbol{k}'} + iV^{(2)}_{\boldsymbol{k}-\boldsymbol{k}'}\right), \tag{3.3}$$

where the spinor

$$\langle \boldsymbol{r}\,|\boldsymbol{k}s\rangle = \frac{1}{\sqrt{2\mathcal{A}}}\begin{pmatrix} 1 \\ se^{i\theta} \end{pmatrix} e^{i\boldsymbol{k}\cdot\boldsymbol{r}}, \tag{3.4}$$

is an eigenstate of H_0^K, $\theta = \tan^{-1}(k_y/k_x)$, s indicates particle ($s = +1$) or hole ($s = -1$) doping, $\mathcal{A}$ is the sample area and

$$V^{(i)}_{\boldsymbol{k}-\boldsymbol{k}'} = \frac{1}{\mathcal{A}}\int d\boldsymbol{r}\, e^{i(\boldsymbol{k}-\boldsymbol{k}')\cdot\boldsymbol{r}}\, V^{(i)}(\boldsymbol{r}) \tag{3.5}$$

is the momentum representation of $V^{(i)}$. Since we deal with elastic processes, we assume in the remaining of the paper that $s = s'$.

3.1 Disordered ripples

The ripple disorder model studied here is defined as follows: We describe the graphene sheet surface by $z = h(\boldsymbol{r})$, where h is the surface displacement with respect to the reference plane $z = 0$ at the position $\boldsymbol{r} = (x, y)$. The average of h is set to zero. In line with the experiments on graphene deposited over a substrate[41, 45, 46, 47, 48], we further assume that the typical heights $h_{\rm rms}$ are much smaller that the ripple lengths λ.

We model the ripple fluctuations in $h(\boldsymbol{r})$ by the correlation function

$$\langle h(\boldsymbol{r})h(\boldsymbol{r}')\rangle = h^2_{\rm rms}\, F\left(\frac{|\boldsymbol{r}-\boldsymbol{r}'|}{\lambda}\right), \tag{3.6}$$

where $\langle\cdots\rangle$ denotes an average over disorder. Although theory predicts a power law height-height correlation function for free-standing membranes [31], experiments support single-parameter correlations for the (static) ripples of graphene deposited over a substrate. For latter convenience, let us define

$$h(\boldsymbol{q}) = \frac{1}{\mathcal{A}}\int d\boldsymbol{r} e^{i\boldsymbol{q}\cdot\boldsymbol{r}} h(\boldsymbol{r}), \tag{3.7}$$

where $\mathcal{A}$ is the sample size. In reciprocal space

$$\langle h(\boldsymbol{q})h(\boldsymbol{q}')\rangle = h_{\rm rms}^2\ \overline{F}(\boldsymbol{q})\delta_{\boldsymbol{q},-\boldsymbol{q}'}, \tag{3.8}$$

where $\overline{F}(\boldsymbol{q})$ is the Fourier transform of the correlation function $F(|\boldsymbol{r}-\boldsymbol{r}'|)$.

We address two mechanisms that generate random magnetic fields. First, we study the case of an external strong magnetic field $\boldsymbol{B}_\parallel$ applied parallel to the graphene sheet. We show that, due to the ripples, $\boldsymbol{B}_\parallel$ gives rise to a random effective magnetic field $B_{\rm ext}(\boldsymbol{r})$ perpendicular to the graphene surface. Next, we discuss the intrinsic pseudo-magnetic field $\boldsymbol{B}_{\rm int}$ originated by the strain field corresponding to the graphene sheet profile height $h(\boldsymbol{r})$.

3.1.1 Random magnetic field due to ripples and an in-plane external B-field

Let us first consider the setup of a magnetic field applied parallel to the sample $z=0$, that has been experimentally investigated in a variety of systems [49, 50, 51, 41]. For notational convenience, in what follows we fix the direction of $B_\parallel$ along the x-axis, namely, $\boldsymbol{B}_\parallel = B_\parallel\hat{\boldsymbol{x}}$.

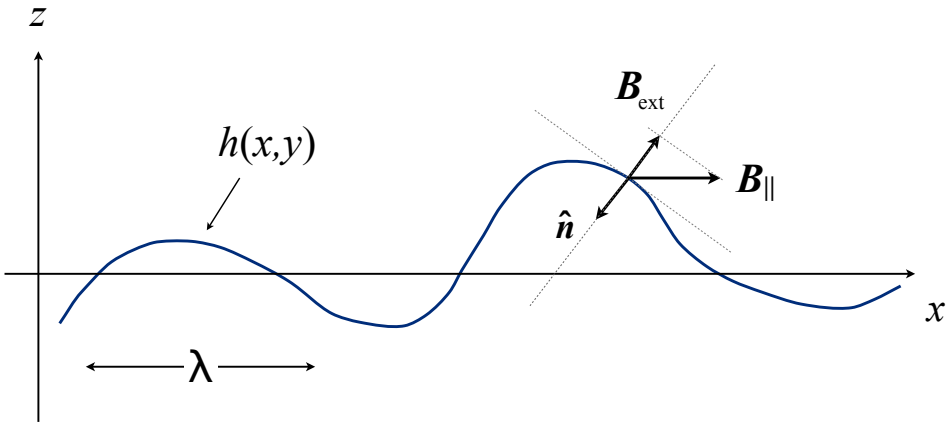

Figure 4: Sketch of $h(\boldsymbol{r})$ along the x direction. The ripple amplitudes δh are enhanced and made comparable with λ to help the illustration.

As illustrated in Fig. 4, the parallel magnetic field $\boldsymbol{B}_\parallel$ has a component perpendicular to the surface $z=h(\boldsymbol{r})$ that is given by

$$B_{\rm ext}(\boldsymbol{r}) = -\boldsymbol{B}_\parallel\cdot\hat{\boldsymbol{n}}(\boldsymbol{r}). \tag{3.9}$$

At the point $\boldsymbol{r}_0 = (x_0, y_0)$, the surface $z = h(\boldsymbol{r})$ has a unit normal vector

$$\hat{\boldsymbol{n}}(\boldsymbol{r}_0) = \frac{1}{\sqrt{1 + \left(\frac{\partial h}{\partial x}\right)^2 + \left(\frac{\partial h}{\partial y}\right)^2}} \left(\begin{array}{c} \partial h/\partial x \\ \partial h/\partial y \\ -1 \end{array} \right) \Bigg|_{\boldsymbol{r}=\boldsymbol{r}_0} . \tag{3.10}$$

We assume that the typical displacement magnitude is characterized by δh. For $\delta h \ll \lambda$, we write

$$\hat{\boldsymbol{n}}(\boldsymbol{r}_0) \approx (\partial h/\partial x, \partial h/\partial y, -1)\Big|_{\boldsymbol{r}=\boldsymbol{r}_0} . \tag{3.11}$$

Hence, the effective local perpendicular magnetic field reads

$$B_{\rm ext}(\boldsymbol{r}) = -\boldsymbol{B}_{\parallel} \cdot \boldsymbol{\nabla} h(\boldsymbol{r}), \tag{3.12}$$

and is expressed, in a convenient gauge for $\boldsymbol{B}_{\parallel} = B_{\parallel}\hat{\boldsymbol{x}}$, by the vector potential

$$A_x(\boldsymbol{r}) = 0 \quad \text{and} \quad A_y(\boldsymbol{r}) = -B_{\parallel} h(\boldsymbol{r}) \, . \tag{3.13}$$

Figure 5(a) illustrates a typical disorder realization of $h(\boldsymbol{r})$ with fluctuations characterized by the Gaussian correlation function $F(x) = \exp\left(-x^2/2\lambda^2\right)$. The corresponding magnetic field $B_{\rm ext}(\boldsymbol{r})$, normal to the graphene sheet, is shown in Fig. 5(b). While $h(\boldsymbol{r})$ displays an isotropic disorder, $B_{\rm ext}(\boldsymbol{r})$ is clearly anisotropic. The anisotropy direction of $B_{\rm ext}(\boldsymbol{r})$ depends on the orientation of $B_{\parallel}$.

The anisotropy is quantified by inspecting the autocorrelation function

$$\langle B_{\rm ext}(\boldsymbol{r}) B_{\rm ext}(\boldsymbol{r}')\rangle = B_{\parallel}^2 \left\langle \frac{\partial h(\boldsymbol{r})}{\partial x} \frac{\partial h(\boldsymbol{r}')}{\partial x'} \right\rangle , \tag{3.14}$$

that can be expressed in terms of F by direct differentiation. Alternatively, going to reciprocal space, one writes

$$\begin{aligned} \left\langle \frac{\partial h(\boldsymbol{r})}{\partial x} \frac{\partial h(\boldsymbol{r}')}{\partial x'} \right\rangle &= h_{\rm rms}^2 \sum_{\boldsymbol{q}} q_x^2 \, \overline{F}(\boldsymbol{q}) e^{-i\boldsymbol{q}\cdot(\boldsymbol{r}-\boldsymbol{r}')} \\ &= -h_{\rm rms}^2 \frac{d^2}{dx^2} F(\boldsymbol{\rho}), \end{aligned} \tag{3.15}$$

with $\boldsymbol{\rho} = \boldsymbol{r} - \boldsymbol{r}'$.

Hence the corresponding $B_{\rm ext}(\boldsymbol{r})$ autocorrelation function reads

$$\langle B_{\rm ext}(\boldsymbol{r}) B_{\rm ext}(\boldsymbol{r}')\rangle = B_{\parallel}^2 \frac{h_{\rm rms}^2}{\lambda^2} \left[1 - \left(\frac{\rho}{\lambda}\right)^2 \cos^2\alpha \right] e^{-\frac{\rho^2}{2\lambda^2}} \tag{3.16}$$

where α is the angle between $\boldsymbol{B}_{\parallel}$ (or the x-axis) and $\boldsymbol{\rho}$.

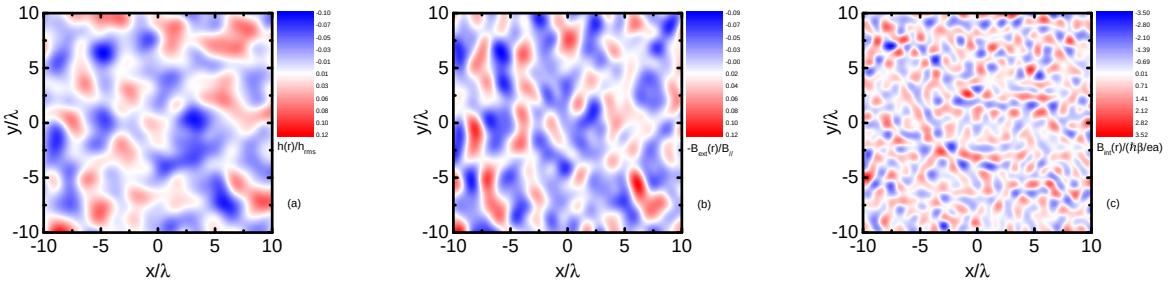

Figure 5: Typical disorder realization of (a) $h(\boldsymbol{r})$, characterized by a Gaussian correlation function F. The corresponding (b) $B_{\rm ext}(\boldsymbol{r})$ for an external $\boldsymbol{B}_{\parallel}$ applied along the x direction, defined in Eq. (14). (c) $B_{\rm int}(\boldsymbol{r})$ due to lattice deformations, given by Eq. (3.18).

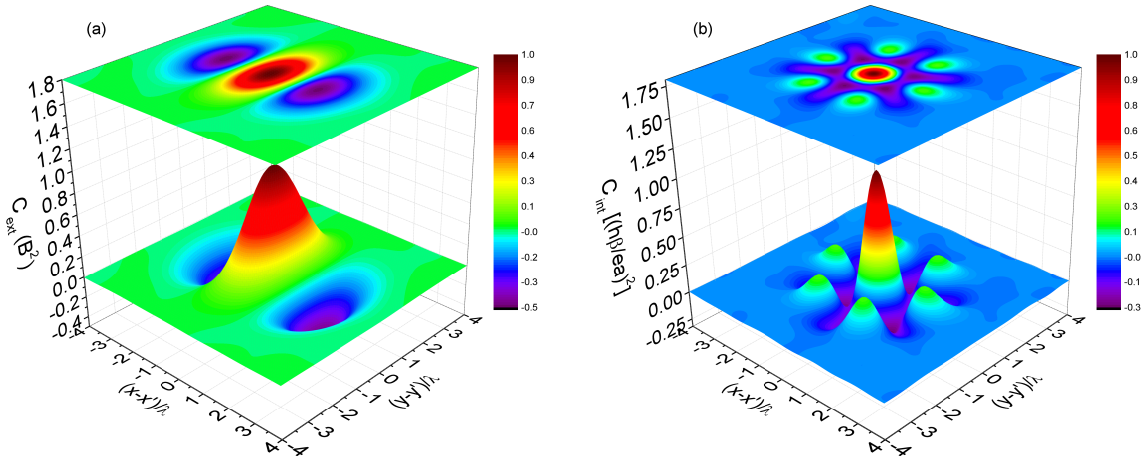

Figure 6: Extrinsic and intrinsic magnetic field correlations functions: (a) $C_{\rm ext}(\boldsymbol{r}-\boldsymbol{r}') = \langle B_{\rm ext}(\boldsymbol{r})B_{\rm ext}(\boldsymbol{r}')\rangle$ for an external $\boldsymbol{B}_{\parallel}$ applied along the x-direction and (b) $C_{\rm int}(\boldsymbol{r}-\boldsymbol{r}') = \langle B_{\rm int}(\boldsymbol{r})B_{\rm int}(\boldsymbol{r}')\rangle$ due to strain in units of $h_{\rm rms}^4/\lambda^6(\hbar\beta/ea)^2$, both corresponding to a ripple disordered surface $h(\mathbf{r})$ characterized by a Gaussian correlation function.

Figure 6(a) shows the $B_{\rm ext}(\boldsymbol{r})$ autocorrelation function obtained by averaging over 10^5 ripple disorder realizations of $h(\boldsymbol{r})$, as defined by Eq. (3.6) with a Gaussian correlation function F (for more details see, for instance, Ref. [23]). As expected, it coincides with Eq. (3.16) and expresses the anisotropy captured by a visual inspection of Fig. 5(b).

3.1.2 Pseudomagnetic field due to strain

The out of plane deformations of a rippled membrane described by $h(\boldsymbol{r})$ can be associated with the strain tensor $u_{ij}(\boldsymbol{r})$ given by [52, 53, 36]

$$u_{xx} \approx \frac{1}{2}\left(\frac{\partial h}{\partial x}\right)^2, \quad u_{yy} \approx \frac{1}{2}\left(\frac{\partial h}{\partial y}\right)^2, \quad \text{and} \quad u_{xy} \approx \frac{1}{2}\left(\frac{\partial h}{\partial x}\frac{\partial h}{\partial y}\right). \tag{3.17}$$

For simplicity we have neglected the effect of in-plane deformations.

As discussed in chapter (2), the effect of strain in the low-energy electronic structure of graphene can be accounted for by introducing a scalar and a vector gauge potential in the Dirac equation [31, 37, 54]. For the K-valley and for a zigzag crystallographic orientation along the x-axis, $\boldsymbol{A} = (A_x, A_y)$ is given by

$$\begin{aligned} A_x(\boldsymbol{r}) &= \frac{\hbar\beta\kappa}{ea}[u_{xx}(\boldsymbol{r}) - u_{yy}(\boldsymbol{r})], \\ A_y(\boldsymbol{r}) &= -2\frac{\hbar\beta\kappa}{ea}u_{xy}(\boldsymbol{r}), \end{aligned} \tag{3.18}$$

with $\kappa \approx 1/3$ [32]. For any given $h(\boldsymbol{r})$ one can readily calculate the pseudo-magnetic field $\boldsymbol{B}_{\rm int} = \nabla \times \boldsymbol{A}$. Since $A_z = 0$ and neither A_x nor A_y depend on z, $\boldsymbol{B}_{\rm int} = B_{\rm int}\hat{\boldsymbol{z}}$. Figure 5(c) shows the $B_{\rm int}$ corresponding to the random rippled surface $h(\boldsymbol{r})$ of Fig. 5(a). Notice that the typical correlation length of $B_{\rm int}(\boldsymbol{r})$ is much shorter than that of $h(\boldsymbol{r})$.

Let us calculate $\langle B_{\rm int}(\boldsymbol{r})B_{\rm int}(\boldsymbol{r}')\rangle$ for a random Gaussian correlated $h(\boldsymbol{r})$, corresponding to Eq. (3.6) with $F(x) = e^{-x^2/2\lambda^2}$. To this end, we calculate the Fourier transform of the intrinsic pseudo magnetic field, namely

$$B_{\rm int}(\boldsymbol{q}) = i\frac{\hbar\beta\kappa}{ea}[q_y u_{xx}(\boldsymbol{q}) + 2q_x u_{xy}(\boldsymbol{q}) - q_y u_{yy}(\boldsymbol{q})], \tag{3.19}$$

with

$$u_{ij}(\boldsymbol{q}) = -\frac{1}{2}\sum_{\boldsymbol{q}'} q'_i(q_j - q'_j)h(\boldsymbol{q}')h(\boldsymbol{q} - \boldsymbol{q}'), \tag{3.20}$$

where i and j label the Cartesian coordinates.

We use Eqs. (3.19) and (3.20) to write the correlation function of $B_{\rm int}$ in momen-

tum space. The evaluation of $\langle B_{\rm int}(\boldsymbol{q})B_{\rm int}(-\boldsymbol{q})\rangle$ amounts to compute the corresponding $\langle u_{ij}(\boldsymbol{q})u_{i'j'}(-\boldsymbol{q})\rangle$, that result in four-point h correlation functions. The calculations can be done exactly for Gaussian fluctuations and provides a good qualitative estimate for other cases[31]. We obtain (See appendix (B) for details)

$$\langle B_{\rm int}(\boldsymbol{q})B_{\rm int}(-\boldsymbol{q})\rangle \;=\; \frac{h_{\rm rms}^4\pi}{32\lambda^2\mathcal{A}}\left(\frac{\hbar\beta\kappa}{ea}\right)^2 q^2\left[16+\lambda^4q^4\sin^2 3\theta\right]e^{-\lambda^2q^2/4}, \qquad (3.21)$$

where θ is the angle between $\boldsymbol{q}$ and the x-direction. By Fourier transforming back to coordinate space, we arrive at

$$C_{\rm int}(\boldsymbol{r}-\boldsymbol{r}')\equiv\langle B_{\rm int}(\boldsymbol{r})B_{\rm int}(\boldsymbol{r}')\rangle = \frac{h_{\rm rms}^4}{\lambda^6}\left(\frac{\hbar\beta\kappa}{ea}\right)^2\left[8-20\frac{\rho^2}{\lambda^2}+9\frac{\rho^4}{\lambda^4}-2\frac{\rho^6}{\lambda^6}\sin^2 3\alpha\right]e^{-\rho^2/\lambda^2}, \qquad (3.22)$$

where α is the angle between $\boldsymbol{\rho}=\boldsymbol{r}-\boldsymbol{r}'$ and the x-axis. [1]

The correlation function $C_{\rm int}(\boldsymbol{r}-\boldsymbol{r}')$ has 6 symmetry axes, reflecting the underlying graphene honeycomb lattice symmetry[36]. In other words, information about the graphene crystal structure survives disorder averaging. Figure 6(b) shows $C_{\rm int}(\boldsymbol{r}-\boldsymbol{r}')$ obtained from 10^5 numerical realizations of Gaussian correlated disorder for $h(\boldsymbol{r})$. The numerical simulations serve as a helpful test to check our analytical results. As in the previous subsection, we verify an excellent agreement within the statistical precision.

[1] Since we only considered the out of plane contribution in the strain tensor, Eq. (3.21) gives a slightly different correlation function than the one found in Ref. [36], where a more general expression for the strain tensor was used.

4 Graphene electronic transport in a random magnetic field

At low temperatures, scalar disorder (short and long ranged) is the main source of momentum relaxation in graphene systems [21, 55]. In this thesis we use a phenomenological transport time τ_s to account for effects of scalar disorder in the conductivity. We assume that τ_s is much shorter than the characteristic transport times due to random gauge fields. In Sec. 5.4, where we compare our results to experiments and, we show that τ_s indeed dominates the conductivity in graphene, but some significant transport properties can only be explained by taking into account random gauge fields effects.

4.1 Drude-Boltzmann conductivity

In this Section we use the effective Dirac Hamiltonian of Eq. (3.1) to calculate the transport time and the Drude-Boltzmann conductivity of graphene monolayers in the presence of random gauge fields.

High mobility graphene samples have typical electronic mean free paths of $\ell \gtrsim 50$ nm [41]. Recalling [44] that the carrier density is related to the Fermi wave number by $k_F = \sqrt{\pi|n|}$, one readily obtains that $k_F\ell \gg 1$ already for a doping of $|n| \approx 10^{11}$ cm^{-2}. This indicates that already for modest carrier densities a semiclassical transport description is justified. For $|n| \gtrsim 10^{11}$ cm^{-2} the typical graphene conductivity in good quality samples is much larger than e^2/h, the order of magnitude of quantum contributions to the electronic transport, such as weak localization [56, 57, 21] and universal conductance fluctuations [58]. In such situations, the Boltzmann approach is very successful in assessing the conductivity, as shown by direct comparison with numerical simulations using an atomistic basis [23, 59]. As one approaches the charge neutrality point, and $k_F\ell \lesssim 1$, the semiclassical method is no longer suited and one has to resort to more sophisticated approaches [24, 21].

We now discuss how to add gauge field disorder in the Boltzmann approach. For long ranged disorder, some authors [60, 61, 62] argue that it can be advantageous to include the disorder potential in the classical Liouvillian evolution, that is, to treat $V(\boldsymbol{r})$ in the *left-hand side* of the Boltzmann equation.

This approach is justified in the "classical" regime, where $k_F\lambda \gg 1$, that is, where the random fields characterized by the scale λ vary slowly in the scale of k_F. In graphene with ripple sizes λ of the order of few to ten nanometers [45, 46, 47, 48], the latter inequality holds for a carrier density $|n| \gg 10^{12}$ cm^{-2}, which is much higher than the doping considered in most experiments [44].

In this thesis, we calculate transport times for both short and long ranged disorder by evaluating the corresponding Boltzmann collision integral (at the *right-hand side* of the equation). As mentioned in the introduction of this chapter, for graphene on standard substrates (the case of interest here), the random gauge field contribution to the conductivity is not the dominant one. Hence, the electron mean free path due to ripples is larger than ℓ and the arguments justifying the semiclassical approximation hold.

The stationary and uniform Boltzmann equation for graphene under a uniform electric field $\boldsymbol{E}$ reads [39, 44]

$$-e\boldsymbol{E}\cdot\frac{\partial\varepsilon_{\boldsymbol{k},s}}{\partial\boldsymbol{p}}\frac{\partial f_0}{\partial\varepsilon} = \sum_{\boldsymbol{k}',s'}(g_{\boldsymbol{k},s} - g_{\boldsymbol{k}',s'})\mathcal{W}_{\boldsymbol{k}',s\leftarrow\boldsymbol{k},s} \tag{4.1}$$

where $\varepsilon_{\boldsymbol{k},s} = sv_F\hbar|\boldsymbol{k}|$, $f_0(\varepsilon)$ is the Fermi distribution function, $g_{\boldsymbol{k}} = f_{\boldsymbol{k}} - f_0$ represents the deviation from the equilibrium distribution due to the electric field, and $W_{\boldsymbol{k}',s'\leftarrow\boldsymbol{k},s}$ is the transition rate from state $(\boldsymbol{k},s)$ to $(\boldsymbol{k}',s)$, that we calculate using Fermi golden rule, namely

$$\mathcal{W}_{\boldsymbol{k}',s'\leftarrow\boldsymbol{k},s} = \frac{2\pi}{\hbar}\left\langle|\langle\boldsymbol{k}'s'|V|\boldsymbol{k}s\rangle|^2\right\rangle\delta(\varepsilon_{\boldsymbol{k},s} - \varepsilon_{\boldsymbol{k}',s'}), \tag{4.2}$$

where V is a generic long-ranged disorder potential parametrized by Eq. (3.2). The δ-function reflects the fact we are dealing with elastic processes and, hence, $s = s'$. In our model, the transition rates do not depend on s. Accordingly we drop this index whenever its omission does not introduce an ambiguity.

The scattering processes we address are anisotropic. The calculation of the transport properties in this case is slightly different [63, 64] than that of the standard isotropic case [39]. Here, we adapt the nice method developed by Tokura [38] – that is briefly described in what follows – to calculate the transport times of massless Dirac electrons in graphene.

In both situations of interest, the scattering potential correlation functions have at

least one symmetry axis. For convenience, we choose the x-axis along a symmetry axis and define [38]

$$g_{\boldsymbol{k}} = \left(-\frac{\partial f_0}{\partial \varepsilon_{\boldsymbol{k}}}\right) e v_{\boldsymbol{k}}\, \boldsymbol{\tau}(\theta) \cdot \boldsymbol{E}, \tag{4.3}$$

where $\boldsymbol{\tau}(\theta)$ is the relaxation time vector to be solved. We recall that θ is the angle between $\boldsymbol{k}$ and the x-axis. Note that $\boldsymbol{\tau}$ depends explicitly on θ and implicitly on $|\boldsymbol{k}|$.

The current density (spin and valley degeneracies included) is given by

$$\begin{aligned} \boldsymbol{j} &= \frac{4}{\mathcal{A}} \sum_{\boldsymbol{k}} e \boldsymbol{v}_{\boldsymbol{k}} g_{\boldsymbol{k}} \\ &= \frac{e^2}{\pi^2} \int_0^\infty dk k \left(-\frac{\partial f_0}{\partial \varepsilon_{\boldsymbol{k}}}\right) \int_0^{2\pi} d\theta\, v_{\boldsymbol{k}}\, \boldsymbol{v}_{\boldsymbol{k}} [\boldsymbol{\tau}(\theta) \cdot \boldsymbol{E}], \end{aligned} \tag{4.4}$$

from which one obtains the conductivity tensor

$$\sigma = \frac{e^2 |\varepsilon_F|}{\hbar^2 \pi^2} \int_0^{2\pi} d\theta \begin{pmatrix} \tau_x(\theta)\cos\theta & \tau_y(\theta)\cos\theta \\ \tau_x(\theta)\sin\theta & \tau_y(\theta)\sin\theta \end{pmatrix}, \tag{4.5}$$

where ε_F is the Fermi energy, measured with respect to the charge neutrality point energy. For the sake of simplicity, in Eq. (4.5) we have taken the zero-temperature limit, namely, $-\partial f_0/\partial \varepsilon = \delta(\varepsilon - \varepsilon_F)$.

By substituting the ansatz (4.3) in the Boltzmann equation, Eq. (4.1), one obtains a set of integral equations for $\boldsymbol{\tau}(\theta)$, namely

$$\cos\theta = \int_0^{2\pi} d\theta' [\tau_x(\theta) - \tau_x(\theta')] \mathcal{W}(\theta, \theta') \tag{4.6}$$

$$\sin\theta = \int_0^{2\pi} d\theta' [\tau_y(\theta) - \tau_y(\theta')] \mathcal{W}(\theta, \theta'), \tag{4.7}$$

where θ' is the angle between $\boldsymbol{k}'$ and the x-axis, and

$$\begin{aligned} \mathcal{W}(\theta, \theta') &= \frac{\mathcal{A}}{(2\pi)^2} \int_0^\infty dk' k' \mathcal{W}_{\boldsymbol{k}', s \leftarrow \boldsymbol{k}, s} \\ &= \frac{\mathcal{A}|\varepsilon_F|}{2\pi v_F^2 \hbar^3} \left\langle |\langle \boldsymbol{k}', s|V|\boldsymbol{k}, s\rangle|^2 \right\rangle, \end{aligned} \tag{4.8}$$

where, due to the zero-temperature limit, $k = k' = k_F$.

The matrix element $\langle \boldsymbol{k}', s|V|\boldsymbol{k}, s\rangle$ depends on $\boldsymbol{q} = \boldsymbol{k} - \boldsymbol{k}'$ and $\varphi = \pi/2 + (\theta + \theta')/2$, the angle between $\boldsymbol{q}$ and the x-axis. Hence, $\mathcal{W}(\theta, \theta')$ is conveniently cast as $\mathcal{W}(q_\zeta, \varphi)$. We use the standard notation $\zeta = |\theta - \theta'|$ and $q_\zeta = 2k_F \sin(\zeta/2)$.

By expressing τ_x and τ_y in terms of a Fourier series, one transforms Eqs. (4.6) and

(4.7) into an (infinite) set of algebraic equations. Using the x-axis symmetry and that $\mathcal{W}(\theta,\theta') = \mathcal{W}(\theta',\theta)$ [1], one shows that[38]

$$\tau_x(\theta) = \sum_{n=1}^{\infty} \tau_x^{(n)} \cos[(2n-1)\theta] \tag{4.9}$$

$$\tau_y(\theta) = \sum_{n=1}^{\infty} \tau_y^{(n)} \sin[(2n-1)\theta]. \tag{4.10}$$

By inserting the above relations in Eq. (4.5), we find that the conductivity tensor is diagonal, with

$$\sigma_{xx} = \frac{e^2|\varepsilon_F|}{\hbar^2\pi}\tau_x^{(1)} \quad \text{and} \quad \sigma_{yy} = \frac{e^2|\varepsilon_F|}{\hbar^2\pi}\tau_y^{(1)}, \tag{4.11}$$

that supports the interpretation of $\boldsymbol{\tau}^{(1)}$ as a transport time vector.

The symmetry $\mathcal{W}(\theta,\theta') = \mathcal{W}(\theta',\theta)$ implies that $\mathcal{W}(q_\zeta,\varphi) = \mathcal{W}(q_\zeta,\varphi+\pi) = \mathcal{W}(q_\zeta,\varphi-\pi)$. In turn

$$\mathcal{W}(q_\zeta,\varphi) = \sum_{n=0}^{\infty} \mathcal{W}_n(q_\zeta)\cos(2n\varphi), \tag{4.12}$$

with an obvious inversion relation.

By using the Fourier expansions for $\boldsymbol{\tau}(\theta)$ and $W(q_\zeta,\varphi)$, Eqs. (4.6) and (4.7) can be cast in matrix form [38]

$$\delta_{l,1} = \sum_{n=1}^{\infty} M^-_{l,n}\tau_x^{(n)} \quad \text{and} \quad \delta_{l,1} = \sum_{n=1}^{\infty} M^+_{l,n}\tau_y^{(n)}, \tag{4.13}$$

where $\delta_{l,1}$ is the Kronecker delta and the matrix elements of $M^\pm$ are[38]

$$M^\pm_{l,n} = \frac{(-1)^{l-n}}{2}\big[(1+\delta_{l,n})J_{|l-n|,n+l-1} \pm J_{n+l-1,|l-n|}\big], \tag{4.14}$$

with

$$J_{n,m} = \int_0^{2\pi} d\zeta\, \mathcal{W}_n(q_\zeta)[\cos(n\zeta) - \cos(m\zeta)]. \tag{4.15}$$

Finally, by inverting $M^\pm$ in Eq. (4.13), one writes the vector transport time components as

$$\tau_x^{(1)} = [(M^-)^{-1}]_{11} \quad \text{and} \quad \tau_y^{(1)} = [(M^+)^{-1}]_{11}. \tag{4.16}$$

Note that for isotropic scattering, all $\mathcal{W}_n$ with $n > 0$ are zero and $M^\pm$ is diagonal, with elements $K_{l,l} = J_{0,2l-1}$. Hence, the vector transport time components coincide,

[1] Microreversibility is usually invoked to guarantee $\mathcal{W}(\theta,\theta') = \mathcal{W}(\theta',\theta)$ and Eq. (4.1). In the presence of an external magnetic field, that breaks time-reversal symmetry, $\mathcal{W}(\theta,\theta') = \mathcal{W}(\theta',\theta)$ still holds true within the Fermi golden rule approximation used in Eq. (4.2)

$\tau_x^{(1)} = \tau_y^{(1)} = \tau^{(1)}$, and read

$$\frac{1}{\tau^{(1)}} = J_{0,1} = \int_0^{2\pi} d\zeta \mathcal{W}_0(q_\zeta)(1 - \cos\zeta), \tag{4.17}$$

which is the standard expression for the transport time in isotropic systems.

4.1.1 Effect of an in-plane magnetic field

Let us now calculate the effect of an external parallel magnetic field on the conductivity. From Eq. (3.13) we write the effective disorder potential for the K-valley as

$$V_{\text{ext}}(\boldsymbol{r}) = v_F e \sigma_y A_y(\boldsymbol{r}) = -v_F e B_\parallel h(\boldsymbol{r}) \sigma_y. \tag{4.18}$$

We recall that $h(\boldsymbol{r})$ varies slowly in the scale of the lattice spacing and, hence, $V_{\text{ext}}(\boldsymbol{r})$ is long-ranged and does not mix valleys [44].

The momentum relaxation rate $W_{\boldsymbol{k}' \leftarrow \boldsymbol{k}}$ reads

$$\mathcal{W}_{\boldsymbol{k}' \leftarrow \boldsymbol{k}} = \delta(k - k') \frac{2\pi e^2 v_F}{\hbar^2} B_\parallel^2 \sin^2\left(\frac{\theta + \theta'}{2}\right) \frac{C_h(q)}{\mathcal{A}}, \tag{4.19}$$

where

$$C_h(q) = \int d\boldsymbol{r}\, e^{i\boldsymbol{q}\cdot\boldsymbol{r}} \left\langle h(0) h(\boldsymbol{r}) \right\rangle \tag{4.20}$$

is the form factor of the height-height correlation function. Here $\langle \cdots \rangle$ indicates disorder average.

From Eq. (4.8) we obtain

$$\mathcal{W}(q, \varphi) = \frac{(eB_\parallel)^2 |\varepsilon_F|}{4\pi\hbar^3} C_h(q)(1 + \cos 2\varphi), \tag{4.21}$$

which has only 2 non-zero Fourier components, namely,

$$\mathcal{W}_n(q) = \frac{(eB_\parallel)^2 |\varepsilon_F|}{4\pi\hbar^3} C_h(q), \quad \text{for} \quad n = 0, 1 \tag{4.22}$$

while $\mathcal{W}_n(q) = 0$ for $n \geq 2$.

In this case, the $M^\pm$ matrix is tridiagonal and reads [38]

$$M^\pm = \begin{pmatrix} (1 \mp \frac{1}{2}) J_{0,1} & -\frac{1}{2} J_{1,2} & 0 & \cdots \\ -\frac{1}{2} J_{1,2} & J_{0,3} & -\frac{1}{2} J_{1,4} & \cdots \\ 0 & -\frac{1}{2} J_{1,4} & J_{0,5} & \cdots \\ \vdots & \vdots & \vdots & \ddots \end{pmatrix}. \tag{4.23}$$

The inverse transport time components are given by

$$\frac{1}{\tau_x^{(1)}} = \frac{3}{2}J_{0,1} - \Gamma_3 \quad \text{and} \quad \frac{1}{\tau_y^{(1)}} = \frac{1}{2}J_{0,1} - \Gamma_3, \tag{4.24}$$

where Γ_3 is isotropic and determined by the continued fraction relation

$$\Gamma_m = \frac{(J_{1,m-1})^2}{4(J_{0,m} - \Gamma_{m+2})}. \tag{4.25}$$

In practice, we compute Γ_3 by assuming that $\Gamma_{\overline{m}} = 0$ as a seed for the iteration of (4.25). The choice of $\overline{m}$ determines the precision of the calculation: The larger $\overline{m}$, the more accurate is Γ_3.

Assuming that $\Gamma_3 \ll J_{0,1}$ leads to an interesting result, that is

$$\frac{1}{\tau_y^{(1)}} = \frac{1}{3\tau_x^{(1)}} = \frac{(eB_\parallel)^2|\varepsilon_F|}{8\pi\hbar^3}\int_0^{2\pi} d\zeta(1-\cos\zeta)C_h(q). \tag{4.26}$$

In this limit $\tau_y^{(1)}/\tau_x^{(1)} = 3$. In other words, for $\Gamma_3 \ll J_{0,1}$ the corrections to the conductivity due to $\boldsymbol{B}_\parallel$ lead to $\Delta\sigma_{yy} = 3\Delta\sigma_{xx}$, regardless of the dependence of correlation function $C_h(q)$ on q.

For the limiting case of $\Gamma_3 = 0$ and $C_h(q) = 2\pi\lambda^2 h_{\rm rms}^2 e^{-\lambda^2 q^2/2}$, we write $\tau_{x,y}^{(1)}$ in closed analytical form, namely

$$\frac{1}{\tau_y^{(1)}} = \frac{1}{3\tau_x^{(1)}} = \frac{(eB_\parallel)^2|\varepsilon_F|}{4\hbar^3}(\lambda h_{\rm rms})^2 e^{-\lambda^2 k_F^2}\left[I_0(\lambda^2 k_F^2) - I_1(\lambda^2 k_F^2)\right], \tag{4.27}$$

where I_0 and I_1 are modified Bessel functions of the first kind. We use [44] $k_F = \sqrt{\pi|n|}$ to express the conductivity in terms of the charge carrier density n. We conclude that the correction to the conductivity due to an in-plane magnetic field depends quadratically on $h_{\rm rms}B_\parallel$ and has a non-trivial dependence on $\lambda^2|n|$.

In the high doping limit of $\lambda|n|^{1/2} \gg 1$, Eq. (4.27) gives

$$\Delta\sigma_{yy} = 3\Delta\sigma_{xx} \approx 2\sqrt{2}\hbar|n|^{3/2}\frac{\lambda}{h_{\rm rms}^2}\frac{1}{B_\parallel^2}. \tag{4.28}$$

in agreement with Ref. [41].

Figure 7 shows the resistivity $\Delta\rho_{yy}$ versus the carrier density n (due to particle hole symmetry, we only show $n > 0$) for $\overline{m} = 3$ and $\overline{m} \to \infty$. The optimal $\overline{m}$ value to obtain convergence depends on $\lambda^2 n$. The inset shows $\Delta\rho_{yy}$ for $\lambda^2 n$ values outside the validity range of the asymptotic expansion. As discussed in the next section, the $\lambda^2 n$

range displayed in the inset corresponds to the typical experimental situation. We find that the $|n|^{-3/2}$ scaling predicted by the asymptotic expansion (4.28) that assumes $\Gamma_3 = 0$ is only a rough approximation.

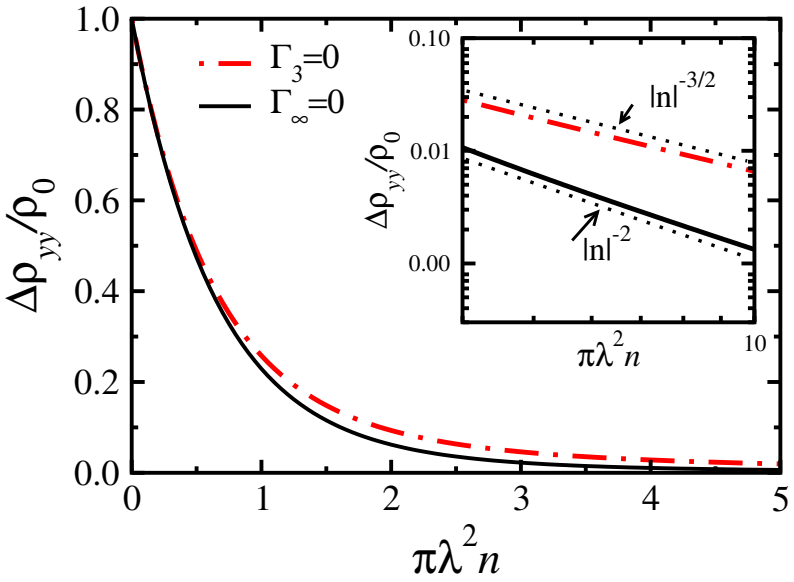

Figure 7: Resistivity $\Delta\rho_{yy}$ in units of $\rho_0 = (\pi\lambda h_{\rm rms}B_\parallel)^2/2\hbar$ due to $\boldsymbol{B}_\parallel$ as a function of $\lambda^2 n$. Inset: The same as in the main plot in log-log scale to illustrate the dependence of $\Delta\rho_{xx}$ on $|n|$.

In general, Γ_3 is a non-vanishing correction to the transport time components, hence $\tau_y^{(1)}/\tau_x^{(1)} \neq 3$. However, for Gaussian ripple height correlations, the ratio $\tau_y^{(1)}/\tau_x^{(1)}$ is a function only of λk_F.

Figure 8 shows $\tau_y^{(1)}/\tau_x^{(1)}$ versus $\lambda^2 n$. It illustrates the importance of Γ_3 in the calculation of the conductivity corrections. We find that by increasing the carrier concentration the anisotropic conductivity is considerably favored.

The transport properties predicted by Eq. (4.27) are only slightly modified for the case of exponential ripple heigh correlations, $\langle h(0)h(\boldsymbol{r})\rangle = h_{\rm rms}^2 e^{-r/\lambda}$: For $\lambda|n|^{1/2} \gg 1$, the resistivity tensor given by Eq. (4.28) is multiplied [65] by a prefactor of order of unity times $\log(\lambda^2|n|)$.

4.1.2 Effect of strain fields

Let us now consider the effect of the pseudo-magnetic fields due to strain, $B_{\rm int}$, in the conductivity of monolayer graphene sheets. In contrast to the mechanism discussed above, $B_{\rm int}(\boldsymbol{r})$ is solely determined by $h(\boldsymbol{r})$ and the material properties. Hence, it is intrinsic to any graphene sample with disordered ripples.

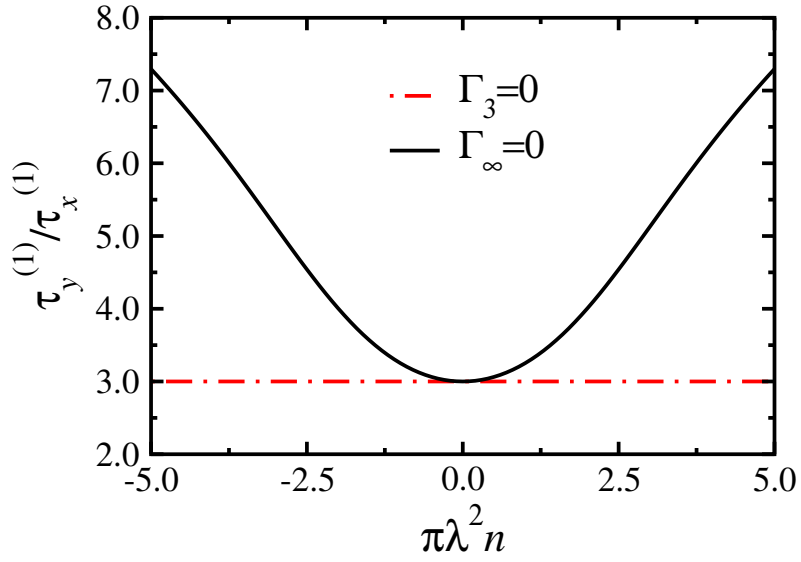

Figure 8: Ratio $\tau_y^{(1)}/\tau_x^{(1)}$ as a function of $\pi\lambda^2 n$. For $\pi\lambda^2 n < 5.0$, the limit $\overline{m} \to \infty$ is attained within 10^{-4} accuracy for $\overline{m} = 13$.

We use Eq. (3.18) to calculate the vector transport time $\boldsymbol{\tau}$ for the intrinsic effective vector potential due to strain. For the K-valley $V_{\rm int}$ reads

$$V_{\rm int}(\boldsymbol{r}) = \hbar v_F \frac{\beta\kappa}{a}\Big\{ \left[u_{xx}(\boldsymbol{r}) - u_{yy}(\boldsymbol{r})\right]\sigma_x - 2u_{xy}(\boldsymbol{r})\sigma_y \Big\}. \tag{4.29}$$

In contrast with the previous subsection, here it is difficult to make quantitative progress without assuming a specific form for the ripple height correlation function. The qualitative behavior of the conductivity corrections due to strain that has been reported in the literature [31] is not sufficient for the analysis we propose.

As in Sec. 3.1.2, we calculate $\langle u_{ij}(\boldsymbol{r}) u_{i'j'}(\boldsymbol{r}')\rangle$ by assuming Gaussian correlated ripple height fluctuations, $C_h(q) = 2\pi\lambda^2 h_{\rm rms}^2 e^{-\lambda^2 q^2/2}$. After some lengthy but straightforward algebra, we obtain

$$\langle |\langle \boldsymbol{k}' s|V_{\rm int}|\boldsymbol{k}s\rangle|^2\rangle = \frac{v_F^2\hbar^2\beta^2\kappa^2}{32a^2}\frac{\pi h_{\rm rms}^4}{\lambda^2\mathcal{A}}\left\{16 + \lambda^4 q^4 \cos^2\left[\frac{3}{2}(\theta+\theta')\right]\right\} e^{-\lambda^2 q^2/4}.$$

Using Eq. (4.8) we arrive at

$$\mathcal{W}(q,\varphi) = \mathcal{W}_{\rm int}\left[16 + \frac{\lambda^4 q^4}{2}(1+\cos 6\varphi)\right] e^{-\lambda^2 q^2/4}, \tag{4.30}$$

where

$$\mathcal{W}_{\rm int} = \frac{\beta^2\kappa^2|\varepsilon_F|}{64a^2\hbar}\frac{h_{\rm rms}^4}{\lambda^2}. \tag{4.31}$$

(The notation is the same as that of the previous section.)

The only non-zero Fourier components of $\mathcal{W}(q,\varphi)$ are

$$\begin{aligned}\mathcal{W}_0(q) &= \mathcal{W}_{\rm int}\left(16+\frac{\lambda^4 q^4}{2}\right)e^{-\lambda^2 q^2/4} \quad \text{and}\\ \mathcal{W}_3(q) &= \mathcal{W}_{\rm int}\frac{\lambda^4 q^4}{2}e^{-\lambda^2 q^2/4}.\end{aligned} \tag{4.32}$$

In this case, the $M^{\pm}$ matrix reads[38]

$$M^{\pm}=\begin{pmatrix} J_{0,1} & 0 & \mp\frac{1}{2}J_{3,2} & -\frac{1}{2}J_{3,4} & \cdots\\ 0 & J_{0,3}\mp\frac{1}{2}J_{3,0} & 0 & 0 & \cdots\\ \mp\frac{1}{2}J_{3,2} & 0 & J_{0,5} & 0 & \cdots\\ -\frac{1}{2}J_{3,4} & 0 & 0 & J_{0,7} & \cdots\\ \vdots & \vdots & \vdots & \vdots & \ddots \end{pmatrix}, \tag{4.33}$$

and the inverse transport time components are given by

$$\frac{1}{\tau^{(1)}_{x/y}} = J_{0,1}-\frac{(J_{3,2})^2}{4J_{0,5}}-\frac{(J_{3,4})^2}{4J_{0,7}}+\cdots. \tag{4.34}$$

Since $\tau^{(1)}_x=\tau^{(1)}_y$, the conductivity corrections due to the strain field are isotropic. This result seems to be at odds with the fact that the pseudo-magnetic field autocorrelation function $\langle B_{\rm int}(\boldsymbol{r})B_{\rm int}(\boldsymbol{r}')\rangle$ clearly shows an hexagonal symmetry, as illustrated by Fig. 6b. As shown by Tokura [38], using general arguments, this is a false paradox: The conductivity tensor becomes anisotropic only for scattering processes characterized by a single symmetry axis, like in the $B_\parallel$ case, analyzed in the previous subsection.

Assuming that $J_{0,1}$ vastly dominates the sum in Eq. (4.34), we obtain

$$\frac{1}{\tau^{(1)}_{x/y}} = \mathcal{W}_{\rm int}\pi e^{-\lambda^2 k_F^2/2}\Big[(32+8\lambda^2k_F^2+16\lambda^4k_F^4)I_0(\lambda^2k_F^2/2)-(64+24\lambda^2k_F^2+16\lambda^4k_F^4)I_1(\lambda^2k_F^2/2)\Big], \tag{4.35}$$

where I_0 and I_1 are modified Bessel functions of the first kind.

In the limit of $\lambda k_F \gg 1$, we write

$$\Delta\sigma_{xx}=\Delta\sigma_{yy}\approx\frac{e^2}{h}\frac{32\pi}{23\beta^2\kappa^2}\frac{\lambda^2a^2}{h_{\rm rms}^4}\lambda^3|n|^{3/2}. \tag{4.36}$$

The above asymptotic expansion for $\Delta\sigma$ helps us to develop some insight on the relevant parameters, but is not accurate for the current experimental situations of interest. As expected the strain corrections to the conductivity depend on material parameters, and are a non-trivial function of λ, $h_{\rm rms}$, and $|n|$. Since these corrections are small compared to

other disorder effects, they are difficult to be noticed in standard transport experiments. This situation changes if we consider the combined effect of intrinsic and extrinsic random magnetic fields, as we discuss in the next section.

4.1.3 Combined effect of extrinsic and intrinsic random magnetic fields

We conclude this chapter by analyzing the combined effect of both previously discussed sources of random magnetic field disorder. As before, we assume that the system transport properties are dominated by other scattering processes, with a corresponding (isotropic) transport time $\tau_{\rm s}$.

It is customary to use Matthiessen's rule when dealing with systems characterized by different competing relaxation time mechanisms. In our case, Matthiessen's rule translates into adding the inverse transport times given by Eqs. (4.24) and (4.34), namely

$$\frac{1}{\tau^{(1)}_{x/y}} = \frac{2\pm 1}{2} J^{\rm ext}_{0,1} - \Gamma^{\rm ext}_3 + J^{\rm int}_{0,1} - \frac{(J^{\rm int}_{3,2})^2}{4J^{\rm int}_{0,5}} - \frac{(J^{\rm int}_{3,4})^2}{4J^{\rm int}_{0,7}} + \cdots . \tag{4.37}$$

This naive approach was shown to be inaccurate when dealing with anisotropic potentials[38].

We analyze the combined effect of intrinsic and extrinsic random magnetic fields by considering an effective M-matrix given by

$$M^{\pm}_{\rm tot} = M^{\pm}_{\rm ext} + M^{\pm}_{\rm int}, \tag{4.38}$$

where $M^{\pm}_{\rm ext}$ and $M^{\pm}_{\rm int}$ are given by Eqs. (4.23) and (4.33) respectively.

The $\boldsymbol{\tau}$ components are

$$\tau^{(1)}_x = [(M^-_{\rm tot})^{-1}]_{11} \quad \text{and} \quad \tau^{(1)}_y = [(M^+_{\rm tot})^{-1}]_{11}, \tag{4.39}$$

that, for $\overline{m} = 5$, explicitly read

$$\begin{aligned}\frac{1}{\tau^{(1)}_{x/y}} \;=\; & (1\pm\frac{1}{2})J^{\rm ext}_{0,1} + J^{\rm int}_{0,1} + \frac{1}{(J^{\rm ext}_{0,3}+J^{\rm int}_{0,3}\mp J^{\rm int}_{3,0}/2)(J^{\rm ext}_{0,5}+J^{\rm int}_{0,5}) - (J^{\rm ext}_{1,4})^2/4} \\ & \left[-\frac{1}{4}(J^{\rm ext}_{0,5}+J^{\rm int}_{0,5})(J^{\rm ext}_{1,2})^2 \mp\frac{1}{4}J^{\rm int}_{3,2}J^{\rm ext}_{1,2}J^{\rm ext}_{1,4} - \frac{1}{4}(J^{\rm int}_{3,2})^2(J^{\rm ext}_{0,3}+J^{\rm int}_{0,3}\mp\frac{1}{2}J^{\rm int}_{3,0})\right] + \cdots\end{aligned} \tag{4.40}$$

This result is clearly different from Eq. (4.37), since it mixes intrinsic and extrinsic effects. Let us now discuss the dependence of $\boldsymbol{\tau}$ on $B_\parallel, \lambda, h_{\rm rms}$, and n. For that purpose we

numerically invert the matrix $M^{\pm}_{\rm tot}$, at order $\overline{m} \approx 30 - 50$ to guarantees an accuracy of 10^{-5} for the analyzed parameter range.

The resistivity corrections obtained from the Matthiessen's rule, Eq. (4.37) depend quadratically on $B_{\parallel}$, in line with the experiment [41]. However, the full M-matrix analysis does not guarantee this simple dependence. In Fig. 9 we plot the resistivity correction $\Delta\rho_{yy}$ calculated using the full M-matrix and compare it with the one obtained from the Matthiessen rule, given by Eq. (4.37), for realistic values of $h_{\rm rms}$, λ, and n. The full M-matrix calculation (indicated as "exact") shows an overall higher resistivity than that obtained from the Matthiessen rule. It depends linearly on $B^2_{\parallel}$ for $B_{\parallel} \gtrsim 5$T and deviates from this dependence only when $B_{\parallel}$ becomes small.

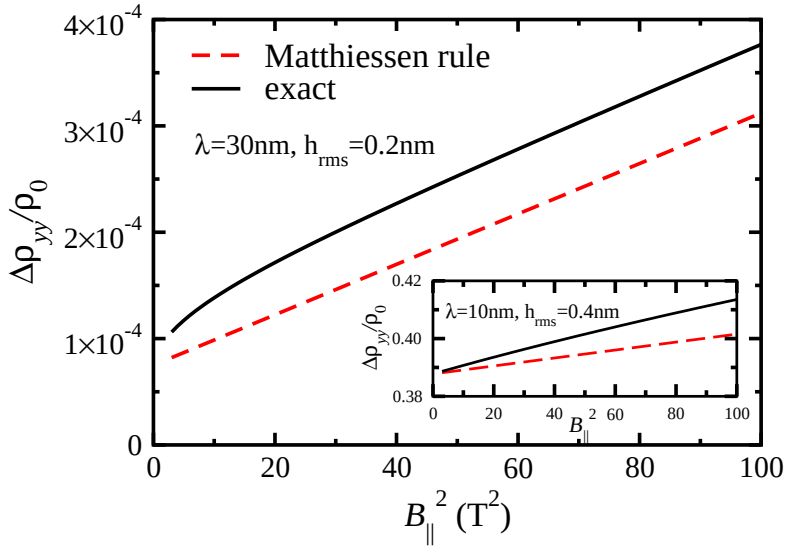

Figure 9: Resistivity correction $\Delta\rho_{yy}$ in units of $\rho_0 = (\pi\lambda h_{\rm rms} B_{\parallel})^2/2\hbar$ as a function of the in-plane magnetic field $B_{\parallel}$ for $h_{\rm rms} = 0.2$ nm, $\lambda = 30$ nm, and $n = 10^{12}\,{\rm cm}^{-2}$. Inset: The same as in the main figure for $h_{\rm rms} = 0.4$ nm and $\lambda = 10$ nm.

In contrast, the dependence of $\Delta\rho$ with $h_{\rm rms}$, λ, and $|n|$ is not trivial. For $h_{\rm rms}$ and λ values taken close to the ones reported by topography experiments [45, 46, 47, 48], a numerical study using the full M-matrix approach gives $\Delta\rho_{yy} \propto \lambda^{-\alpha}$ with $\alpha \approx 3 \cdots 4$, $\Delta\rho_{yy} \propto h^{\beta}_{\rm rms}$ with $\beta \approx 3$, and $\Delta\rho_{yy} \propto |n|^{-\gamma}$ with $\gamma \approx 2$. In summary, $\Delta\rho$ is very sensitive on small variations of $h_{\rm rms}$ and λ.

In Fig. 10 we compare Eqs. (4.24), (4.37), and (4.40) to gain insight on how the strain mechanism affects the ratio $\tau^{(1)}_y/\tau^{(1)}_x$. We find that the strain fields contribute to a strong suppression of the anisotropy in the transport time due to a strong $B_{\parallel}$. However, for realistic parameter values the anisotropy is still very large and of the order of $\tau^{(1)}_y/\tau^{(1)}_x \approx 10$

for $|n| \approx 10^{12}$ cm^{-2}.

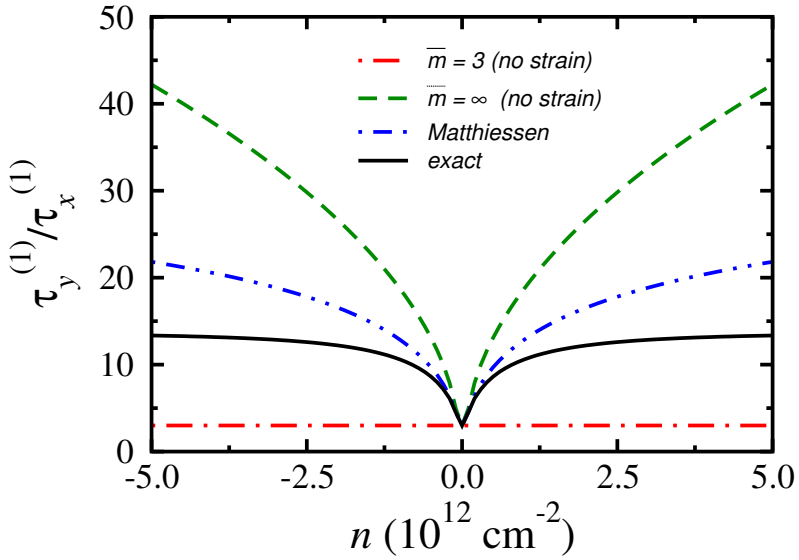

Figure 10: Anisotropy $\tau_y^{(1)}/\tau_x^{(1)}$ as a function of the carrier concentration n using different approximation schemes, for $h_{\rm rms} = 0.2$ nm, $\lambda = 30$ nm, and $B_\parallel = 8$ T. The red and green lines stand for the contribution of $B_\parallel$ without accounting for strain fields. The blue line represents the contributions of both external and strain fields using the conventional Matthiessen's rule. The black line stands for the combined effect of intrinsic and extrinsic fields obtained for the full M-matrix analysis.

In order to further compare our results with the experiment[41], let us introduce the magnetoresistance $\Delta\rho = \boldsymbol{E}\cdot\boldsymbol{j}/j^2$, where $j_x = j\cos\xi$, $j_y = j\sin\xi$, and ξ is the angle between $\boldsymbol{B}_\parallel$ and $\boldsymbol{j}$. Using the relation $E_i = \rho_{ij}J_j$ one writes [66]

$$\Delta\rho(\xi) = \Delta\rho_{xx}\cos^2\xi + \Delta\rho_{yy}\sin^2\xi. \tag{4.41}$$

Ref. [41] reports $\Delta\rho(70^{\rm o})/\Delta\rho(20^{\rm o}) \approx 0.13 - 0.26$. Using λ and $h_{\rm rms}$ values obtained from AFM measurements, we obtain $\tau_y^{(1)}/\tau_x^{(1)} \approx 10$ for $n = 10^{12}$ cm^{-2}. This ratio leads to $\Delta\rho(70^{\rm o})/\Delta\rho(20^{\rm o}) \approx 0.2$ in good agreement with the experiment [41].

4.2 Conclusions

In this chapter we studied the effect of random magnetic fields on the transport properties of a rippled graphene flake. We used the Boltzmann equation, adapted to the case of anisotropic disorder [38], to address the case of an external magnetic field applied in-plane, the effect of intrinsic strain fields caused by the graphene corrugation, as well as the combination of both.

We find that an external in-plane magnetic field $B_\parallel$ gives rise to very anisotropic conductivity corrections. By neglecting the effect of strain fields and using a parametrization of the ripple disorder that is consistent with experiments, we find conductivity corrections that scale with $B_\parallel^2$ and $|n|^{-2}$, consistent with Ref. [41]. In contrast, we obtain $\tau_y^{(1)}/\tau_x^{(1)}$ ratios as large as $20 \cdots 30$.

Random gauge fields due to ripples give a small *isotropic* contribution to the electron momentum relaxation in graphene. We find, however, that their effect cannot be neglected in the analysis of the conductivity in the presence of a large $B_\parallel$. We also concluded that, due to the anisotropic nature of the problem, the Matthiessen's rule is not accurate to address both intrinsic and extrinsic random fields at the same footing. For that purpose we have to invert the total M-matrix.

This approach allows us to successfully describe the corrections to the Drude conductivity reported in the experiment [41] using typical λ and $h_{\rm rms}$ parameters taken from the AMF literature. In addition, we also obtain a suppression of the resistivity anisotropy (with respect to the case where strain is neglected) that is consistent with Ref. [41]. We believe that the anisotropic nature of the random magnetic-field disorder also significantly changes the quantum correction to the conductivity with respect to the isotropic results and deserves further investigation.

Our results suggest that the investigation of anisotropy corrections to the Drude conductivity can be a new and insightful path to experimentally quantify effects of random pseudo-magnetic fields due to strain.

5 Weiss Oscillations

When a 2DEG is subjected to an electrical modulation and to a perpendicular magnetic field a kind of oscillatory behavior, called Weiss oscillations [6, 7], appears in the conductivity for low magnetic fields. These oscillations are periodic with inverse magnetic field, as in the case of Shubnikov de Hass (SdH)[67, 68] oscillations which show up and dominate for higher magnetic fields. Semi-classically, Weiss oscillation can be explained as a consequence of the commensurability between the cyclotron ratio of the electrons at the Fermi energy and the period of the modulation. This oscillations were theoretically studied by many authors from a quantum mechanical point of view [69, 70, 71, 72, 7, 73] and from a classical point of view for isotropic relaxation time [74] and for anisotropic relaxation time [75]. In these 2DEG systems, a periodic potential can be achieved by two interfering laser beams[6, 7] or by depositing an array of parallel metallic strips on the surface[69].

In this chapter we study Weiss oscillations in graphene due to uniaxial strain. The source of modulated electric and magnetic potential is the deformation of the sheet.

5.1 Theoretical background

Our model Hamiltonian reads

$$H = H_0 + H', \tag{5.1}$$

where H_0 accounts for the dynamics of low-energy electrons in graphene monolayers under a uniform external magnetic field and H' is the effective Hamiltonian due to the modulated deformation of the graphene sheet.
In the presence of an external applied magnetic field, the effective Hamiltonian for low

energy electrons in graphene reads [40, 76]

$$H_0 = v_F \boldsymbol{\sigma} \cdot (\boldsymbol{p} + e\boldsymbol{A}_{\text{ext}}), \tag{5.2}$$

where $v_F \approx 10^6$m/s is the Fermi velocity and $\boldsymbol{\sigma} = (\sigma_x, \sigma_y)$ are Pauli matrices in the lattice subspace [40].

For a uniform magnetic field perpendicular to the graphene plane, $\boldsymbol{B}_{\text{ext}} = B_\perp \hat{\mathbf{z}}$, the vector potential can be written in the Landau gauge

$$\boldsymbol{A}_{\text{ext}} = B_\perp[(1-\alpha)y\hat{\boldsymbol{x}} + \alpha x\hat{\boldsymbol{y}}]. \tag{5.3}$$

We postpone the discussion of the most convenient choice of α to the next section.

In what follows we obtain the effective perturbation Hamiltonian H' that describes the effects of strain due to a periodic out of plane deformation of the graphene sheet given by

$$h(x) = h_0 \cos(2\pi x/\lambda), \tag{5.4}$$

where λ is the modulation period.

5.1.1 Strain induced magnetic and electric fields

As explained in chapter 2, strain modifies the graphene inter-atomic distances and changes its electronic properties, and this can be accounted for by a term in the Hamiltonian given by

$$H' = ev_F \boldsymbol{\sigma} \cdot \boldsymbol{A} \tag{5.5}$$

where

$$\mathbf{A}(\theta) = \frac{\hbar\beta_{\text{G}}\kappa}{ae} \begin{pmatrix} \frac{u_{xx}-u_{yy}}{2}\cos 3\theta + u_{xy}\sin 3\theta \\ \frac{u_{xx}-u_{yy}}{2}\sin 3\theta - u_{xy}\cos 3\theta \end{pmatrix} \tag{5.6}$$

In addition to the pseudo vector potential, strain also induces a scalar potential [77, 78, 79] given by

$$V(\boldsymbol{r}) = g[u_{xx}(\boldsymbol{r}) + u_{yy}(\boldsymbol{r})]I \tag{5.7}$$

where I is the identity matrix in sublattice space and $g \approx 4$ eV [80]. For a periodic modulation in one direction, such as $h(x)$ given by Eq. (5.4) the minimization of the elastic energy (see chapter 2) leads to a relaxed configuration where the strain tensor components are negligibly small [34]. Such analysis does not account for the fact that, in general, the graphene sheet is pinned to the substrate at random positions [34] that in-

troduce non trivial minimization constraints. In this study we consider quenched ripples, setting $u_x(\boldsymbol{r}) = u_y(\boldsymbol{r}) = 0$. Hence, we present an upper bound for the strain fields and for the corresponding vector gauge potential.

The strain tensor corresponding to $h(x)$ of Eq.(5.4) reads

$$\begin{aligned} u_{xx}(x) &= 2\pi^2 \left(\frac{h_0}{\lambda}\right)^2 \sin^2(2\pi x/\lambda), \\ u_{yy}(x) &= u_{xy}(x) = 0. \end{aligned} \tag{5.8}$$

Hence, the pseudo vector potential reads

$$\mathbf{A}(\theta) = A_0 \sin^2(2\pi x/\lambda) \begin{pmatrix} \cos 3\theta \\ \sin 3\theta \end{pmatrix}, \tag{5.9}$$

where

$$A_0 = \frac{\hbar \beta_{\mathrm{G}} \pi^2 \kappa}{ae} \left(\frac{h_0}{\lambda}\right)^2. \tag{5.10}$$

The pseudo scalar potential is given by

$$V(x) = V_0 \sin^2(2\pi x/\lambda), \tag{5.11}$$

with

$$V_0 = 2g\pi^2 \left(\frac{h_0}{\lambda}\right)^2. \tag{5.12}$$

We finish this section pointing out that the electrons of the substrate can screen $V(x)$ and significantly quench the pseudo scalar potential [81]. Screening modifies the coupling g as

$$g \to \frac{g}{\epsilon(\boldsymbol{q}, \omega \to 0)}, \tag{5.13}$$

where

$$\frac{1}{\epsilon(\boldsymbol{q}, \omega)} = 1 + v(\boldsymbol{q}) \Pi^R(\boldsymbol{q}, \omega), \tag{5.14}$$

is $\epsilon(\boldsymbol{q}, \omega)$ the dynamical dielectric function, $v(\boldsymbol{q}) = 2\pi e^2/\epsilon_0 |\boldsymbol{q}|$ the Coulomb interaction with ϵ_0 being the substrate dielectric constant, and $\Pi^R(\boldsymbol{q}, \omega)$ is the retarded density-density correlation function. Within the random phase approximation (RPA) the dielectric function can be expressed as $\epsilon(\boldsymbol{q}, \omega) = 1 - v(\boldsymbol{q}) \chi^0(\boldsymbol{q}, \omega)$, where $\chi^0(\boldsymbol{q}, \omega)$ is the pair bubble diagram. This function was already calculated in Ref. [82]. Explicitly the static

dielectric function reads:

$$\epsilon(\boldsymbol{q},0)=\begin{cases}1+v(\boldsymbol{q})\rho(E_F), & q\leq 2k_F,\\ 1+v(\boldsymbol{q})\rho(E_F)\left[1-\frac{1}{2}\sqrt{1-\left(\frac{2k_F}{q}\right)^2}-\frac{q}{4k_F}\arcsin\left(\frac{2k_F}{q}\right)+\frac{\pi q}{8k_F}\right], & q>2k_F.\end{cases} \tag{5.15}$$

where $\rho(E_F)$ is the density of states at the Fermi energy. We have checked that $\epsilon(\boldsymbol{q},0)\geqslant 40$ for SiO_2, suggesting a strong suppression of the pseudo electric field.

5.1.2 External in-plane magnetic field

A modulated magnetic field can also be realized by applying an external magnetic field parallel to a grated patterned graphene sheet. The external magnetic field has a component perpendicular to the graphene surface profile given by [33]

$$B'(\boldsymbol{r})=-\boldsymbol{B}_{\parallel}\cdot\hat{\boldsymbol{n}}(\boldsymbol{r}). \tag{5.16}$$

The normal vector to the surface $z=h(\boldsymbol{r})$ is

$$\hat{\boldsymbol{n}}(\boldsymbol{r})=\frac{1}{\sqrt{1+(\partial h/\partial x)^2+(\partial h/\partial y)^2}}\begin{pmatrix}\partial h(\boldsymbol{r})/\partial x\\ \partial h(\boldsymbol{r})/\partial y\\ -1\end{pmatrix}. \tag{5.17}$$

Since $h_0\ll\lambda$, we write

$$\hat{\boldsymbol{n}}(\boldsymbol{r})\approx(\partial h(\boldsymbol{r})/\partial x,\partial h(\boldsymbol{r})/\partial y,-1)^T. \tag{5.18}$$

Hence, the effective local perpendicular magnetic field reads

$$B_{\text{ext}}(\boldsymbol{r})=-\boldsymbol{B}_{\parallel}\cdot\boldsymbol{\nabla}h(\boldsymbol{r}), \tag{5.19}$$

and for $\boldsymbol{B}_{\parallel}=B_{\parallel}\hat{\boldsymbol{x}}$ is expressed in a convenient gauge, by the vector potential

$$A_x(\boldsymbol{r})=0\quad\text{and}\quad A_y(\boldsymbol{r})=-A_{\parallel}\cos(2\pi x/\lambda)\,. \tag{5.20}$$

with $A_{\parallel}=B_{\parallel}h_0$. The perturbation term is given by

$$V_{\text{ext}}(\boldsymbol{r})=v_F e\sigma_y A_y(\boldsymbol{r})=-v_F eA_{\parallel}\cos(2\pi x/\lambda)\sigma_y. \tag{5.21}$$

5.2 Weiss oscillations in graphene

In this section we briefly review the calculations of the Weiss oscillations for modulated magnetic [83] and electric [84] fields, adapting the results to the vector and scalar fields obtained in the previous section.

We study the corrections to the conductivity caused by the modulated strain restricting ourselves to the regime where the latter correspond to small perturbation to the electronic spectrum. In this case, an analytical expression for the Weiss conductivity oscillations can be obtained following the approach put forward in Refs. [69, 70, 71].

The scalar potential of Eq. (5.11) breaks the translational invariance along the x-axis. Hence, it is convenient to solve the unperturbed Hamiltonian H_0 in the Landau gauge with $\alpha = 1$. Hence, the Schrödinger equation $H_0\Psi(\boldsymbol{r}) = E\Psi(\boldsymbol{r})$ has eigenvalues [85, 40, 76]

$$E_n = \mathrm{sgn}(n)\frac{v_F\hbar}{l_B}\sqrt{2|n|}, \tag{5.22}$$

with

$$\mathrm{sgn}(n) = \begin{cases} 1 & n > 0, \\ 0 & n = 0, \\ -1 & n < 0. \end{cases} \tag{5.23}$$

The corresponding eigenfunctions are [86]

$$\Psi_{n,k_y}(\boldsymbol{r}) = \frac{C_n}{\sqrt{L_y l_B}} e^{ik_y y} \begin{pmatrix} -i\mathrm{sgn}(n)\Phi_{|n|-1}(\frac{x-x_0}{l_B}) \\ \Phi_{|n|}(\frac{x-x_0}{l_B}) \end{pmatrix}, \tag{5.24}$$

where $l_B = \sqrt{\hbar/eB} \approx (26\,\mathrm{nm})/\sqrt{B(\mathrm{T})}$ is the magnetic length, $x_0 = l_B^2 k_y$ gives the center of the wave function,

$$C_n = \begin{cases} 1 & n = 0, \\ 1/\sqrt{2} & n \neq 0, \end{cases} \tag{5.25}$$

and

$$\Phi_n(x) = \frac{e^{-x^2/2}}{\sqrt{2^n n!\sqrt{\pi}}} H_n(x), \tag{5.26}$$

where $H_n(x)$ are Hermite polynomials.

Starting from the Kubo formula for the conductivity, it has been shown [72] that the main contribution to the Weiss oscillations comes from the diagonal diffusive conductivity,

that in the quasielastic scattering regime can be written as [87]

$$\Delta\sigma_{yy} = g_v g_s \frac{e^2}{L_x L_y} \sum_{\zeta} \left(-\frac{\partial f}{\partial \varepsilon} \right) \Big|_{\varepsilon = E_\zeta} \tau(E_\zeta) v_{\zeta,y} v_{\zeta,y}, \tag{5.27}$$

where g_v and g_s stand for valley and spin degeneracy (for graphene $g_v g_s = 4$), $\zeta = (n, k_y)$ are the quantum numbers of the single-particle electronic states, L_x and L_y are the dimensions of the graphene layer, $f(E_\zeta)$ is the Fermi-Dirac distribution function, $\tau(E_\zeta)$ is the electron relaxation time, and v_y^ζ is the electron velocity given by the semiclassical relation

$$v_{\zeta,y} = \frac{1}{\hbar} \frac{\partial}{\partial k_y} E_{n,k_y}, \tag{5.28}$$

with E_{n,k_y} calculated in first order perturbation theory as

$$E_{n,k_y} = E_n + \langle n, k_y | H' | n, k_y \rangle. \tag{5.29}$$

Note that this correction lifts the degeneracy of Landau levels. The dc diffusive conductivity is then obtained by explicitly summing over the quantum numbers, namely

$$\sum_{\zeta} \big[\cdots \big] = \frac{L_y}{2\pi} \int_0^{L_x/l_B^2} dk_y \sum_{n=0}^{\infty} \big[\cdots \big]. \tag{5.30}$$

5.2.1 Modulated scalar potential

Let us now present the theory for Weiss oscillations for graphene monolayers in a modulated electric field [84]. We highlight the main results that are relevant to our analysis, deferring the details of the derivation to the original literature [84]. For the scalar potential, the expectation value of the velocity operator

$$v_{\zeta,y}^{\mathrm{s}} = \hbar^{-1} \partial \langle n, k_y | V | n, k_y \rangle / \partial k_y$$

reads

$$v_{\zeta,y}^{\mathrm{s}} = \frac{2\pi V_0 l_B^2}{\hbar \lambda} e^{-u/2} [\mathrm{sgn}^2(n) L_{|n|-1}(u) + L_{|n|}(u)] \sin\left(4\pi \frac{x_0}{\lambda} \right), \tag{5.31}$$

where $u = 8\pi^2 (l_B/\lambda)^2$ and $L_n(u)$ is a Laguerre polynomial.

Inserting the above expression in Eq. (5.27) and using (5.30), $\Delta\sigma_{yy}$ reads

$$\Delta\sigma_{yy}^{\mathrm{s}} \approx \frac{e^2}{h} \frac{V_0^2 \beta \tau}{\hbar} F^{\mathrm{s}}(u, \beta, E_F) \tag{5.32}$$

with

$$F^{\mathrm{s}} = \frac{ue^{-u}}{\beta} \sum_{n=-\infty}^{\infty} \left(-\frac{\partial f}{\partial \varepsilon}\right)\Big|_{\varepsilon=E_n} [(1-\delta_{0,n})L_{|n|-1}(u) + L_{|n|}(u)]^2 \tag{5.33}$$

where $\beta = 1/k_B T$ and we assume a constant relaxation time [1] $\tau = \tau(E_F)$, as well as that $\Delta E_{n,k_y} = |E_{n,ky} - E_n|$ is smaller than the Landau level spacing.

Eq. (5.27) indicates that $\Delta\sigma_{yy}$ is dominated by the Landau levels with energy close to the Fermi energy. In the limit where many Landau levels are filled (for $E_F > 0$) or empty (for $E_F < 0$), it is possible [84] to obtain an analytical expression for $\Delta\sigma^{\mathrm{s}}_{yy}$ by using the asymptotic expression for the Laguerre polynomials

$$e^{-u/2}L_n(u) \xrightarrow{n\gg 1} \frac{1}{\pi^{1/2}(nu)^{1/4}} \cos(2\sqrt{nu} - \pi/4) \tag{5.34}$$

and taking the continuum limit

$$\sum_{n=-\infty}^{\infty} \big[\cdots\big] \approx \left(\frac{l_B}{v_F\hbar}\right)^2 \int_{-\infty}^{\infty} dE E\big[\cdots\big]. \tag{5.35}$$

The latter is obtained using Eq. (5.22). Hence

$$F^s = \frac{1}{\pi^2}\frac{T}{T_*}\cos^2\left(\frac{2\pi}{k_F\lambda}\right)\left[1 + S\left(\frac{T}{T_*}\right)\sin\left(8\pi\frac{k_F l_B^2}{\lambda}\right)\right], \tag{5.36}$$

where

$$S(x) = \frac{x}{\sinh(x)} \quad \text{and} \quad \frac{T}{T_*} = \frac{8\pi^2 l_B^2}{\lambda v_F \hbar\beta}. \tag{5.37}$$

5.2.2 Modulated vector potential

Let us now turn our attention to the magnetic modulations. In the case of the pseudo vector potential, the expectation value of the velocity operator is

$$\begin{aligned} v^{\mathrm{v}}_{\zeta,y} &= A_0 \frac{l_B v_F e}{\hbar}\frac{2}{\sqrt{2}}\cos(2Kx_0) \\ &\times \; e^{-u/2}\mathrm{sgn}(n)\sqrt{|n|+1}[L_{|n|+1}(u) - L_{|n|}(u)]\sin(3\theta), \end{aligned} \tag{5.38}$$

[1] The consequences of a constant relaxation time is to neglect quantum oscillation (see Ref. [73]). Since we are interested in $\rho_{xx} \propto \sigma_{yy}$ which has a classical origin(see Ref. [74, 75]) this is a good approximation in our case.

where $u = 8\pi^2(l_B/\lambda)^2$ and $L_n(u)$ is a Laguerre polynomial. For the external in-plane magnetic field the velocity is

$$v^{\parallel}_{\zeta,y} = A_{\parallel}\frac{l_B v_F e}{\hbar}\frac{2}{\sqrt{2}}\cos(Kx_0)e^{-u/2}\mathrm{sgn}(n)\sqrt{|n|+1}[L_{|n|+1}(u)-L_{|n|}(u)], \quad (5.39)$$

with $u = 2\pi^2(l_B/\lambda)^2$. Note that here the periodicity is different than that for the strain case. Inserting Eq. (5.38) and Eq. (5.39) in Eq. (5.27) and using (5.30), the $\Delta\sigma^{\mathrm{v}}_{yy}$ reads

$$\Delta\sigma^{\mathrm{v}}_{yy} \approx \frac{e^2}{h}\frac{(v_F e A_0)^2\tau\beta}{\hbar}\sin^2(3\theta)\,F^{\mathrm{v}}(u,\beta,E_F) \quad (5.40)$$

with

$$F^{\mathrm{v}} = \frac{4e^{-u}}{\beta}\sum_{n=-\infty}^{\infty}\left(-\frac{\partial f}{\partial\varepsilon}\right)\Big|_{\varepsilon=E_n}(1-\delta_{0,n})(|n|+1)\left[L_{|n|}(u)-L_{|n|+1}(u)\right]^2, \quad (5.41)$$

and a similar relation for the in-plane magnetic field. Following the same strategy as before we obtain

$$F^{\mathrm{v}} = \frac{1}{4\pi^4}(\lambda k_F)^2\left(\frac{T}{T_*}\right)\sin^2\left(\frac{2\pi}{k_F\lambda}\right)\left[1-S\left(\frac{T}{T_*}\right)\sin\left(8\pi\frac{k_F l_B^2}{\lambda}\right)\right], \quad (5.42)$$

where $S(x)$ and T/T_* are defined in Eq. (5.37). The conductivity correction for the case of an external modulated magnetic field i given by

$$\Delta\sigma^{\mathrm{v}}_{yy} \approx \frac{e^2}{h}\frac{(v_F e A_{\parallel})^2\tau\beta}{\hbar}F^{\parallel}(u,\beta,E_F) \quad (5.43)$$

where $F^{\parallel}(u,\beta,E_F)$ is obtained by taking $\lambda\to 2\lambda$ in the expression for $F^{\mathrm{v}}(u,\beta,E_F)$.

5.3 Results and discussion

In this section we discuss the validity range of our results and propose a physical realization of the Weiss oscillation due to strain and a parallel magnetic field in graphene.

The theory discussed in the previous section is based on three main assumptions, namely:

(i)The electronic transport is diffusive and in the semiclassical regime, that justified the calculation of the conductivity using Eq. (5.27). Accordingly, we are addressing disordered graphene samples characterized by an electron momentum relaxation mean free path l_e, where $k_F l_e \gg 1$.

(ii) In the calculation of $\Delta\sigma_{yy}$ we use perturbation theory assuming that the Landau

level spacing at the Fermi energy is much larger than the perturbation correction.

(iii)The analytic results for $\Delta\sigma_{yy}$ rely on the asymptotic expression given by Eq. (5.34). Hence, it requires that the Landau levels close to the Fermi energy have $n \gg 1$, which limits the analytic results to a region of weak fields.

The condition (i) $k_F l_e \gg 1$ can be expressed as $\sqrt{\pi n_e} v_F \tau \gg 1$. For good quality graphene samples, where $l \gtrsim 100\text{nm} \cdots 1000\text{nm}$, $n_e \gtrsim 3 \times 10^9 \cdots 10^7 \text{cm}^{-2}$, a carrier concentration easy to attain in experiments.

The derivative of the Fermi distribution in Eq.(5.36) selects only the Landau levels near the Fermi energy to contribute to the conductivity $\Delta\sigma_{yy}$. This means that the Weiss oscillations are dominated by the LL with

$$n_F \approx \frac{1}{2}\left(\frac{l_B E_F}{\hbar v_F}\right)^2. \tag{5.44}$$

The applicability of perturbation theory (ii) demands that the LL spacing $E_{n+1} - E_n$ is large as compare with the correction ΔE_n given by equation Eq. (5.29). Let us consider the different cases separately. For the scalar potential $E_{n+1} - E_n > \Delta E_n$ leads to

$$n < \frac{1}{32\pi^8}\left(\frac{\lambda}{l_B}\right)^2 \left(\frac{\hbar v_F}{g\lambda}\right)^4 \left(\frac{\lambda}{h_0}\right)^8. \tag{5.45}$$

that at the Fermi energy, reads

$$16\pi^9 \left(\frac{g l_B}{\hbar v_F}\right)^4 n_e < \frac{\lambda^6}{h_0^8}. \tag{5.46}$$

For the case of the modulated magnetic fields, $E_{n+1} - E_n > \Delta E_n$ restricts n to

$$n < \left[\left(\frac{\hbar\pi}{2Ae\lambda}\right)^4 \left(\frac{8\pi^4 l_B^2}{\lambda^2}\right)\right]^{1/3}, \tag{5.47}$$

where $A = A_0$ or $A_\parallel$ for the intrinsic pseudo magnetic or for the external magnetic field, respectively. At the Fermi energy we write for the strain generated gauge field

$$\frac{\pi}{4}\left(\frac{2\beta_G \kappa l_B}{a}\right)^{4/3} n_e < \left[\left(\frac{\lambda^2}{h_0^8}\right)\right]^{1/3}. \tag{5.48}$$

and

$$\frac{\pi}{4}\left(\frac{2eB_\parallel l_B}{\hbar\pi^2}\right)^{4/3} n_e < \left[\left(\frac{1}{h_0^4\lambda^6}\right)\right]^{1/3}, \tag{5.49}$$

for the external parallel magnetic field.

The asymptotic limit addressed in (iii) is the simplest to account for. In Fig.11 we

compare $\Delta\sigma_{yy}$ versus $1/B$ obtained using the analytical expression Eq. (5.42) , with the explicit summation of Eq. (5.41) for the external magnetic field.

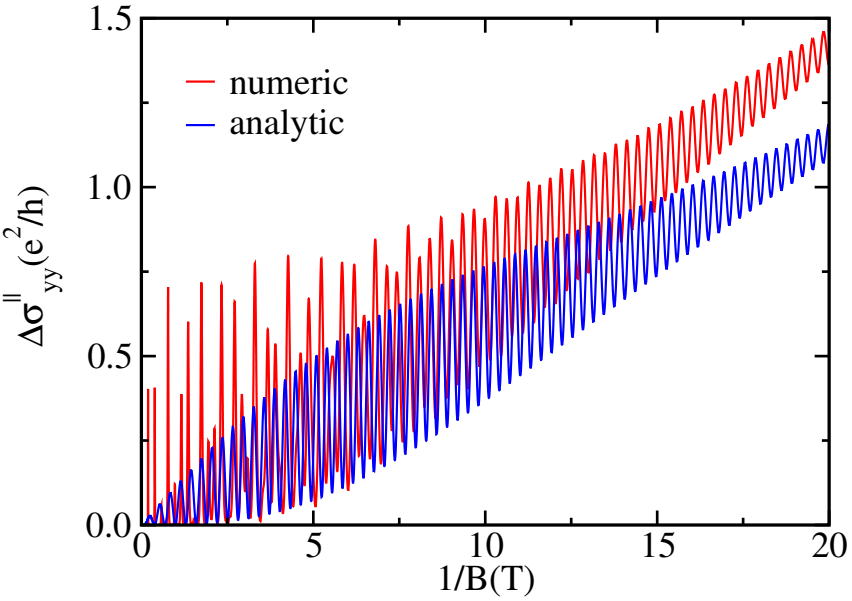

Figure 11: External magnetic field contribution to transversal conductivity $\Delta\sigma^{\parallel}_{yy}$ as a function of $1/B$ for 150 Landau levels. We used an electronic density of $n_e = 5\times10^{11}\text{cm}^{-2}$, $\lambda = 50\text{nm}$, $h_0 = 1.5\text{nm}$, $T = 4\text{K}$ and $\tau = 10^{-13}\text{s}$ and $B_{\parallel} = 1.5\text{T}$.

By decreasing the magnitude of the perpendicular magnetic field the Landau level that crosses the Fermi energy has an increasing n and the agreement between the analytical and the numerical results become increasingly better.

To study the joint effect of the three modulated potentials considered in this paper, we again use Eq. (5.27) with the total velocity

$$v^{\mathrm{T}}_{\zeta,y} = v^{\mathrm{s}}_{\zeta,y} + v^{\mathrm{v}}_{\zeta,y} + v^{\parallel}_{\zeta,y}. \tag{5.50}$$

Following the same steps as before, we write the conductivity as a sum of three independent contributions

$$\sigma^{\mathrm{T}}_{yy} \;=\; \Delta\sigma^{\mathrm{s}}_{yy} + \Delta\sigma^{\mathrm{v}}_{yy} + \Delta\sigma^{\parallel}_{yy}, \tag{5.51}$$

since upon integration the cross terms average to zero. We show the three contributions separately in Fig. 12, rescaling the contribution for the intrinsic modulated potentials since the external modulation dominates. For the sake of definition, we take an average on the lattice orientation in Eq. (5.40). In a experimental realization it is possible to measure the angle θ. The total conductivity is plotted in Fig. 13.

Having stablished that the external parallel magnetic field mechanism dominates the

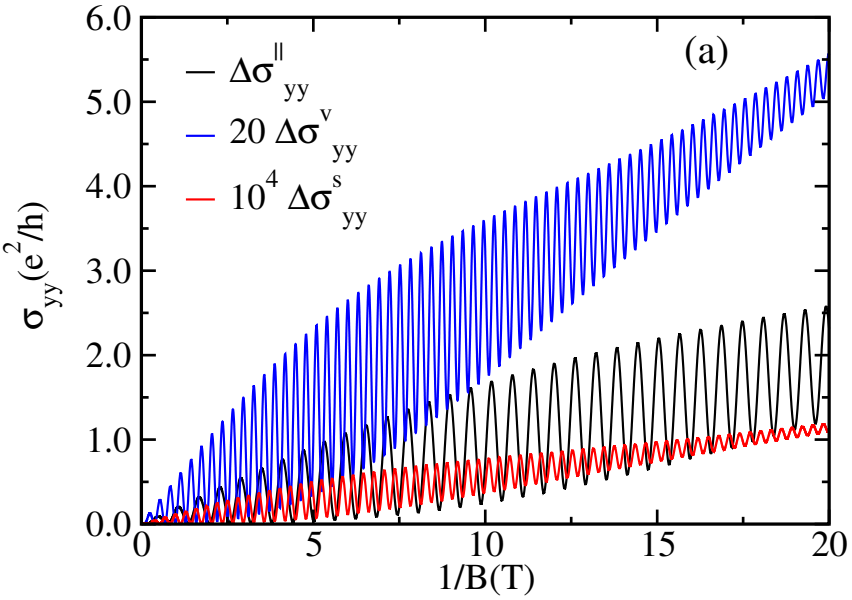

Figure 12: Conductivity as a function of $1/B$ for the external in-plane magnetic field. We used $B_{\parallel} = 8\text{T}$, $\lambda = 100\text{nm}$, $h_0 = 0.5\text{nm}$ and $\tau \approx 10^{-13}\text{s}$.

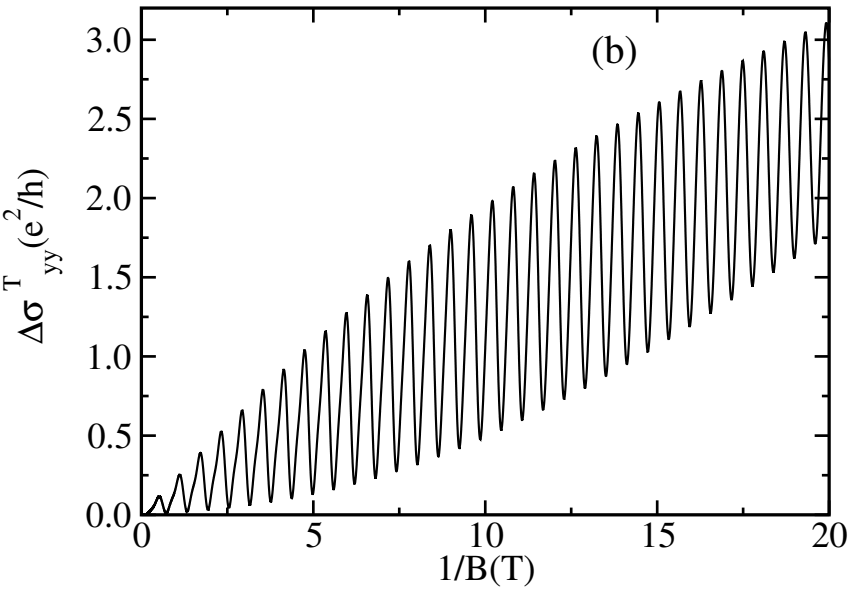

Figure 13: Total transversal conductivity as a function of $1/B$. The parameters used are $B_{\parallel} = 8\text{T}$, $\lambda = 100\text{nm}$, $h_0 = 0.5\text{nm}$, $T = 4\text{K}$ and $\tau = 10^{-13}\text{s}$.

Weiss oscillations we now study the temperature dependence. In Fig. 14 we have used different parameters for which perturbations theory fails for the intrinsic modulations, but works well for the external one. We show here that the effect of temperature is to reduce the amplitude of the oscillations. To see whether or not Weiss oscillations dominates against the Shubnikov de Haas (SdH) we compare the critical temperature for each of them. For Weiss oscillations, one finds form Eq. (5.37)

$$k_B T^{\text{Weiss}} = \left(\frac{\hbar\omega_0}{2\pi^2}\right)\left(\frac{\lambda}{4\sqrt{2}l_B}\right), \tag{5.52}$$

while for the SdH[67, 68]

$$k_B T^{\text{SdH}} = \left(\frac{\hbar\omega_0}{2\pi^2}\right)\left(\frac{1}{\sqrt{2}k_F l_B}\right), \tag{5.53}$$

with $\omega_0 = \sqrt{2}v_F/l_B$. For the parameter we use here $k_B T^{\text{Weiss}}/k_B T^{\text{SdH}} > 1$, consequently we expect the Weiss oscillation to be more robust than SdH with temperature.

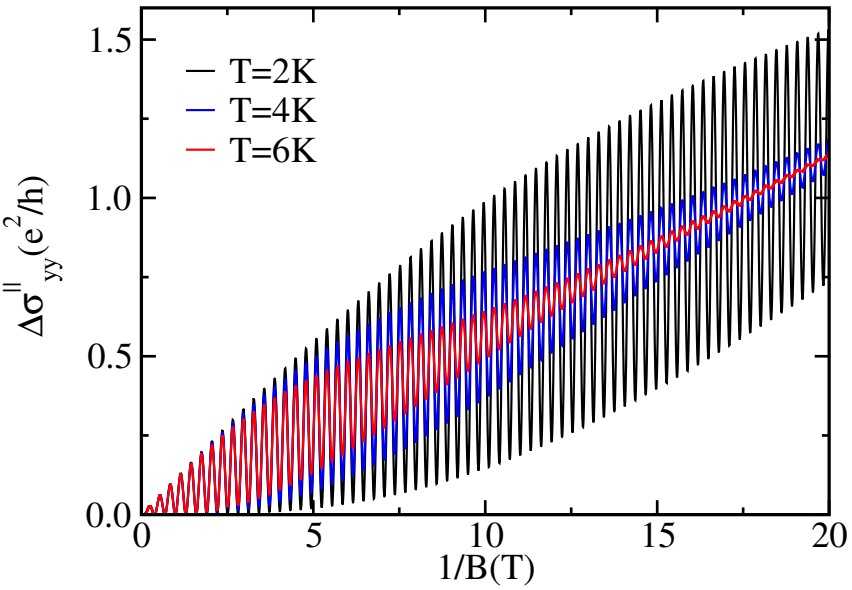

Figure 14: Conductivity as a function of $1/B$ for the external in-plane magnetic field. We used $B_{\parallel} = 1.5\text{T}$, $\lambda = 50\text{nm}$, $h_0 = 1.5\text{nm}$, $T = 4\text{K}$ and $\tau \approx 10^{-13}\text{s}$.

We finish this section making some estimates of the relevant parameters in our theory to establish a link with the semiclassical picture presented in Ref.[74] for 2DEG. For a magnetic field in a range of $2\text{T}^{-1} \leqslant 1/B(\text{T}) \leqslant 10\text{T}^{-1}$ we have $26\text{nm} \leqslant l_B \leqslant 57\text{nm}$. The typical extension of the wave function at high Landau levels is the cyclotron radio, namely $R_c = \sqrt{n}l_B$, which at the Fermi energy reads $R_c = k_F l_B^2/\sqrt{2}$. For the window of magnetic fields we are interested in, $116\text{nm} \leqslant R_c \leqslant 580\text{nm}$. Accordingly to the semiclassical theory, one expects to observe Weiss oscillations only if $R_c \lesssim l_e$, that is, the electron is typically

scattered after completing a cyclotron orbit. Fortunately, this requirement can be fulfilled by the nowadays high mobility graphene samples, that have reported a mean free path of the order of $l_e \gtrsim 1\mu$m [88, 89, 90]. This value will enhance our calculation of the conductivity $\Delta\sigma_{yy}$ by a factor of 10.

To see the commensurability between the cyclotron radio and the modulation, let us consider, for instance, Eq. (5.42) for the magnetic modulation, which is of course out off phase with respect to the scalar modulation. This equation has maximum when

$$2R_c = \frac{1}{2\sqrt{2}}\left(m + \frac{1}{4}\right)\lambda, \quad m = 1, 2, 3, \cdots \tag{5.54}$$

which is quite similar to the case of a 2DEG apart from a factor of $1/2\sqrt{2}$ for the intrinsic magnetic modulation and a factor of $1/\sqrt{2}$ for the external magnetic modulation.

5.4 Conclusions

We have studied how periodic modulation of the substrate profile can give origin to Weiss oscillation in the conductivity in monolayer graphene, both by strain induce pseudofields and by applying a parallel magnetic field. The effect of lattice orientation has also been taken into account. We used first order perturbation theory and a quantum Boltzmann equation in order to find the conductivity. Within this framework, we showed that measurable Weiss oscillation can appear in the transversal conductivity for suitable parameters of the modulation.

We also studied the behavior of Weiss oscillations with temperature. These are damped with increasing temperatures, as in the case of SdH oscillation. We think that, as in the case of 2DEG, Weiss oscillations in graphene are less damped than the SdH ones. This is because the amplitude of SdH oscillations depends on the LL separation as compared with the thermal energy[67, 68], while for Weiss oscillations the relevant energy to be compared with the thermal energy is the difference between flat bands.

Finally, we want to remark that pseudo fields in graphene due to strain has been the subject of many investigations. The aim of this study is to propose and experiment to test the effect of this pseudo field in low magnetic fields, namely through Weiss oscillations.

6 Weak localization corrections in ripples grephene sheets

In this chapter we study the quantum corrections to the Drude-Boltzmann conductivity analysed in chapter 4 [33]. Our focus is on the analysis of the weak localization correction in the presence of a strong in-plane magnetic field. In 2DEG systems, it was shown experimentally and theoretically [91] that an external $B_{\parallel}$ applied in a randomly corrugated interface causes an increase of the dephasing rate. This idea was used by Lundeberg and Folk in the analysis of their weak localization experiment on monolayer graphene sheets [41]. In what follows we adapt the theory of weak localization due to random magnetic field in 2DEG to graphene and reinterpret the experimental results.

6.1 Description of graphene low energy Hamiltonian

When short-range disorder is present in graphene, the two valleys are coupled and a more general spinor description than the one presented in chapter 2 is needed in order to treat them on the same footing. To this end, one writes the low energy Hamiltonian for pristine graphene as

$$\mathcal{H}_0 = v_F \boldsymbol{\Sigma} \cdot \boldsymbol{p}, \tag{6.1}$$

where

$$\Sigma_x = \Pi_z \otimes \sigma_x, \quad \Sigma_y = \Pi_z \otimes \sigma_y, \quad \Sigma_z = \Pi_0 \otimes \sigma_z, \quad \Sigma_0 = I, \tag{6.2}$$

with $\boldsymbol{\Pi}$ acting in the valley space and $\boldsymbol{\sigma}$ acts in the sublattice space and v_F is the Fermi velocity. The Hamiltonian (6.1), in contrast to the $H^{\boldsymbol{K}}$ and $H^{\boldsymbol{K}'}$ presented in chapter 2,

operates in the spinors $\Psi^T = (\Psi_A^{\boldsymbol{K}}, \Psi_B^{\boldsymbol{K}}, \Psi_B^{\boldsymbol{K}'}, \Psi_A^{\boldsymbol{K}'})$. For electrons in the conduction band

$$\begin{aligned}\psi_{\boldsymbol{K}}(\boldsymbol{r}) &= \frac{e^{i\boldsymbol{k}\cdot\boldsymbol{r}}}{\sqrt{2}}\left[e^{i\theta/2}|\boldsymbol{K}-\rangle + e^{-i\theta/2}|\boldsymbol{K}+\rangle\right] \\ &= \frac{e^{i\boldsymbol{k}\cdot\boldsymbol{r}}}{\sqrt{2}}\left[e^{i\theta/2}\begin{pmatrix}0\\1\\0\\0\end{pmatrix} + e^{-i\theta/2}\begin{pmatrix}1\\0\\0\\0\end{pmatrix}\right]. \end{aligned} \tag{6.3}$$

$$\begin{aligned}\psi_{\boldsymbol{K}'}(\boldsymbol{r}) &= \frac{e^{i\boldsymbol{k}\cdot\boldsymbol{r}}}{\sqrt{2}}\left[e^{i\theta/2}|\boldsymbol{K}'-\rangle - e^{-i\theta/2}|\boldsymbol{K}'+\rangle\right] \\ &= \frac{e^{i\boldsymbol{k}\cdot\boldsymbol{r}}}{\sqrt{2}}\left[e^{i\theta/2}\begin{pmatrix}0\\0\\0\\1\end{pmatrix} - e^{-i\theta/2}\begin{pmatrix}0\\0\\1\\0\end{pmatrix}\right]. \end{aligned} \tag{6.4}$$

Here $\langle\boldsymbol{r}|\boldsymbol{K}+\rangle$ represents the wave function of an electron polarized in the sublattice A of the valley $\boldsymbol{K}$ and $\langle\boldsymbol{r}|\boldsymbol{K}-\rangle$ represents the wave function of an electron polarized in the sublattice B of the valley $\boldsymbol{K}$. Note also that

$$I = \sum_{\xi,\alpha} |\xi\alpha\rangle\langle\alpha\xi|, \tag{6.5}$$

with $\xi = \{\boldsymbol{K}, \boldsymbol{K}'\}$ and $\alpha = \{\uparrow, \downarrow\}$ representing valleys and sub-lattice degree of freedom respectively. In order to describe all possible symmetry breaking classes of disorder, we define the matrices

$$\Lambda_x = \Pi_x \otimes \sigma_z, \quad \Lambda_y = \Pi_y \otimes \sigma_z, \quad \Lambda_z = \Pi_z \otimes \sigma_z, \quad \Lambda_0 = I, \tag{6.6}$$

which clearly commute with the Hamiltonian for pristine graphene. Explicitly, these matrices read

$$\Sigma_x = \begin{bmatrix}0 & 1 & 0 & 0\\ 1 & 0 & 0 & 0\\ 0 & 0 & 0 & -1\\ 0 & 0 & -1 & 0\end{bmatrix}, \quad \Sigma_y = \begin{bmatrix}0 & -i & 0 & 0\\ i & 0 & 0 & 0\\ 0 & 0 & 0 & i\\ 0 & 0 & -i & 0\end{bmatrix}, \quad \Sigma_z = \begin{bmatrix}1 & 0 & 0 & 0\\ 0 & -1 & 0 & 0\\ 0 & 0 & 1 & 0\\ 0 & 0 & 0 & -1\end{bmatrix} \tag{6.7}$$

$$\Lambda_x = \begin{bmatrix} 0 & 0 & 1 & 0 \\ 0 & 0 & 0 & -1 \\ 1 & 0 & 0 & 0 \\ 0 & -1 & 0 & 0 \end{bmatrix}, \quad \Lambda_y = \begin{bmatrix} 0 & 0 & -i & 0 \\ 0 & 0 & 0 & i \\ i & 0 & 0 & 0 \\ 0 & -i & 0 & 0 \end{bmatrix}, \quad \Lambda_z = \begin{bmatrix} 1 & 0 & 0 & 0 \\ 0 & 1 & 0 & 0 \\ 0 & 0 & -1 & 0 \\ 0 & 0 & 0 & -1 \end{bmatrix}. \tag{6.8}$$

With these matrices the trigonal warping term discussed in chapter 2 can be written as [56]

$$H_w = -\mu\Sigma_x(\boldsymbol{\Sigma}\cdot\boldsymbol{p})\Lambda_z\Sigma_x(\boldsymbol{\Sigma}\cdot\boldsymbol{p})\Sigma_x, \tag{6.9}$$

and we can write a Hamiltonian for weakly disorder graphene as [56]

$$H = \mathcal{H}_0 + H_w + \hat{I}V(\boldsymbol{r}) + \sum_{s,l=x,y,z}\Sigma_s\Lambda_l V_{s,l}(\boldsymbol{r}). \tag{6.10}$$

Hence, the most general form for a disorder term in the long wave-length limit reads [56].

$$\hat{U} = \sum_{s,l=x,y,z}\Sigma_s\Lambda_l V_{s,l}(\boldsymbol{r}). \tag{6.11}$$

6.2 Drude-Boltzmann conductivity: diagrammatic approach

In order to introduce the diagammatic technique, we derive here the Drude-Boltzmann conductivity within this approach. Let us start considering the free single particle Green's function, namely [56]

$$\mathcal{G}_0(\epsilon,\boldsymbol{p}) = \frac{\epsilon + v_F\boldsymbol{\Sigma}\cdot\boldsymbol{p}}{\epsilon^2 - v_F^2p^2}. \tag{6.12}$$

Assuming that isotropic (diagonal) disorder $\hat{I}u(\hat{\boldsymbol{r}})$ dominates the elastic scattering process and

$$\langle V(\boldsymbol{r})V(\boldsymbol{r}')\rangle = u^2\delta(\boldsymbol{r}-\boldsymbol{r}'), \tag{6.13}$$

we can use Dyson equation

$$\mathcal{G}(\epsilon,\boldsymbol{p}) = \mathcal{G}_0(\epsilon,\boldsymbol{p}) + \mathcal{G}_0(\epsilon,\boldsymbol{p})V\mathcal{G}(\epsilon,\boldsymbol{p}) \tag{6.14}$$

to calculate the single particle disorder averaged Green's function. In the first Born approximation [1] and for $\epsilon_F \gg \hbar/\tau_0$, this reads

$$\langle\mathcal{G}(\epsilon,\boldsymbol{p})\rangle = G(\epsilon,\boldsymbol{p}) = \frac{\bar{\epsilon} + v_F\boldsymbol{\Sigma}\cdot\boldsymbol{p}}{\bar{\epsilon}^2 - v_F^2p^2}, \quad \bar{\epsilon}^{R/A} = \epsilon \pm \frac{1}{2}i\hbar\tau_0^{-1}, \tag{6.15}$$

[1] Here we do not consider crossing terms in the self-energy. See for instance [24].

where $\langle \cdots \rangle$ denotes impurity average and $\pm$ stands for $G^R(\epsilon, \boldsymbol{p})$ or $G^A(\epsilon, \boldsymbol{p})$ respectively. Fig 15 shows the disorder diagrams taken into account to write the self-energy. Here the scattering rate is $1/\tau_0 = \pi\gamma u^2/\hbar$ with $\gamma = p_F/(2\pi\hbar^2 v_F)$.

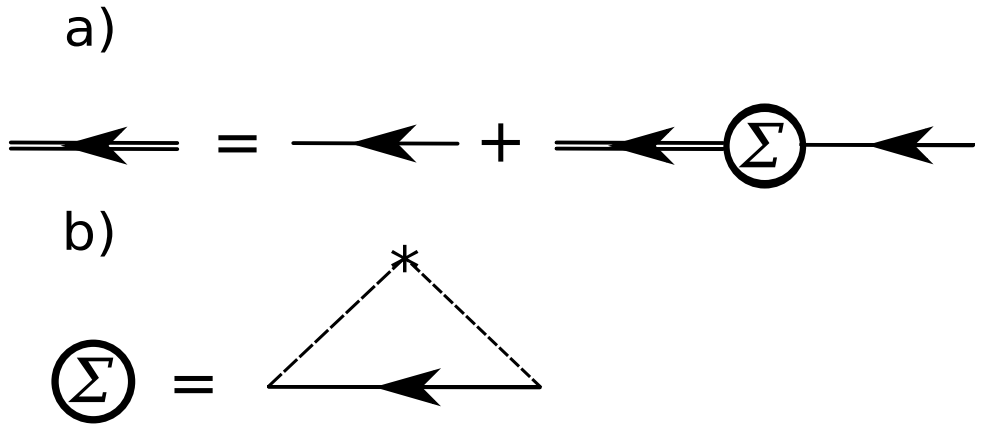

Figure 15: Diagram representing Dyson series. a) single lines represent free electron Green's functions and double lines represet the disorder average Green function. b) Self-energy where dotted lines represent the disorder potential in first born approximation.

The Drude conductivity can be calculated from Kubo's formula, namely

$$g_{jj} = \frac{e^2}{\pi\hbar} \int \frac{d\boldsymbol{p}}{(2\pi)^2} \mathrm{Tr}\left[\tilde{\boldsymbol{v}}_j G^R(\epsilon, \boldsymbol{p}) \hat{\boldsymbol{v}}_j G^A(\epsilon, \boldsymbol{p})\right] \tag{6.16}$$

where $\tilde{\boldsymbol{v}} = 2\hat{\boldsymbol{v}} = 2v_F\boldsymbol{\Sigma}$. The disorder average Kubo conductivity is diagrammatically represented by Fig. 16. By inserting $G^{R/A}$ of Eq.(6.15) in Eq. (6.16) one can show that

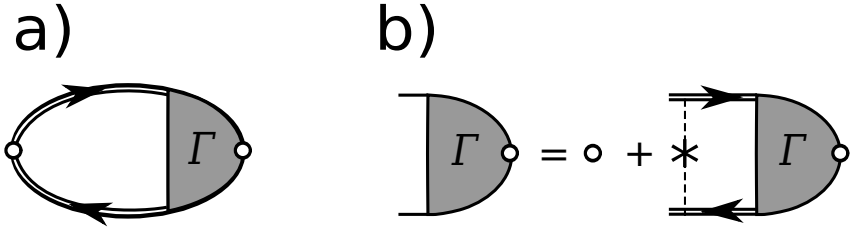

Figure 16: a)Diagrammatic representation of the Green function disorder contraction for the Drude conductivity and b) vertex correction.

$$\mathrm{Tr}\left[\tilde{\boldsymbol{v}}_j G^R(\epsilon, \boldsymbol{p}) \hat{\boldsymbol{v}}_j G^A(\epsilon, \boldsymbol{p})\right] = \frac{2\tau_0 v_F^2}{\hbar}\left[\frac{\frac{1}{2}\hbar\tau_0^{-1}}{(\epsilon + v_F p)^2 + \frac{1}{4}\hbar^2\tau_0^{-2}} + \frac{\frac{1}{2}\hbar\tau_0^{-1}}{(\epsilon - v_F p)^2 + \frac{1}{4}\hbar^2\tau_0^{-2}}\right] \tag{6.17}$$

In the limit of weak impurity scattering, $\hbar/\tau_0 \ll \epsilon_F$, one can use the approximation

$$\frac{\frac{1}{2}\hbar\tau_0^{-1}}{(\epsilon \pm v_F p)^2 + \frac{1}{4}\hbar^2\tau_0^{-2}} \approx \pi\delta(\epsilon_F \pm v_F p), \tag{6.18}$$

that leads to

$$\begin{aligned} g_{xx} &= 4e^2 \left(\frac{p_F}{2\pi\hbar^2 v_F} \right) v_F^2 \tau_0 \\ &= 4e^2 \gamma D, \end{aligned} \tag{6.19}$$

with $\gamma = p_F/(2\pi\hbar^2 v_F)$ and $D = v_F^2 \tau_0$.

6.3 Weak localization corrections due to random gauge fields

Weak localization (WL) is a quantum correction to the conductivity which arises from the interference of electronic pairs of paths related by time reversal symmetry, as sketched in Fig. 17. In the weak disorder limit, $k_F l_e \gg 1$, we associate a path to the electron from one point to another and give a probability amplitude for each path. Within the

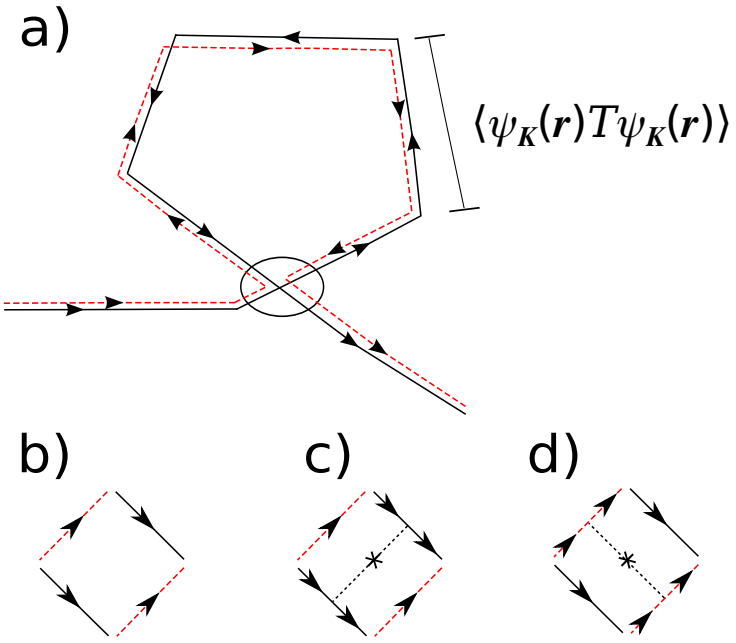

Figure 17: Sketch of weak localization correction to the conductivity. a) semiclassical interpretation b) bare Hikami box c) and d) dressed Hikami boxes.

representation we are using here, the time-reversal operator is $\hat{T} = (\Pi_x \otimes \sigma_x)\mathcal{C}_\theta$, where $\mathcal{C}_\theta$ a complex conjugate operator. Now take the correlation between a wave function in one valley for a ballistic segment of a close loop and its time reversal partner in Fig. (17), namely

$$\langle \psi_{\boldsymbol{K}}(\boldsymbol{r}) \hat{T} \psi_{\boldsymbol{K}}(\boldsymbol{r}) \rangle \propto |\boldsymbol{K}-\rangle |\boldsymbol{K}'+\rangle - |\boldsymbol{K}+\rangle |\boldsymbol{K}'-\rangle, \tag{6.20}$$

where $\langle \cdots \rangle$ means angular average. The WL correction can be expressed in terms of a quantity called Cooperon (see below), which is proportional to this correlation function, as depicted in Fig. 17. This preliminary analysis considered in Ref. [56] suggests that only singlet isospin[2] modes contribute to the conductivity. In fact, in Ref. [56] this correction was found to be (represented diagrammatically in Fig. 18)

$$\delta g_{\mathrm{WL}} = \frac{2e^2 D}{\pi\hbar} \int \frac{d^2q}{(2\pi)^2} [C_0^x + C_0^y + C_0^z - C_0^0], \tag{6.21}$$

where C_0^0 represents singlet channel in the iso/pseudospin degree of freedom and $C_0^{x,y,z}$, singlet channel in isospin and triplet channel in pseudospin degree of freedom [56].

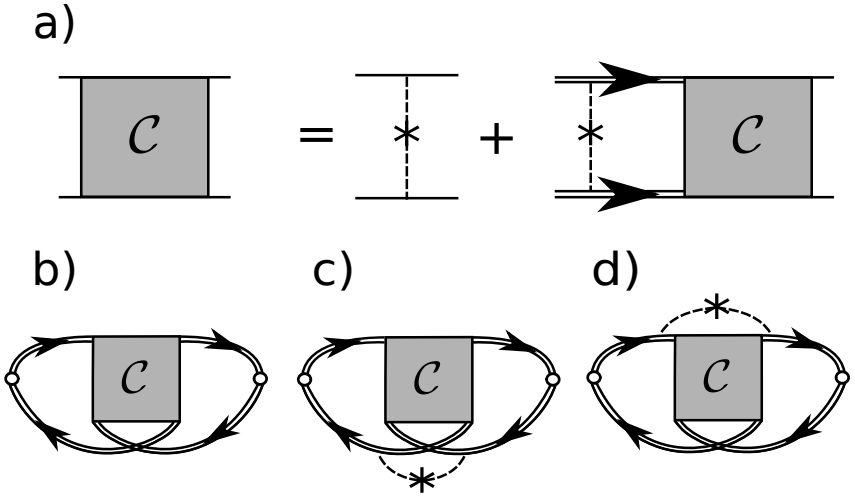

Figure 18: Diagrammatic representation of weak localization correction to the Drude conductivity. a) the cooperon b) weak localization correction with bare Hikami box c) and d) weak localization correction with dressed Hikami boxes.

The equation for the Cooperon channels is [56]

$$[D(i\nabla - \frac{2e}{\hbar}\boldsymbol{A})^2 + \Gamma_0^l + \tau_\phi^{-1} - i\omega] C_0^l(\boldsymbol{r}, \boldsymbol{r}') = \delta(\boldsymbol{r} - \boldsymbol{r}'), \tag{6.22}$$

where $\boldsymbol{A}$ represents a gauge field for an external perpendicular magnetic field, Γ_0^l represents relaxation rates for different sources of disorder that suppress the different channels [56] and τ_ϕ^{-1} is a dephasing time, namely a time that destroys the constructive interferences of time reversal related wave functions.

The effective magnetic field due to strain does not break time reversal symmetry since it has opposite effect in both valleys. This is why it is called pseudo-magnetic. However, the Cooperon channels $C_0^{x,y}$ are responsible for intravalley scattering and are suppressed

[2]Hereafter we call isospin the sub-lattice degree of freedom and pseudospin the valley degree of freedom.

by strain. In the next section we calculate this daphasing time.

6.4 Dephasing due to random gauge fields

In this section we calculate the dephasing time of the weak localization correction due to both the extrinsic and intrinsic random gauge fields considered in Chapter (4). We begin describing the procedure put forward by Mathur and Baranger [91] to calculate the effect of a parallel magnetic field in weak localization peak for a corrugated quasi-2D systems. These results can be adapted to graphene system with ripple disorder, as done in Ref. [41]. Next, we adapt the presented derivation to compute the dephasing time due to an intrinsic strain field.

Let us start considering the integral equation obeyed by the cooperon

$$C(\boldsymbol{r},\boldsymbol{r}') = C^{(0)}(\boldsymbol{r},\boldsymbol{r}') + \int d\boldsymbol{r}'' C^{(0)}(\boldsymbol{r},\boldsymbol{r}'')C(\boldsymbol{r}'',\boldsymbol{r}'), \tag{6.23}$$

where, in the limits $|\boldsymbol{r}-\boldsymbol{r}'| \gg \lambda_F$ and $k_F l_e \gg 1$, one can show [91] that (at zero magentic field $B=0$)

$$C^{(0)}_{B=0}(\boldsymbol{r},\boldsymbol{r}') \approx \frac{1}{2\pi l_e^2}\exp\left(-\frac{|\boldsymbol{r}-\boldsymbol{r}'|}{l_e}\right) \tag{6.24}$$

The solution to equation (6.23) is found by solving an eigenvalue equation for $C^{(0)}(\boldsymbol{r},\boldsymbol{r}')$

$$\int d\boldsymbol{r}' C^{(0)}(\boldsymbol{r},\boldsymbol{r}')\boldsymbol{Q}_\gamma(\boldsymbol{r}') = \gamma \boldsymbol{Q}_\gamma(\boldsymbol{r}), \tag{6.25}$$

from which follows

$$C(\boldsymbol{r},\boldsymbol{r}') = \sum_\gamma \frac{\gamma}{1-\gamma}\boldsymbol{Q}_\gamma(\boldsymbol{r})\boldsymbol{Q}_\gamma(\boldsymbol{r}') \tag{6.26}$$

For a slowly varying eigenfunction of $C^0(\boldsymbol{r},\boldsymbol{r}')$, equation (6.25) can be transformed in an diffusion equation [91]

$$D\tau_e\nabla^2\boldsymbol{Q}_\gamma(\boldsymbol{r}) + \boldsymbol{Q}_\gamma(\boldsymbol{r}) = \left(\gamma + \frac{\tau_e}{\tau_\phi}\right)\boldsymbol{Q}_\gamma(\boldsymbol{r}) \tag{6.27}$$

The parameter τ_e/τ_ϕ is included phenomenologically to consider sources of dephasing, like electron-electron interaction and electron-phonon interaction, that can diminish the quantum interference effect of the weak localization. For mathematical simplicity, it is better to work with a modified cooperon, namely

$$\mathcal{C}^{(0)}_{B=0}(\boldsymbol{r},\boldsymbol{r}') \approx \frac{1}{2\pi l_e^2}\exp\left(-\frac{|\boldsymbol{r}-\boldsymbol{r}'|^2}{2l_e}\right), \tag{6.28}$$

whose slowly varying eigenfunctions obey the same diffusion equation as the ones of $C^{(0)}(\boldsymbol{r},\boldsymbol{r}')$.

Let us now study the effect of a magnetic field on the cooperon. In Ref. [91] it was shown that in the limit of weak magnetic field, the only effect is to change the phase,

$$\mathcal{C}_B(\boldsymbol{r},\boldsymbol{r}') = \mathcal{C}^{(0)}_{B=0}(\boldsymbol{r},\boldsymbol{r}')\exp\left(i\frac{2e}{\hbar}\int_{\boldsymbol{r}'}^{\boldsymbol{r}} d\boldsymbol{l}\cdot\boldsymbol{A}\right). \tag{6.29}$$

In our problem, $\boldsymbol{A}$ can be either the gauge field that originates the intrinsic or the extrinsic random magnetic fields discussed in previous chapter. Let us take the average over the surface roughness. This is better done by solving equation (6.23) by iteration, namely

$$\mathcal{C}_B(\boldsymbol{r},\boldsymbol{r}) = \sum_n \mathcal{C}^{(n)}_B(\boldsymbol{r},\boldsymbol{r}), \tag{6.30}$$

with

$$\mathcal{C}^{(n)}_B(\boldsymbol{r},\boldsymbol{r}) \;=\; \int d\boldsymbol{r}_1\cdots d\boldsymbol{r}_n \mathcal{C}^{(n)}_{B=0}(\boldsymbol{r},\boldsymbol{r}_1)\cdots\mathcal{C}^{(n)}_{B=0}(\boldsymbol{r}_n,\boldsymbol{r})\exp\left(2\pi i n\frac{\phi_g}{\phi_{sc}}\right),$$

where $\phi_{sc} = h/2e$ is the superconducting flux quantum and

$$\phi_g = \int_{\boldsymbol{r}}^{\boldsymbol{r}} d\boldsymbol{l}\cdot\boldsymbol{A} \tag{6.31}$$

The disorder average of equation (6.30) reads

$$\langle\mathcal{C}_B(\boldsymbol{r},\boldsymbol{r})\rangle = \sum_n \langle\mathcal{C}^{(n)}_B(\boldsymbol{r},\boldsymbol{r})\rangle, \tag{6.32}$$

by assuming that the phases ϕ_g are Gaussian random variables with zero mean, the following equality holds

$$\langle\exp(i\xi\phi_g)\rangle = \exp\left(-\frac{1}{2}\xi^2\langle\phi_g^2\rangle\right). \tag{6.33}$$

With these elements one can calculate the cooperon suppression for the different situations of interest.

6.4.1 The case of the parallel external magnetic field

The calculation for an external parallel magnetic field was already worked out in Ref. [91] in the regime of short-ranged roughness $\lambda \ll l_e$, which is the one met for slowly varying corrugations in graphene [41, 33]. The result is

$$\langle\mathcal{C}^{(0)}_{B_\parallel}(\boldsymbol{r},\boldsymbol{r}')\rangle = \mathcal{C}^{(0)}_{B=0}(\boldsymbol{r},\boldsymbol{r}')\exp\left(-2\sqrt{\pi}\frac{e^2}{\hbar^2}B_\parallel^2 h_{rms}^2\lambda\frac{(y-y')^2}{|\boldsymbol{r}-\boldsymbol{r}'|}\right) \tag{6.34}$$

Using the above expression for the cooperon, we again transform equation (6.25) in a diffusion-like equation

$$(1 + D\tau_e\nabla^2)\boldsymbol{Q}_\gamma(\boldsymbol{r}) = \left(\gamma + \frac{\tau_e}{\tau_\phi} + \frac{\tau_e}{\tau_\parallel}\right)\boldsymbol{Q}_\gamma(\boldsymbol{r}), \tag{6.35}$$

where the extra term is

$$\frac{\tau_e}{\tau_\parallel} \approx \sqrt{\pi}\frac{e^2}{\hbar^2}B_\parallel^2 h_{\rm rms}^2 \lambda l_e = \sqrt{\pi}\frac{e^2}{\hbar^2}\left[\left(\frac{B_\parallel h_{\rm rms}}{\lambda}\right)^2\right]\lambda^3 l_e \tag{6.36}$$

The conclusion here is that the effect of a parallel external magnetic field on disorder ripples in graphene is to enhance the dephasing, this is

$$\frac{\tau_e}{\tau_\phi} \to \frac{\tau_e}{\tau_\phi} + \frac{\tau_e}{\tau_\parallel}, \tag{6.37}$$

making the effective τ_ϕ shorter. As a result, the WL peak is suppressed, in line with experiments [41].

6.4.2 The case of the intrinsic pseudo magnetic field

In the case of strain, the random vector field which enters the cooperon phase correction is given in equation (3.18). Working in the same form as in last section, we find (see Appendix D.1)

$$\langle \mathcal{C}^{(0)}_{B_{strain}}(\boldsymbol{r},\boldsymbol{r}')\rangle = \mathcal{C}^{(0)}_{B=0}(\boldsymbol{r},\boldsymbol{r}')\exp\left[-\frac{1}{2}\xi^2\left(\langle\phi_g^2\rangle_1^{(0)} + \langle\phi_g^2\rangle_2^{(0)} + \langle\phi_g^2\rangle_3^{(0)} + \langle\phi_g^2\rangle_4^{(0)}\right)\right], \tag{6.38}$$

where

$$\begin{aligned}
\langle\phi_g^2\rangle_1^{(0)} &= \left(\frac{\hbar\beta}{ea}\right)^2 \frac{3\sqrt{\pi}h_{rms}^4}{8\lambda^3}|\boldsymbol{r}-\boldsymbol{r}'|\left[\frac{2}{3}\cos^2(\theta) + \frac{1}{2}\cos^2(\theta)\cos^2(2\theta)\right] \\
\langle\phi_g^2\rangle_2^{(0)} &= \left(\frac{\hbar\beta}{ea}\right)^2 \frac{3\sqrt{\pi}h_{rms}^4}{8\lambda^3}|\boldsymbol{r}-\boldsymbol{r}'|\cos^2(\theta)\sin^2(\theta)\cos(2\theta) \\
\langle\phi_g^2\rangle_3^{(0)} &= \left(\frac{\hbar\beta}{ea}\right)^2 \frac{3\sqrt{\pi}h_{rms}^4}{8\lambda^3}|\boldsymbol{r}-\boldsymbol{r}'|\cos^2(\theta)\sin^2(\theta)\cos(2\theta) \\
\langle\phi_g^2\rangle_4^{(0)} &= \left(\frac{\hbar\beta}{ea}\right)^2 \frac{3\sqrt{\pi}h_{rms}^4}{8\lambda^3}|\boldsymbol{r}-\boldsymbol{r}'|\left[\frac{2}{3}\sin^2(\theta) + 2\sin^4(\theta)\cos^2(\theta)\right]
\end{aligned}$$

We use $\langle \mathcal{C}^{(0)}_{B_{strain}}(\boldsymbol{r},\boldsymbol{r}')\rangle$ to transform equation (6.25) in a diffusion-like equation.

$$(1 + D\tau_e\nabla^2)\boldsymbol{Q}_\gamma(\boldsymbol{r}) = \left(\gamma + \frac{\tau_e}{\tau_\phi} + \frac{\tau_e}{\tau_{strain}}\right)\boldsymbol{Q}_\gamma(\boldsymbol{r}), \tag{6.39}$$

where

$$\frac{\tau_e}{\tau_{strain}} \approx \frac{11\sqrt{2}\pi^3\beta^2 h_{\rm rms}^4 l_e}{16a^2\lambda^3} = \frac{11\sqrt{2}\pi^3}{16}\frac{e^2}{\hbar^2}\left[\frac{h_{\rm rms}^4}{\lambda^6}\left(\frac{\beta\hbar}{ea}\right)^2\right]\lambda^3 l_e \tag{6.40}$$

As before, we conclude that pseudo magnetic field due to strain has the effect of enhance the dephasing.

The rate $\tau_e/\tau_\parallel$ was measured in Ref. [41] in graphene by fitting the weak localization correction curve with and without in-plane magnetic field. The aim of this experiment was to extract a relation between $h_{\rm rms}$ and λ. Since the strain field suppressed the intravalley contributions to the weak localization correction, τ_e/τ_{strain} should be taken into account. Actually, for values $h_{\rm rms} = 10$nm and $\lambda = 10$nm from STM experiments [41], we obtain $1/\tau_{strain} \approx 1 \times 10^{13}\text{s}^{-1}$ and for values $h_{\rm rms} = 0.19$nm and $\lambda = 32$nm from AFM experiments[41], we obtain $1/\tau_{strain} \approx 1 \times 10^{10}\text{s}^{-1}$, that theoretically explain relaxations rates observed in experiments [41].

7 Many-body density of states in disorder systems

In this chapter we calculate the effects of disorder in the N-particle density of states. We briefly describe the general procedure to find this quantity and show explicitly the results for free Fermions in 2-dimensions.

Let us start by explaining the main difference between the one and many particle density of states. To this end, we begin by calculating the single particle one. Consider the transition amplitude (propagator)

$$K(\boldsymbol{x},t;\boldsymbol{x}',t') \;=\; \langle \boldsymbol{x}|e^{\frac{1}{\hbar}iH(t-t')}|\boldsymbol{x}'\rangle. \tag{7.1}$$

By making analytical continuation to imaginary time, $t = -i\tau$, inserting an identity resolution of energy eigenstates and taking the trace of this propagator[1], we get

$$\mathrm{Tr}[K(\boldsymbol{x},\boldsymbol{x},\tau-\tau')] \;=\; \sum_n e^{-\frac{1}{\hbar}E_n(\tau-\tau')}. \tag{7.2}$$

By evaluating the propagator at $\tau - \tau' = \hbar\beta$ we obtain the single-particle canonical partition function

$$\begin{aligned} Z(\beta) = \mathrm{Tr}K(\boldsymbol{x},\hbar\beta) &= \sum_n e^{-\beta E_n} \\ &= \int_{-\infty}^{\infty} dE' \sum_n e^{-\beta E'}\delta(E'-E_n) \\ &= \int_{-\infty}^{\infty} dE' e^{-\beta E'}\rho(E')\theta(E'). \end{aligned} \tag{7.3}$$

Thus, the density of states is the inverse Laplace transform of the canonical partition function, namely

$$\rho(E) = \mathcal{L}^{-1}\{Z\}(E). \tag{7.4}$$

[1]The trace is defined as $\int d\boldsymbol{x}d\boldsymbol{x}'\delta(\boldsymbol{x}-\boldsymbol{x}')$

This expression can be represented diagrammatically as shown in Fig.19a for the single particle density of states. Hereafter, we use black lines to represent the propagator and red lines to represent a trace.

Let us discuss how to extend the diagrammatic approach for $N > 1$ particles. In Fig.(19)b we represent the density of states for two particles. Note that due to indistinguishability, there are two contributions: one that looks like a single particle and another that looks as two independent ones. To give a better insight on the role played by indistinguishability of particles we present in Fig. 20 the case for three particles. Observe that we see three different contributions due to the exchange of final coordinates. First, Fig. 20a shows a contribution that looks like three independent particles, Fig. 20b, a contribution that looks like two independent particles and Fig. 20c, a contribution that looks like just one particle.

An important contribution of Prof. Klaus Richter group to this problem was recently published [92]. They used a geometrical interpretation of the symmetrization postulate (which we remark that is a quantum characteristic of many-body physics) to calculate the many-particle density of states for free Bosons and Fermions in 1,2 and 3 dimensions using only semiclassical tools.

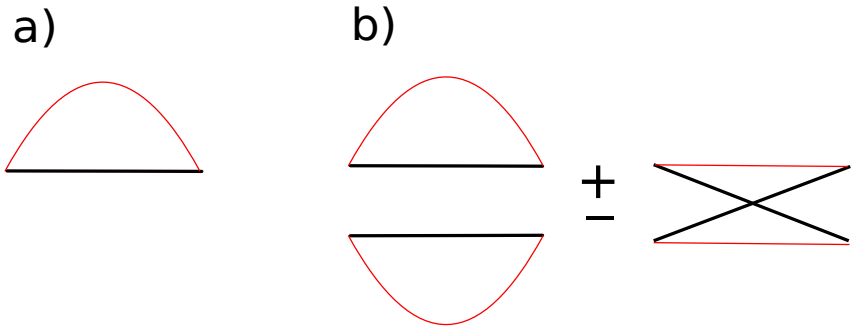

Figure 19: Diagrammatic representation of the density of states a) single particle and b) two particles. Plus and minus sign are for Bosons and Fermions. Black lines represent propagators and red lines, the trace.

The procedure explained before to calculate the DOS is more suitable to give a diagrammatic interpretation of the density of states. Another way to calculate this quantity is through the imaginary part of the retarded Green function, namely

$$\rho(E) = -\frac{1}{N!}\frac{1}{\pi}\mathrm{Im}\mathrm{Tr}\hat{G}^R, \tag{7.5}$$

with $\hat{G}^R$ the N-particle Green function. Let us explicitly calculate the two particle DOS

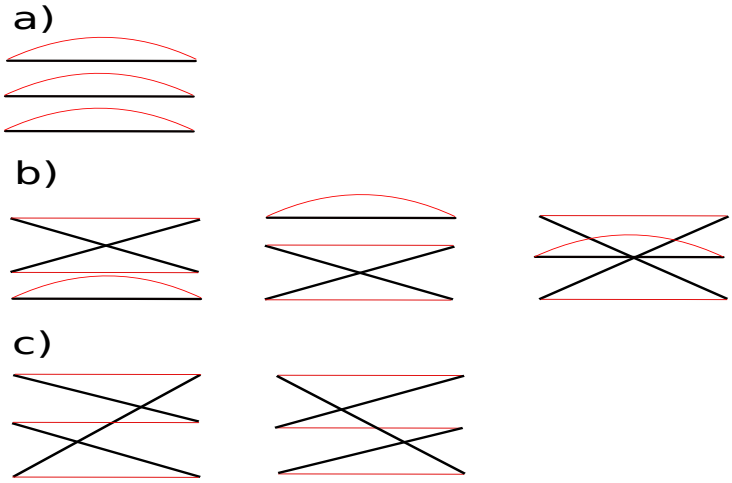

Figure 20: Sketch of diagrammatic contributions to the density of states for three particles.

including disorder [2].

7.1 Effect of disorder in the two-particle density of states

The Hilbert space for two particles is $\mathcal{H} = \mathcal{H}^{(1)} \otimes \mathcal{H}^{(2)}$. The total Hamiltonian operator is given by

$$\hat{H} = \hat{H}_0^{(1)} \otimes \mathbb{I} + V^{(1)}(\hat{x}) \otimes \mathbb{I} + \mathbb{I} \otimes \hat{H}_0^{(2)} + \mathbb{I} \otimes V^{(2)}(\hat{x}). \tag{7.6}$$

where the Hamiltonian operator for each particle is given by

$$\hat{H} = \hat{H}_0 + V(\hat{x}). \tag{7.7}$$

Let us assume we know how to solve $\hat{H}_0$, and $V(\hat{x})$ represents a disorder potential defined by its first and second moments

$$\langle V(x) \rangle = 0 \tag{7.8}$$

$$\langle V(x)V(x') \rangle = n_0 \delta(x - x'), \tag{7.9}$$

where $\langle \cdots \rangle$ stands for a mean over disorder and n_0 accounts for the strength of disorder. For simplicity we consider here the first born approximation, which means $n_0 = 1/2\pi\rho_0\tau$

[2] We work in 2 dimensions. So far, we have not found analytic expressions neither for 1d nor 3d.

with ρ the single particle density of states. The two particle propagator is[3]

$$\begin{aligned} K(x_1', x_2'; x_1, x_2, t'-t) &:= \sum_{P_f} \langle x_1', t', x_2', t' | x_1, t_1 x_2, t_2 \rangle \\ &= \langle x_1' | \hat{U}(t', t) | x_1 \rangle \langle x_2' | \hat{U}(t', t) | x_2 \rangle \\ &\pm \langle x_2' | \hat{U}(t', t) | x_1 \rangle \langle x_1' | \hat{U}(t', t) | x_2 \rangle, \end{aligned} \tag{7.10}$$

where $\hat{U} = i(\hat{G}^R(t', t) - \hat{G}^A(t', t))$, is the time evolution operator with $\hat{G}^{R/A}(t', t)$ retarded and advanced single particle Green's functions. We now use identity resolutions (the eigenstates of $\hat{H}_0$ taken here as the kinetic energy) and take the trace, namely

$$\begin{aligned} \mathrm{Tr}[\langle K(x_1, x_2; x_1, x_2, t'-t) \rangle] &= \sum_{n,n',m,m'} \langle \langle n' | \hat{U}(t', t) | n \rangle \langle m' | \hat{U}(t', t) | m \rangle \rangle \\ &\times \begin{vmatrix} \int dx_1 \varphi_{n'}(x_1) \varphi_n^*(x_1) & \int dx_1 \varphi_{m'}(x_1) \varphi_n^*(x_1) \\ \int dx_2 \varphi_{n'}(x_2) \varphi_m^*(x_2) & \int dx_2 \varphi_{m'}(x_2) \varphi_m^*(x_2) \end{vmatrix}. \end{aligned} \tag{7.11}$$

Changing to energy and momentum domain

$$\mathrm{Tr}[\langle K(x_1, x_2; E) \rangle] = \sum_{\boldsymbol{k}_1, \boldsymbol{k}_2} \mathcal{F}(E, \varepsilon_1, \varepsilon_2) \mathcal{D}(\boldsymbol{k}_1, \boldsymbol{k}_2), \tag{7.12}$$

where

$$\mathcal{F}(E, \varepsilon_1, \varepsilon_2) = \frac{1}{2\pi} \int_{-\infty}^{\infty} dE_1 \langle G(\boldsymbol{k}_1, E_1) G(\boldsymbol{k}_2, E - E_1) \rangle \tag{7.13}$$

where ε stands for single-particle kinetic energy and $\mathcal{D}(\boldsymbol{k}_1, \boldsymbol{k}_2)$ is a determinant given by

$$\mathcal{D}(\boldsymbol{k}_1, \boldsymbol{k}_2) = \begin{vmatrix} 1 & \delta_{\boldsymbol{k}_1, \boldsymbol{k}_2} \\ \delta_{\boldsymbol{k}_2, \boldsymbol{k}_1} & 1 \end{vmatrix}. \tag{7.14}$$

Explicitly, we have [4]

$$\begin{aligned} \mathrm{Tr} \langle K(x_{1f} x_{2f}; x_{1i}, x_{2i}; E) \rangle &= (i)^2 \sum_{\boldsymbol{k}_1, \boldsymbol{k}_2} \Big[\mathcal{F}^{RR}(E, \varepsilon_1, \varepsilon_2) + \mathcal{F}_C^{RR}(E, \varepsilon_1, \varepsilon_2) \\ &+ \mathcal{F}^{AA}(E, \varepsilon_1, \varepsilon_2) + \mathcal{F}_C^{AA}(E, \varepsilon_1, \varepsilon_2) \Big] \mathcal{D}(\boldsymbol{k}_1, \boldsymbol{k}_2), \end{aligned} \tag{7.15}$$

where $R(A)$ stands for retarded(advanced) Green's function. Neglecting correlation between the two particles (see Fig. 21a), we write

$$\mathcal{F}^{RR}(E, \varepsilon_1, \varepsilon_2) = -i \frac{1}{(E - \varepsilon_1 - \varepsilon_2 + i/\tau)}, \tag{7.16}$$

[3]Plus or minus sign stands for bosons or fermions respectively.

[4]We will consider here only explicit calculations for Fermion. For Bosons, we only have to take the permanent instead of the determinant in Eq.(7.14).

$$\mathcal{F}^{AA}(E,\varepsilon_1,\varepsilon_2) = i\frac{1}{(E-\varepsilon_1-\varepsilon_2-i/\tau)}, \tag{7.17}$$

$$\mathcal{F}^{RA}(E,\varepsilon_1,\varepsilon_2) = \mathcal{F}^{AR}(E,\varepsilon_1,\varepsilon_2) = 0. \tag{7.18}$$

where $\hbar/\tau$ is the imaginary part of the self energy. If we include correlations (see Fig. 21b), we need to compute

$$\begin{aligned}\mathcal{F}_C(E,\varepsilon_1,\varepsilon_2) &= \frac{1}{2\pi}\int_{-\infty}^{\infty} dE_1 G(k_1,E_1)G(k_2,E-E_1)\Lambda(k_1+k_2,E_1,E-E_1) \\ &\times\ G(k_1,E_1)G(k_2,E-E_1),\end{aligned} \tag{7.19}$$

where

$$\Lambda(\boldsymbol{q},E_1,E-E_1) = \frac{n_0}{1-\frac{n_0}{L}\sum_{q_1} G(q_1,E_1)G(q-q_1,E-E_1)}.$$

Computing all the contributions for retarded and advanced Green's functions explicitly we get

$$\Lambda^{RR}(\boldsymbol{q},E_1,E-E_1) = \Lambda^{AA}(\boldsymbol{q},E_1,E-E_1) \approx n_0 \tag{7.20}$$

$$\Lambda^{AR}(\boldsymbol{q},E_1,E-E_1) \approx \frac{n_0}{Dq^2\tau + i(2E_1\tau - E\tau)} = \frac{-in_0}{2E_1\tau - E\tau - iDq^2\tau}$$

$$\Lambda^{RA}(\boldsymbol{q},E_1,E-E_1) \approx \frac{n_0}{Dq^2\tau - i(2E_1\tau - E\tau)} = \frac{in_0}{2E_1\tau - E\tau + iDq^2\tau}$$

with $D = v_F^2\tau$ the diffusion constant and

$$\mathcal{F}_C^{RR}(E,\varepsilon_1,\varepsilon_2) = \frac{-2in_0}{(E-\varepsilon_1-\varepsilon_2+i/\tau)^3}$$

$$\mathcal{F}_C^{AA}(E,\varepsilon_1,\varepsilon_2) = \frac{2in_0}{(E-\varepsilon_1-\varepsilon_2-i/\tau)^3}$$

$$\begin{aligned}\mathcal{F}_C^{AR}(E,\varepsilon_1,\varepsilon_2) &= 0 \\ \mathcal{F}_C^{RA}(E,\varepsilon_1,\varepsilon_2) &= 0\end{aligned}$$

Note that the average between retarded and advanced Green's functions gives rise to a diffusive term, but gives no contribution to the whole 2-particle propagator. As in the case for the 1-particle DOS, we take only the retarded-retarded contribution, finally the

DOS reads

$$\begin{aligned}\rho(E) &= -\frac{1}{2!}\frac{1}{\pi}\sum_{\boldsymbol{k}_1,\boldsymbol{k}_2}\mathrm{Im}\left[\frac{1}{(E-\varepsilon_1-\varepsilon_2+i/\tau)}+\frac{2n_0}{(E-\varepsilon_1-\varepsilon_2+i/\tau)^3}\right]\mathcal{D}(\boldsymbol{k}_1,\boldsymbol{k}_2)\\ &= -\frac{1}{2!}\frac{1}{\pi}\sum_{\boldsymbol{k}_1,\boldsymbol{k}_2}\mathrm{Im}\left[\frac{1}{(E-\varepsilon_1-\varepsilon_2+i/\tau)}+\frac{2n_0}{(E-\varepsilon_1-\varepsilon_2+i/\tau)^3}\right]\\ &+ \frac{1}{2!}\frac{1}{\pi}\sum_{\boldsymbol{k}_1}\mathrm{Im}\left[\frac{1}{(E-2\varepsilon_1+i/\tau)}+\frac{2n_0}{(E-2\varepsilon_1+i/\tau)^3}\right]\end{aligned} \tag{7.21}$$

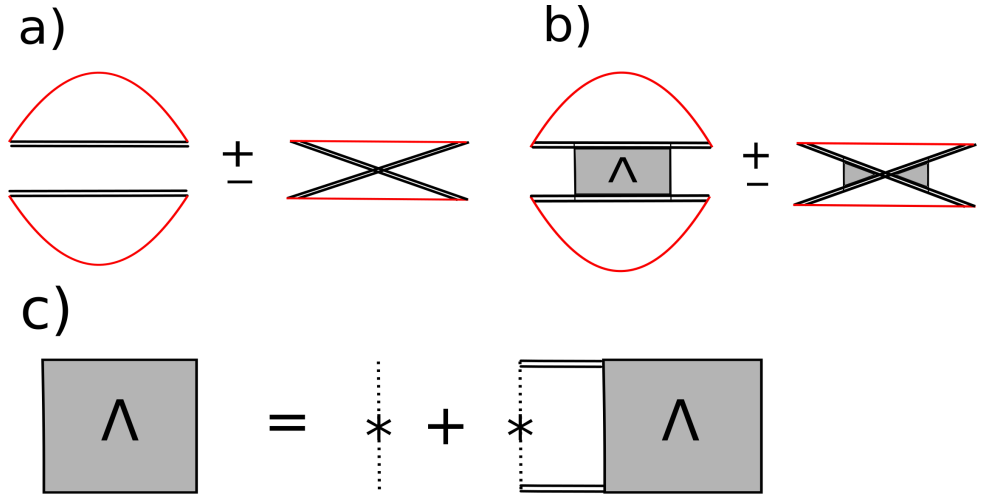

Figure 21: Diagrammatic representation of the density of states with disorder a) without correlations b) with correlations and c) the kernel with gives raise to the contraction of two independent particles with the disorder potential. We call correlations the contraction of disorder potential for different particles. Double lines represents disorder Green's function.

Performing the integrals,

$$\begin{aligned}\rho(E) &\approx \frac{1}{2\pi}\rho_0\left(\rho_0 E-\frac{1}{2}\right)\left[\frac{\pi}{2}+\tan^{-1}(\tau E)\right]-\frac{1}{2\pi}\rho_0^2 E\left[\frac{\ln(1+E^2\tau^2)}{2E\tau}\right]\\ &- n_0\frac{1}{2\pi}\rho_0^2\frac{1}{E}\left[\frac{E\tau}{(1+\tau^2E^2)}\right]+n_0\frac{1}{2\pi}\rho_0\frac{1}{E^2}\left[\frac{E^3\tau^3}{(1+E^2\tau^2)^2}\right],\end{aligned} \tag{7.22}$$

with ρ_0 the single particle density of states. This equation is shown diagrammatically in Fig. 21. We can take the zero disorder limit ($\tau=\infty$) to find the free two particle density of states. It is

$$\rho(E)=\frac{1}{2}\rho_0^2E-\frac{1}{4}\rho_0, \tag{7.23}$$

and is represented diagrammatically in Fig. 19b.

7.2 General procedure to find the many particles density of states

To calculate the many particle DOS let us consider the Hilbert space of the N-particle system. This is

$$\mathcal{H} = \mathcal{H}^{(1)} \otimes \mathcal{H}^{(2)} \cdots \otimes \mathcal{H}^{(N)} \tag{7.24}$$

For *non-interacting particles*, we can separate the time evolution operator of the many particle system as a product of single particle ones, namely

$$\hat{U}(t,t') = \hat{U}^{(1)}(t,t') \otimes \hat{U}^{(2)}(t,t') \cdots \otimes \hat{U}^{(N)}(t,t'). \tag{7.25}$$

Using now the relation

$$\hat{U}(t',t) = i(\hat{G}^R(t',t) - \hat{G}^A(t',t)), \tag{7.26}$$

for each single particle time evolution operator, we can write the many particle one as

$$\hat{U}(t,t') = i^N[\hat{G}^R(t',t) - \hat{G}^A(t',t)]_1 \otimes [\hat{G}^R(t',t) - \hat{G}^A(t',t)]_2 \otimes \cdots \otimes [\hat{G}^R(t',t) - \hat{G}^A(t',t)]_N. \tag{7.27}$$

Now we ask for the transition amplitude

$$\begin{aligned} K^{(N)} &= \langle x_1(t')x_2(t')x_3(t') \cdots x_N(t')|x_1(t)x_2(t)x_3(t) \cdots x_N(t)\rangle \\ &= \sum_{Permutations(x')} \langle x'_1|U(t',t)|x_1\rangle\langle x'_2|U(t',t)|x_2\rangle \cdots \langle x'_N|U(t',t)|x_N\rangle \end{aligned} \tag{7.28}$$

taking care that we have to sum over all the possible permutations of the final coordinates. In terms of retarded and advanced time evolution operators

$$\begin{aligned} K_N &= i^N \sum_{Permutation} \langle x'_1|[\hat{G}^R(t',t) - \hat{G}^A(t',t)]|x_1\rangle\langle x'_2|[\hat{G}^R(t',t) - \hat{G}^A(t',t)]|x_2\rangle \cdots \\ &\times \langle x'_N|[\hat{G}^R(t',t) - \hat{G}^A(t',t)]|x_N\rangle \end{aligned} \tag{7.29}$$

The trace of the (average) many particle propagator in energy and momentum domain can be expressed as

$$\mathrm{Tr}\langle K_N(E)\rangle = i^N \sum_{\boldsymbol{k}_1,\cdots,\boldsymbol{k}_N} \mathcal{F}(\varepsilon_1,\cdots,\varepsilon_N;E)\mathcal{D}(\boldsymbol{k}_1,\cdots,\boldsymbol{k}_N) \tag{7.30}$$

where

$$\begin{aligned} \mathcal{F}(\varepsilon_1,\cdots,\varepsilon_N;E) &= \int_{-\infty}^{\infty}\frac{dE_1}{2\pi}\int_{-\infty}^{\infty}\frac{dE_2}{2\pi}\cdots\int_{-\infty}^{\infty}\frac{dE_{N-1}}{2\pi} \\ &\times \langle G(\boldsymbol{k}_1,E_1)G(\boldsymbol{k}_2,E_2)\cdots G(\boldsymbol{k}_{N-1},E_{N-1})\cdots G(\boldsymbol{k}_N,E-\cdots-E_{N-1})\rangle \end{aligned} \tag{7.31}$$

and we have to take all the possible combinations of product of retarded and advanced propagators. $\mathcal{D}(\boldsymbol{k}_1, \cdots, \boldsymbol{k}_N)$ is a determinant that takes into account the permutations of all the final coordinates. The general calculation follows the same steps discused in the $N = 2$ case. As N increases, the algebra becomes more and more involved. Let us explicitly show the final result for $N = 6$ particles. Separating the contributions without correlation and with correlation, namely

$$\rho(E) = \rho_{WC}(E) + \rho_C(E), \tag{7.32}$$

The 6-particle density of states reads

$$\begin{aligned}
\rho_{WC}(E) \;\approx\; & \left[\frac{1}{720\pi}(\rho_0)^6 \frac{1}{2}\frac{1}{3}\frac{1}{4}\frac{1}{5}E^5 - \frac{15}{720\pi}(\rho_0)^5 \frac{1}{2}\frac{1}{2}\frac{1}{3}\frac{1}{4}E^4 + \frac{40}{720\pi}(\rho_0)^4 \frac{1}{3}\frac{1}{2}\frac{1}{3}E^3\right. \\
+ \; & \frac{45}{720\pi}(\rho_0)^4 \frac{1}{2}\frac{1}{2}\frac{1}{2}\frac{1}{3}E^3 - \frac{90}{720\pi}(\rho_0)^3 \frac{1}{4}\frac{1}{2}E^2 - \frac{120}{720\pi}(\rho_0)^3 \frac{1}{3}\frac{1}{2}\frac{1}{2}E^2 \\
- \; & \frac{15}{720\pi}(\rho_0)^3 \frac{1}{2}\frac{1}{2}\frac{1}{2}\frac{1}{2}E^2 + \frac{144}{720\pi}(\rho_0)^2 \frac{1}{5}E + \frac{90}{720\pi}(\rho_0)^2 \frac{1}{4}\frac{1}{2}E \\
+ \; & \left.\frac{40}{720\pi}(\rho_0)^2 \frac{1}{3}\frac{1}{3}E - \frac{120}{720\pi}(\rho_0)\frac{1}{6}\right]\left[\frac{\pi}{2} + \arctan\left(\frac{2\tau}{6}E\right)\right]
\end{aligned}$$

and

$$\begin{aligned}
\rho_C(E) \;=\; & \frac{6!n_0^3}{6!\pi}(\rho_0)^6 \frac{1}{720}\frac{1}{E}\left[\frac{\tau E}{(1+(2\tau E/6)^2)}\right] \\
+ \; & \frac{6!n_0^3}{6!\pi}(\rho_0)^5 15\frac{1}{360}\frac{1}{2}\frac{1}{E^2}\left[\frac{(2\tau E/6)^3}{(1+(2\tau E/6)^2)^2}\right] \\
+ \; & \frac{6!n_0^3}{6!\pi}(\rho_0)^4 \frac{1}{360}\left(40\frac{1}{3} + 45\frac{1}{2}\frac{1}{2}\right)\frac{1}{E^3}\left[\frac{3(2\tau E/6)^5 - (2\tau E/6)^3}{(1+(2\tau E/6)^2)^3}\right] \\
+ \; & \frac{6!n_0^3}{6!\pi}(\rho_0)^3 \frac{1}{30}\left(90\frac{1}{4} + 120\frac{1}{3}\frac{1}{2} + 15\frac{1}{2}\frac{1}{2}\frac{1}{2}\right)\frac{1}{E^4}\left[\frac{(2\tau E/6)^7 - (2\tau E/6)^5}{(1+(2\tau E/6)^2)^4}\right] \\
+ \; & \frac{6!n_0^3}{6!\pi}(\rho_0)^2 \frac{1}{30}\left(144\frac{1}{5} + 90\frac{1}{4}\frac{1}{2} + 40\frac{1}{3}\frac{1}{3}\right)\frac{1}{E^5}\left[\frac{(2\tau E/6)^5 - 10(2\tau E/6)^7 + 5(2\tau E/6)^9}{(1+(2\tau E/6)^2)^5}\right] \\
+ \; & \frac{6!n_0^3}{6!\pi}(\rho_0)\frac{1}{3}\frac{1}{6}\frac{1}{E^6}\left[\frac{3(2\tau E/6)^7 - 10(2\tau E/6)^9 + 3(2\tau E/6)^{11}}{(1+(2\tau E/6)^2)^6}\right],
\end{aligned}$$

We show a plot of $\rho_{WC}(E)$ in Fig.22 for N=5,6,7 and 8 particles. We do not show $\rho_C(E)$ because this part only gives non negligible contributions very close $E = 0$, which is not a physical region, as explained below.

Some comments are pertinent here. First of all, it is clear that the density of states can not be negative, so the oscillatory part of this quantity in Fig. 22 is not physical. An

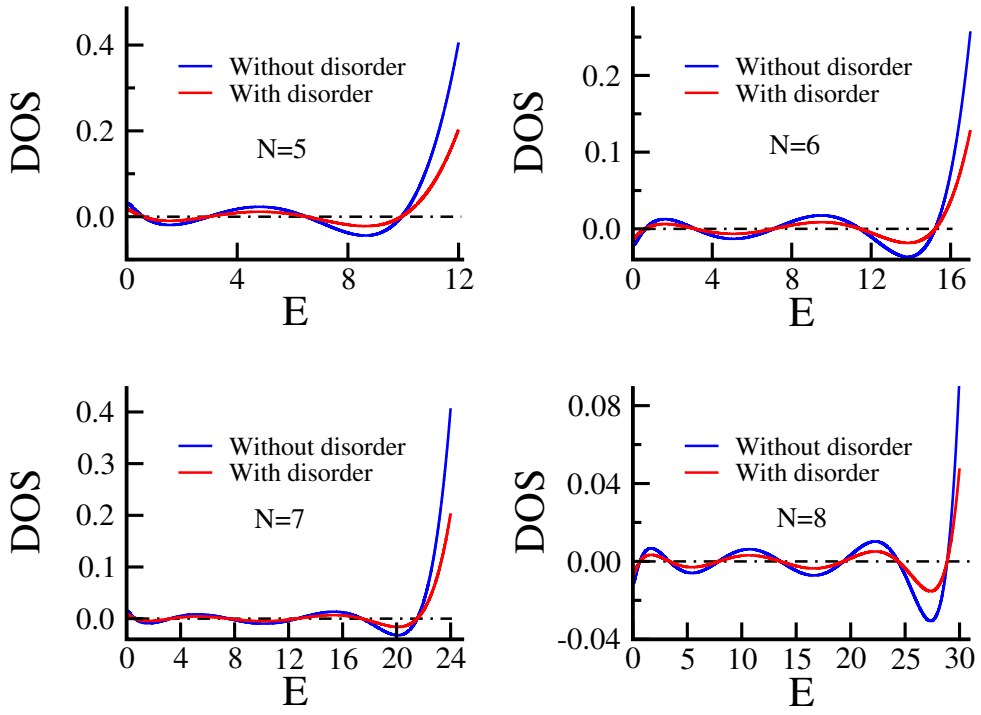

Figure 22: Evolution of the many particle density of states with increasing particle number N. We have rescaled the DOS and the energy putting $\rho_0 = 1$. We also used $\tau \to 0$ and $\tau \to 100$ in units of $1/\rho_0$s for high and low disorder respectively.

important feature of this calculation is the emergence of the ground state of the systems[5], which here occurs only as a consequence of the exchange symmetry of the wave function. This can be seen from the definition of the ground state

$$E_{GS} = \int_{-\infty}^{E_F} dE' \rho_0(E') E', \tag{7.33}$$

with the Fermi energy calculated with

$$N = \int_{-\infty}^{E_F} \rho_0(E') dE'. \tag{7.34}$$

The conclusion we draw from the calculations presented here is that disorder does not affect to much the many particle density of states. This conclusion is valid at least in the first Born approximation used here. We plan to go beyond this approximation to see if correlations are important.

[5]The ground state happens to be the point where the DOS stops to oscillate. This fact is more accurate if we increase the number of particles, see for instance Ref. [92].

7.3 Problems with the Lieb-Liniger model

The Lieb-Liniger model considers a system of Bosons in one dimension with contact interaction and confined in a finite region. The Hamiltonian reads [6] ($\hbar = 2m = 1$)

$$\left[-\sum_i \frac{\partial^2}{\partial x_i^2} + \sum_{\langle i,j \rangle} 2c\delta(x_i - x_j) \right] \psi(x_1, x_2, \cdots x_N) = E\psi(x_1, x_2, \cdots x_N), \tag{7.35}$$

in the domain,

$$R : 0 \leqslant x_i \leqslant L, \tag{7.36}$$

where $\langle i, j \rangle$ means sum over pairs and c is a positive constant related to the interaction strength.

To better understand this system, let us consider two bosons. Following the original approach [96], we consider a finite region of space with subdomain [7]

$$R_1 : 0 \leqslant x_1 \leqslant x_2 \leqslant L. \tag{7.37}$$

The Schrödinger's equation then reads

$$\left[-\frac{\partial^2}{\partial x_1^2} - \frac{\partial^2}{\partial x_2^2} + 2c\delta(x_1 - x_2) \right] \psi(x_1, x_2) = E\psi(x_1, x_2). \tag{7.38}$$

Following Lieb and Liniger [96], we take into account the contact interaction as boundary condition on the wave function by solving the equation

$$\left(-\frac{\partial^2}{\partial x_1^2} - \frac{\partial^2}{\partial x_2^2} \right) \psi(x_1, x_2) = E\psi(x_1, x_2), \tag{7.39}$$

with the mixed boundary conditions

$$\left(\frac{\partial}{\partial x_2} - \frac{\partial}{\partial x_1} \right) \psi(x_1, x_2)\Big|_{x_1 = x_2} = c\psi(x_1, x_2)\Big|_{x_1 = x_2}, \tag{7.40}$$

and periodic boundary conditions

$$\psi(0, x_2) \quad = \quad \psi(x_2, L). \tag{7.41}$$

At this point, the effect of the delta-like interaction has been replaced by boundary con-

[6] This system has been experimentally realized using optical lattices[93, 94, 95].

[7] Knowing the wave function in the subdomain R_1 allows us to know the wave function R just by requiring the full symmetry of the wave function.

ditions on R_1. Now we make the Bethe ansatz (valid in R_1)

$$\begin{aligned} \psi(x_1, x_2) &= \sum_{\mathcal{P}} A_{\mathcal{P}} e^{i\sum_j k_{\mathcal{P}_j} x_j} && (7.42) \\ &= A(k_1, k_2) e^{ik_1 x_1 + ik_2 x_2} + A(k_2, k_1) e^{ik_2 x_1 + ik_1 x_2}. && (7.43) \end{aligned}$$

We see that $\psi(x_1, x_2)$ is an eigenstate of Eq.(7.39) with

$$E = k_1^2 + k_2^2, \tag{7.44}$$

and, also an eigenstate of the momentum operator

$$\hat{\mathcal{K}} = -i \sum_j \frac{\partial}{\partial x_j}, \tag{7.45}$$

with eigenvalue

$$\mathcal{K} = k_1 + k_2. \tag{7.46}$$

Using Eq. (7.40) we get

$$\frac{A_{12}}{A_{21}} = \frac{i(k_2 - k_1) - c}{i(k_2 - k_1) + c}, \tag{7.47}$$

and since this number has unit modulus, it should be a pure phase, namely

$$\frac{A_{12}}{A_{21}} = e^{i\theta}, \tag{7.48}$$

with

$$\theta := \theta(k_2 - k_1) = \pi - 2 \arctan\left(\frac{k_2 - k_1}{c}\right), \quad 0 \leqslant \theta \leqslant 2\pi. \tag{7.49}$$

We can redefine the phase as

$$\tilde{\theta} := \theta(k_2 - k_1) - \pi = -2 \arctan\left(\frac{k_2 - k_1}{c}\right), \quad -\pi \leqslant \tilde{\theta} \leqslant \pi, \tag{7.50}$$

and

$$-\frac{A_{12}}{A_{21}} = e^{i\tilde{\theta}}. \tag{7.51}$$

Using the periodic boundary conditions Eq. (7.41), we get

$$\begin{aligned} k_1 L &= (2n_1 + 1)\pi - 2 \arctan\left(\frac{k_2 - k_1}{c}\right) && (7.52) \\ k_2 L &= (2n_2 + 1)\pi + 2 \arctan\left(\frac{k_2 - k_1}{c}\right). \end{aligned}$$

These are the Bethe equations for unknows k_i.

Now we are ready to discuss the difficulty in calculating the DOS for this model. We

ask for the probability amplitude

$$\begin{aligned} \langle x_1' x_2'; t' | x_1 x_2; t \rangle &= \langle x_1' x_2' | U(t', t) | x_1 x_2 \rangle \\ &= \langle x_1' x_2' | e^{-i\hat{H}(t-t')} | x_1 x_2 \rangle. \end{aligned} \tag{7.53}$$

Using energy eigenstates and going to energy domain

$$\mathrm{Tr} G(k_1, k_2 : E) = \sum_{k_1, k_2} \frac{1}{E - E(k_1, k_2)}. \tag{7.54}$$

We can add an infinitesimal positive constant and use the imaginary part to arrive at the density of states, but note here that the quantization condition given in Eq. (7.52) makes the change of the sum to integrals a non trivial task, and so far we have not found a way to do it. This is a key technical difficulty within this approach. The goal is to calculate the propagator directly in real space and take the inverse Laplace transform to find the DOS [8].

Another problem appears when considering disorder. All the perturbation theory described above works well for fermionic systems with a well defined Fermi surface, where a small parameter to do perturbation theory is $\delta = \hbar / E_F \tau$. This parameter does not exist for bosons. Actually, what we calculated before in Sec. (7.2) can be interpreted as the effect of disorder on the many *quasiparticles* density of states. Our goal is to find out how to adapt disorder perturbation theory for bosonic systems.

[8] This approach is being considered in the group of professor Klaus Richter.

APPENDIX A

A.1 Strain contribution for zigzag orientation

Let us now explicitly work out the strain contribution in zigzag orientation for the $\boldsymbol{K}$-valley. By inserting (2.17) in (2.14) the Hamiltonian reads

$$H_{\mathrm{s}}^{K} = t\sum_{n} i\frac{\boldsymbol{\sigma}\cdot\boldsymbol{\delta}_n}{a}\sigma_z\left(\frac{\beta}{a^2}\boldsymbol{\delta}_n\cdot\boldsymbol{u}\cdot\boldsymbol{\delta}_n\right) \tag{A.1}$$

Now, we use some brute force to calculate $\boldsymbol{\delta}_n\cdot\boldsymbol{u}\cdot\boldsymbol{\delta}_n$. First

$$\boldsymbol{\delta}_1^T\cdot\boldsymbol{u}\cdot\boldsymbol{\delta}_1 = \frac{a^2}{4}(3u_{xx}+2\sqrt{3}u_{xy}+u_{yy}) \tag{A.2}$$

$$\boldsymbol{\delta}_2^T\cdot\boldsymbol{u}\cdot\boldsymbol{\delta}_2 = \frac{a^2}{4}(3u_{xx}-2\sqrt{3}u_{xy}+u_{yy}) \tag{A.3}$$

$$\boldsymbol{\delta}_3^T\cdot\boldsymbol{u}\cdot\boldsymbol{\delta}_3 = a^2u_{yy} \tag{A.4}$$

Expanding the sum and collecting all results

$$H_s^{\boldsymbol{K}} = -v_F\hbar\left[\sigma_x\left(\frac{\beta}{2a}(u_{xx}-u_{yy})\right)+\sigma_y\left(-\frac{\beta}{a}u_{xy}\right).\right] \tag{A.5}$$

By using the minimal coupling $\mathbf{p}\to\mathbf{p}-q\mathbf{A}$, we associate the vector potential to

$$\mathbf{A} = \frac{\beta}{2ae}\left(u_{xx}-u_{yy},-2u_{xy}\right). \tag{A.6}$$

For the $\boldsymbol{K}'$ valley

$$H_{\mathrm{s}}^{\boldsymbol{K}'} = -v_0\hbar\left[\sigma_x\left(\frac{\beta}{2a}(u_{xx}-u_{yy})\right)+\sigma_y^*\left(-\frac{\beta}{a}u_{xy}\right)\right] \tag{A.7}$$

A.2 Armchair geometry

For armchair lattice orientation shown in Fig. 23a the primitive translation vectors are

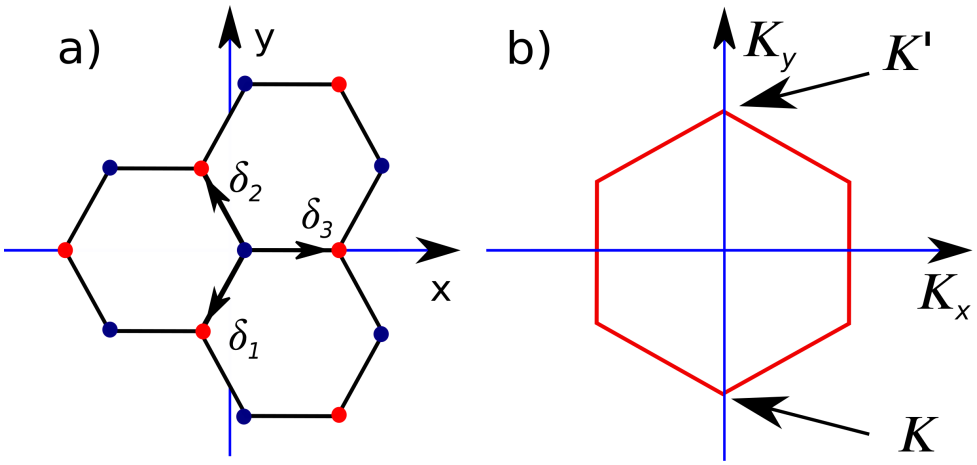

Figure 23: Lattice structure of graphene. a) Armchair orientation and b) Corresponding Brillouin zone.

$$\boldsymbol{a}_1 = \frac{a}{2}\begin{pmatrix} 3 \\ \sqrt{3} \end{pmatrix}, \quad \boldsymbol{a}_2 = \frac{a}{2}\begin{pmatrix} 3 \\ -\sqrt{3} \end{pmatrix}, \tag{A.8}$$

and the nearest neighbors vectors are

$$\boldsymbol{\delta}_1 = \frac{a}{2}\begin{pmatrix} 1 \\ -\sqrt{3} \end{pmatrix}, \quad \boldsymbol{\delta}_2 = \frac{a}{2}\begin{pmatrix} 1 \\ \sqrt{3} \end{pmatrix}, \quad \text{and} \quad \boldsymbol{\delta}_3 = a\begin{pmatrix} -1 \\ 0 \end{pmatrix}. \tag{A.9}$$

The corresponding reciprocal lattice vectors are

$$\boldsymbol{b}_1 = \frac{2\pi}{3a}\begin{pmatrix} 1 \\ \sqrt{3} \end{pmatrix} \quad \boldsymbol{b}_2 = \frac{2\pi}{3a}\begin{pmatrix} 1 \\ -\sqrt{3} \end{pmatrix} \tag{A.10}$$

and the high symmetry points

$$\boldsymbol{K} = \frac{4\pi}{3a}\begin{pmatrix} 0 \\ -\sqrt{3}/3 \end{pmatrix} \quad \boldsymbol{K}' = \frac{4\pi}{3a}\begin{pmatrix} 0 \\ \sqrt{3}/3 \end{pmatrix}. \tag{A.11}$$

The useful identity (2.17) is modified for the armchair geometry. For the $\boldsymbol{K}$ valley one writes

$$\begin{pmatrix} 0 & e^{-i\boldsymbol{K}\cdot\boldsymbol{\delta}_n} \\ e^{i\boldsymbol{K}\cdot\boldsymbol{\delta}_n} & 0 \end{pmatrix} = -\frac{\boldsymbol{\sigma}\cdot\boldsymbol{\delta}_n}{a}. \tag{A.12}$$

The Dirac Hamiltonian for the valley $\boldsymbol{K}$ then reads

$$\begin{aligned} H_0^{\boldsymbol{K}} &= t\sum_n \frac{\boldsymbol{\sigma}\cdot\boldsymbol{\delta}_n}{a}\left(i\sigma_z \boldsymbol{q}'\cdot\boldsymbol{\delta}_n\right) \\ &= v_0\hbar(\sigma_x q'_x + \sigma_y q'_y)(i\sigma_z) \qquad (A.13) \\ &= v_0\hbar(\sigma_y q'_x - \sigma_x q'_y) \end{aligned}$$

$$(A.14)$$

This expression is obviously **not** what we want. We can recover the standard Dirac equation by rotating the coordinate axis by $\pi/2$. Before doing it, let us analyse the strain term.

The strain Hamiltonian for the $\boldsymbol{K}$ valley

$$H_{\rm s} = -t\sum_n \frac{\boldsymbol{\sigma}\cdot\boldsymbol{\delta}_n}{a}\left(\frac{\beta}{a^2}\boldsymbol{\delta}_n^T\cdot\boldsymbol{u}\cdot\boldsymbol{\delta}_n\right). \qquad (A.15)$$

It can be calculated by "brute force" as done for the zigzag case

$$\frac{1}{a^2}\boldsymbol{\delta}_1^T\cdot\boldsymbol{u}\cdot\boldsymbol{\delta}_1 = \frac{1}{4}(u_{xx} - 2\sqrt{3}u_{xy} + 3u_{yy}) \qquad (A.16)$$

$$\frac{1}{a^2}\boldsymbol{\delta}_2^T\cdot\boldsymbol{u}\cdot\boldsymbol{\delta}_2 = \frac{1}{4}(u_{xx} + 2\sqrt{3}u_{xy} + 3u_{yy}) \qquad (A.17)$$

$$\frac{1}{a^2}\boldsymbol{\delta}_3^T\cdot\boldsymbol{u}\cdot\boldsymbol{\delta}_3 = u_{xx}. \qquad (A.18)$$

Expanding the sum and collecting all terms

$$H_{\rm s}^{\boldsymbol{K}} = v_0\left[\sigma_x\left(-\frac{\beta\hbar}{2a}\right)(u_{xx} - u_{yy}) + \sigma_y\left(\frac{\beta\hbar}{a}\right)u_{xy}\right] \qquad (A.19)$$

The full Hamiltonian(Dirac and strain contributions) reads

$$H^{\boldsymbol{K}} = v_0\left[\sigma_x\left(-p_y - \frac{\beta\hbar}{2a}(u_{xx} - u_{yy})\right) + \sigma_y\left(p_x + \frac{\beta\hbar}{a}u_{xy}\right)\right] \qquad (A.20)$$

Let us define

$$H^{\boldsymbol{K}} = v_0(\sigma_x\Pi_{x'} + \sigma_y\Pi_{y'}) \qquad (A.21)$$

with

$$\Pi_{x'} = -p_y - \frac{\beta\hbar}{2a}(u_{xx} - u_{yy}) \quad \text{and} \quad \Pi_{y'} = p_x + \frac{\beta\hbar}{a}u_{xy} \qquad (A.22)$$

By rotating the coordinate system $\mathrm{O}x'y'$ by $\pi/2$, the canonical momentum transforms as

$\mathbf{\Pi} = R(\pi/2)\mathbf{\Pi}'$

$$\begin{pmatrix} \Pi_x \\ \Pi_y \end{pmatrix} = \begin{pmatrix} 0 & 1 \\ -1 & 0 \end{pmatrix} \begin{pmatrix} \Pi_{x'} \\ \Pi_{y'} \end{pmatrix}$$

and we arrive to

$$\Pi_x = p_x + \frac{\beta\hbar}{a} u_{xy} \quad \text{and} \quad \Pi_y = p_y + \frac{\beta\hbar}{2a}(u_{xx} - u_{yy}) \tag{A.23}$$

which is the desired result.

APPENDIX B

B.1 Correlation function for the pseudo magnetic field due to strain

Here we explicitly derive the expression for the correlation function of the pseudo magnetic field. We start with the equations for the vector potential

$$A_x(\boldsymbol{r}) = \frac{\hbar\beta}{ea}[u_{xx}(\boldsymbol{r}) - u_{yy}(\boldsymbol{r})] \tag{B.1}$$

$$A_y(\boldsymbol{r}) = -2\frac{\hbar\beta}{ea}u_{xy}(\boldsymbol{r}), \tag{B.2}$$

where

$$u_{xx} \approx \frac{1}{2}\frac{\partial h(\boldsymbol{r})}{\partial x}\frac{\partial h(\boldsymbol{r})}{\partial x}, \quad u_{xy} \approx \frac{1}{2}\frac{\partial h(\boldsymbol{r})}{\partial y}\frac{\partial h(\boldsymbol{r})}{\partial x}, \quad u_{yy} \approx \frac{1}{2}\frac{\partial h(\boldsymbol{r})}{\partial y}\frac{\partial h(\boldsymbol{r})}{\partial y}. \tag{B.3}$$

With these equations, we can compute the effective magnetic field due to strain as

$$\begin{aligned} B_z^s(\boldsymbol{r}) &= \frac{\partial A_y}{\partial x} - \frac{\partial A_x}{\partial y} \\ &= \frac{\hbar\beta}{ea}\left[u_{yyy}(\boldsymbol{r}) - 2u_{xxy}(\boldsymbol{r}) - u_{yxx}(\boldsymbol{r})\right]. \end{aligned} \tag{B.4}$$

Defining

$$h(\boldsymbol{r}) = \sum_{\boldsymbol{q}} e^{-i\boldsymbol{q}\cdot\boldsymbol{r}}h(\boldsymbol{q}) \tag{B.5}$$

we get

$$u_{yyy}(\boldsymbol{r}) \approx \frac{1}{2}\frac{\partial}{\partial y}\frac{\partial h(\boldsymbol{r})}{\partial y}\frac{\partial h(\boldsymbol{r})}{\partial y} = \frac{i}{2}\sum_{\boldsymbol{q}_1}\sum_{\boldsymbol{q}_2} q_{1y}q_{2y}(q_{1y}+q_{2y})e^{-i(\boldsymbol{q}_1+\boldsymbol{q}_2)\cdot\boldsymbol{r}}h(\boldsymbol{q}_1)h(\boldsymbol{q}_2) \tag{B.6}$$

with the Fourier transform

$$\begin{aligned} u_{yyy}(\boldsymbol{q}) &= \frac{1}{\mathcal{A}}\int d\boldsymbol{r}\, u_{yyy}(\boldsymbol{r})e^{i\boldsymbol{q}\cdot\boldsymbol{r}} = \frac{i}{2}q_y\sum_{\boldsymbol{q}_1} q_{1y}(q_y - q_{1y})h(\boldsymbol{q}_1)h(\boldsymbol{q}-\boldsymbol{q}_1) \\ &= -iq_y u_{yy}(\boldsymbol{q}). \end{aligned} \tag{B.7}$$

In the same way

$$u_{yxx}(\boldsymbol{r}) \approx \frac{1}{2}\frac{\partial}{\partial y}\frac{\partial h(\boldsymbol{r})}{\partial x}\frac{\partial h(\boldsymbol{r})}{\partial x} = \frac{i}{2}\sum_{\boldsymbol{q}_1}\sum_{\boldsymbol{q}_2} q_{1x}q_{2x}(q_{1y}+q_{2y})e^{-i(\boldsymbol{q}_1+\boldsymbol{q}_2)\cdot\boldsymbol{r}}h(\boldsymbol{q}_1)h(\boldsymbol{q}_2) \quad \text{(B.8)}$$

$$\begin{aligned} u_{yxx}(\boldsymbol{q}) &= \frac{1}{\mathcal{A}}\int d\boldsymbol{r}\, u_{yxx}(\boldsymbol{r})e^{i\boldsymbol{q}\cdot\boldsymbol{r}} = \frac{i}{2}q_y\sum_{\boldsymbol{q}_1} q_{1x}(q_x-q_{2x})h(\boldsymbol{q}_1)h(\boldsymbol{q}-\boldsymbol{q}_1) \\ &= -iq_y u_{xx}(\boldsymbol{q}) \end{aligned} \quad \text{(B.9)}$$

and finally

$$u_{xxy}(\boldsymbol{r}) \approx \frac{1}{2}\frac{\partial}{\partial x}\frac{\partial h(\boldsymbol{r})}{\partial x}\frac{\partial h(\boldsymbol{r})}{\partial y} = \frac{i}{2}\sum_{\boldsymbol{q}_1}\sum_{\boldsymbol{q}_2} q_{1x}q_{2y}(q_{1x}+q_{2x})e^{-i(\boldsymbol{q}_1+\boldsymbol{q}_2)\cdot\boldsymbol{r}}h(\boldsymbol{q}_1)h(\boldsymbol{q}_2) \quad \text{(B.10)}$$

(B.11)

$$\begin{aligned} u_{xxy}(\boldsymbol{q}) &= \frac{1}{\mathcal{A}}\int d\boldsymbol{r}\, u_{yxx}(\boldsymbol{r})e^{i\boldsymbol{q}\cdot\boldsymbol{r}} = \frac{i}{2}q_x\sum_{\boldsymbol{q}_1} q_{1x}(q_y-q_{2y})h(\boldsymbol{q}_1)h(\boldsymbol{q}-\boldsymbol{q}_1) \\ &= -iq_x u_{xy}(\boldsymbol{q}) \end{aligned} \quad \text{(B.12)}$$

The Fourier transform of the effective magnetic field due to strain is then

$$B_z^s(\boldsymbol{q}) = \frac{1}{\mathcal{A}}\int d\boldsymbol{r}\, B_z^s(\boldsymbol{r})e^{i\boldsymbol{q}\cdot\boldsymbol{r}} = i\frac{\hbar\beta}{ea}[q_y u_{xx}(\boldsymbol{q}) + 2q_x u_{xy}(\boldsymbol{q}) - q_y u_{yy}(\boldsymbol{q})], \quad \text{(B.13)}$$

and the correlation function in reciprocal space is then

$$\begin{aligned} \langle B(\boldsymbol{q})B(-\boldsymbol{q})\rangle &= \left(\frac{\hbar\beta}{ea}\right)^2\Big[q_y^2\langle u_{xx}(\boldsymbol{q})u_{xx}(-\boldsymbol{q})\rangle + 2q_yq_x\langle u_{xx}(\boldsymbol{q})u_{xy}(-\boldsymbol{q})\rangle - q_y^2\langle u_{xx}(\boldsymbol{q})u_{yy}(-\boldsymbol{q})\rangle \\ &+ 2q_yq_x\langle u_{xy}(\boldsymbol{q})u_{xx}(-\boldsymbol{q})\rangle + 4q_x^2\langle u_{xy}(\boldsymbol{q})u_{xy}(-\boldsymbol{q})\rangle - 2q_yq_x\langle u_{xy}(\boldsymbol{q})u_{yy}(-\boldsymbol{q})\rangle \\ &- q_y^2\langle u_{yy}(\boldsymbol{q})u_{xx}(-\boldsymbol{q})\rangle - 2q_yq_x\langle u_{yy}(\boldsymbol{q})u_{xy}(-\boldsymbol{q})\rangle + q_y^2\langle u_{yy}(\boldsymbol{q})u_{yy}(-\boldsymbol{q})\rangle\Big] \end{aligned} \quad \text{(B.14)}$$

$$\begin{aligned} \langle B(\boldsymbol{q})B(-\boldsymbol{q})\rangle &= \left(\frac{\hbar\beta}{ea}\right)^2\Bigg[q_y^2\Big(\langle u_{xx}(\boldsymbol{q})u_{xx}(-\boldsymbol{q})\rangle - \langle u_{xx}(\boldsymbol{q})u_{yy}(-\boldsymbol{q})\rangle - \langle u_{yy}(\boldsymbol{q})u_{xx}(-\boldsymbol{q})\rangle \\ &+ \langle u_{yy}(\boldsymbol{q})u_{yy}(-\boldsymbol{q})\rangle\Big) + 2q_yq_x\Big(\langle u_{xx}(\boldsymbol{q})u_{xy}(-\boldsymbol{q})\rangle + \langle u_{xy}(\boldsymbol{q})u_{xx}(-\boldsymbol{q})\rangle \\ &- \langle u_{xy}(\boldsymbol{q})u_{yy}(-\boldsymbol{q})\rangle - \langle u_{yy}(\boldsymbol{q})u_{xy}(-\boldsymbol{q})\rangle\Big) + 4q_x^2\langle u_{xy}(\boldsymbol{q})u_{xy}(-\boldsymbol{q})\rangle\Bigg]. \end{aligned} \quad \text{(B.15)}$$

Now we use the equations

$$\langle u_{xx}(\boldsymbol{q})u_{xx}(-\boldsymbol{q})\rangle = \frac{h_{rms}^4}{4\lambda^4} + \frac{h_{rms}^4\pi}{32\lambda^2\mathcal{A}}(12 - 4\lambda^2q_x^2 + \lambda^4q_x^4)e^{-\frac{\lambda^2}{4}\boldsymbol{q}^2} \quad \text{(B.16)}$$

$$\langle u_{xx}(\boldsymbol{q})u_{yy}(-\boldsymbol{q})\rangle = \frac{h_{rms}^4}{4\lambda^4} + \frac{\pi h_{rms}^4}{32\lambda^2\mathcal{A}}(2-\lambda^2 q_x^2)(2-\lambda^2 q_y^2)e^{-\frac{\lambda^2}{4}\boldsymbol{q}^2} \tag{B.17}$$

$$\langle u_{yy}(\boldsymbol{q})u_{xx}(-\boldsymbol{q})\rangle = \frac{h_{rms}^4}{4\lambda^4} + \frac{\pi h_{rms}^4}{32\lambda^2\mathcal{A}}(2-\lambda^2 q_y^2)(2-\lambda^2 q_x^2)e^{-\frac{\lambda^2}{4}\boldsymbol{q}^2} \tag{B.18}$$

$$\langle u_{yy}(\boldsymbol{q})u_{yy}(-\boldsymbol{q})\rangle = \frac{h_{rms}^4}{4\lambda^4} + \frac{h_{rms}^4\pi}{32\lambda^2\mathcal{A}}(12-4\lambda^2 q_y^2+\lambda^4 q_y^4)e^{-\frac{\lambda^2}{4}\boldsymbol{q}^2} \tag{B.19}$$

$$\langle u_{xx}(\boldsymbol{q})u_{xy}(-\boldsymbol{q})\rangle = \frac{\pi h_{rms}^4 q_x q_y(\lambda^2 q_x^2-2)}{32\mathcal{A}}e^{-\frac{\lambda^2\boldsymbol{q}^2}{4}} \tag{B.20}$$

$$\langle u_{yy}(\boldsymbol{q})u_{xy}(-\boldsymbol{q})\rangle = \frac{\pi h_{rms}^4 q_x q_y(\lambda^2 q_y^2-2)}{32\mathcal{A}}e^{-\frac{\lambda^2\boldsymbol{q}^2}{4}} \tag{B.21}$$

$$\langle u_{xy}(\boldsymbol{q})u_{yy}(-\boldsymbol{q})\rangle = \frac{\pi q_x q_y h_{rms}^4}{32\mathcal{A}}(q_y^2\lambda^2-2)e^{-\frac{\lambda^2\boldsymbol{q}^2}{4}} \tag{B.22}$$

$$\langle u_{xy}(\boldsymbol{q})u_{xx}(-\boldsymbol{q})\rangle = \frac{\pi q_x q_y h_{rms}^4}{32\mathcal{A}}(\lambda^2 q_x^2-2)e^{-\frac{\lambda^2\boldsymbol{q}^2}{4}} \tag{B.23}$$

$$\langle u_{xy}(\boldsymbol{q})u_{xy}(-\boldsymbol{q})\rangle = \frac{\pi h_{rms}^4}{32\lambda^2\mathcal{A}}(4+q_x^2 q_y^2\lambda^4)e^{-\frac{\lambda^2\boldsymbol{q}^2}{4}} \tag{B.24}$$

from which we get

$$\begin{aligned}\langle B(\boldsymbol{q})B(-\boldsymbol{q})\rangle &= \frac{h_{rms}^4\pi}{32\lambda^2\mathcal{A}}\left(\frac{\hbar\beta}{ea}\right)^2\left[q_y^2\left(16+\lambda^4(q_x^2-q_y^2)^2\right)+2q_yq_x\left(2\lambda^4 q_x q_y(q_x^2-q_y^2)\right)\right.\\ &+ \left.4q_x^2\left(4+\lambda^4 q_x^2 q_y^2\right)\right]e^{-\frac{\lambda^2}{4}\boldsymbol{q}^2}.\end{aligned} \tag{B.25}$$

Making the parametrization

$$q_x = q\cos\theta \tag{B.26}$$

$$q_y = q\sin\theta \tag{B.27}$$

we finally find the expression

$$\langle B(\boldsymbol{q})B(-\boldsymbol{q})\rangle = \frac{h_{rms}^4\pi}{32\lambda^2\mathcal{A}}\left(\frac{\hbar\beta}{ea}\right)^2\left[16q^2+\lambda^4 q^6\sin^2 3\theta\right]e^{-\frac{\lambda^2}{4}\boldsymbol{q}^2} \tag{B.28}$$

In real space, the correlator reads

$$\begin{aligned}\langle B(\boldsymbol{r})B(-\boldsymbol{r}')\rangle &= \sum_{\boldsymbol{q}} e^{-i\boldsymbol{q}\cdot\boldsymbol{r}}\langle B(\boldsymbol{q})B(-\boldsymbol{q})\rangle \qquad \text{(B.29)}\\ &= \frac{h_{rms}^4}{\lambda^6}\left(\frac{\hbar\beta}{ea}\right)^2\left[8-\frac{20}{\lambda^2}(x^2+y^2)+\frac{9}{\lambda^4}(x^2+y^2)^2-\frac{2y^2}{\lambda^6}(y^2-3x^2)^2\right]e^{-\frac{r^2}{\lambda^2}}.\end{aligned}$$

We set the parametrization

$$x = r\cos\theta \qquad \text{(B.30)}$$

$$y = r\sin\theta \qquad \text{(B.31)}$$

and finally

$$\langle B(\boldsymbol{r})B(-\boldsymbol{r}')\rangle = \frac{h_{rms}^4}{\lambda^6}\left(\frac{\hbar\beta}{ea}\right)^2\left[8-20\frac{r^2}{\lambda^2}+9\frac{r^4}{\lambda^4}-2\frac{r^6}{\lambda^6}\sin^2(3\theta)\right]e^{-\frac{r^2}{\lambda^2}} \qquad \text{(B.32)}$$

The variance is given by

$$\langle B(\boldsymbol{r})B(-\boldsymbol{r}')\rangle|_{r=0} = 8\frac{h_{rms}^4\pi}{\lambda^6}\left(\frac{\hbar\beta}{ea}\right)^2 \qquad \text{(B.33)}$$

APPENDIX C

C.1 Electrons in high magnetic field

The Hamiltonian for pristine graphene in a magnetic field(one valley only) reads

$$H = v_F \begin{pmatrix} 0 & \pi_x - i\pi_y \\ \pi_x + i\pi_y & 0 \end{pmatrix} \tag{C.1}$$

with the kinetic momentum given by $\pi_x = p_x + eA_x$ and $\pi_y = p_y + eA_y$. We define operators

$$\Pi_+ = \pi_x + i\pi_y = \sqrt{2e\hbar B}b^+ \tag{C.2}$$

$$\Pi_- = \pi_x - i\pi_y = \sqrt{2e\hbar B}b^- \tag{C.3}$$

so that the Hamiltonian can be written as

$$H = \frac{\sqrt{2}v_F\hbar}{l_B} \begin{pmatrix} 0 & b^- \\ b^+ & 0 \end{pmatrix}. \tag{C.4}$$

The eigenvalue problem to solve is then

$$\frac{\sqrt{2}v_F\hbar}{l_B} \begin{pmatrix} 0 & b^- \\ b^+ & 0 \end{pmatrix} \begin{pmatrix} \varphi_1 \\ \varphi_2 \end{pmatrix} = E \begin{pmatrix} \varphi_1 \\ \varphi_2 \end{pmatrix}, \tag{C.5}$$

and explicitly we have two equations, namely

$$\frac{\sqrt{2}v_F h}{l_B} b^- \varphi_2 = E\varphi_1 \tag{C.6}$$

and

$$\frac{\sqrt{2}v_F h}{l_B} b^+ \varphi_1 = E\varphi_2. \tag{C.7}$$

solving for φ_2 we have

$$\left(\frac{\sqrt{2}v_F h}{l_B}\right)^2 b^+ b^- \varphi_2 = E^2\varphi_2 \tag{C.8}$$

what suggests that φ is an eigenstate of the number operator with eigenvalues

$$E = \left(\frac{v_F h}{l_B}\right)\sqrt{2n}. \tag{C.9}$$

Suppose now the gauge $\boldsymbol{A} = \{0, xB\}$. For this particular choice of gauge, y is a cyclic variable and the functions can be taken as $\varphi_{1,2} = e^{ik_y y}\varphi_{1,2}(x)$. Using the explicit form of the operators in eq. (C.6) and eq. (C.7) and changing variable to

$$X = \frac{(k_y l^2 + x)}{l} \quad \rightarrow \frac{\partial}{\partial x} = \frac{1}{l}\frac{\partial}{\partial X} \tag{C.10}$$

we arrive at the equations

$$\frac{1}{l}\left(\frac{\partial}{\partial X} + X\right)\varphi_2 = \frac{iE}{\hbar v_F}\varphi_1 \tag{C.11}$$

$$\frac{1}{l}\left(\frac{\partial}{\partial X} - X\right)\varphi_1 = \frac{iE}{\hbar v_F}\varphi_2 \tag{C.12}$$

Solving for φ_2 we get

$$\left(\frac{\partial^2}{\partial X^2} + \left(\frac{lE}{\hbar v_F}\right)^2 - X^2 + 1\right)\varphi_2 = 0 \tag{C.13}$$

with solution

$$\varphi_2(X) = \frac{1}{\sqrt{l_B 2^n n! \sqrt{\pi}}} e^{-X^2/2} H_n(X). \tag{C.14}$$

φ_1 follows from the equation

$$\varphi_1(X) = -i\frac{\hbar v_F}{lE}\left(\frac{\partial}{\partial X} + X\right)e^{-X^2/2}H_n(X) \tag{C.15}$$

whose solution is now

$$\varphi_1(X) = \frac{-i}{\sqrt{l_B 2^n n! \sqrt{\pi}}} e^{-X^2/2} H_{n-1}(X) \tag{C.16}$$

The total eigenspinor then reads

$$\Psi_{n,k_y}(\boldsymbol{r}) = \frac{e^{ik_y y}}{\sqrt{2L_y l_B}}\begin{pmatrix}\varphi_1(X)\\ \varphi_2(X)\end{pmatrix}. \tag{C.17}$$

APPENDIX D

D.1 Dephasing time

In this appendix we explicitly calculate the dephasing time due to the strain pseudo magnetic field. To this end, we have to compute[91]

$$\langle \exp(i\xi\phi_g)\rangle = \exp\left(-\frac{1}{2}\xi^2\langle\phi_g^2\rangle\right), \tag{D.1}$$

where $\xi = \frac{2\pi}{\phi_{sc}}$ and $\phi_{sc} = \frac{h}{2e}$ and

$$\langle\phi_g^2\rangle = \sum_{i=1}^{n+1}\sum_{j=1}^{n+1}\left\langle \int d\boldsymbol{l}_i\cdot\boldsymbol{A}(\boldsymbol{r}_i)\int d\boldsymbol{l}'_j\cdot\boldsymbol{A}(\boldsymbol{r}'_j)\right\rangle. \tag{D.2}$$

We can consider only diagonal elements, assuming that the off diagonal part is uncorrelated ($\lambda << l_e$). We recall here that the strain gauge field is

$$A_x(\boldsymbol{r}) = \frac{\hbar\beta}{ea}[u_{xx}(\boldsymbol{r}) - u_{yy}(\boldsymbol{r})] \tag{D.3}$$

$$A_y(\boldsymbol{r}) = -2\frac{\hbar\beta}{ea}u_{xy}(\boldsymbol{r}), \tag{D.4}$$

with

$$u_{xx} \approx \frac{1}{2}\frac{\partial h(\boldsymbol{r})}{\partial x}\frac{\partial h(\boldsymbol{r})}{\partial x} \tag{D.5}$$

$$u_{xy} \approx \frac{1}{2}\frac{\partial h(\boldsymbol{r})}{\partial y}\frac{\partial h(\boldsymbol{r})}{\partial x} \tag{D.6}$$

$$u_{yy} \approx \frac{1}{2}\frac{\partial h(\boldsymbol{r})}{\partial y}\frac{\partial h(\boldsymbol{r})}{\partial y}. \tag{D.7}$$

Then, we need to calculate the phase

$$\begin{aligned}
\langle\phi_g^2\rangle &= \sum_{i=1}^{n+1}\sum_{j=1}^{n+1}\left\langle\int d\boldsymbol{l}_i\cdot\boldsymbol{A}(\boldsymbol{r}_i)\int d\boldsymbol{l}'_j\cdot\boldsymbol{A}(\boldsymbol{r}'_j)\right\rangle = \left\langle\int dx_i A_x(\boldsymbol{r}_i)\int dx'_j A_x(\boldsymbol{r}'_j)\right\rangle \quad \text{(D.8)}\\
&+ \left\langle\int dx_i A_x(\boldsymbol{r}_i)\int dy'_j A_y(\boldsymbol{r}'_j)\right\rangle + \left\langle\int dy_i A_y(\boldsymbol{r}_i)\int dx'_j A_x(\boldsymbol{r}'_j)\right\rangle\\
&+ \left\langle\int dy_i A_y(\boldsymbol{r}_i)\int dy'_j A_y(\boldsymbol{r}'_j)\right\rangle\\
&= \sum_{i=1}^{n+1}\sum_{j=1}^{n+1}\int dx_i\int dx'_j\left\langle A_x(\boldsymbol{r}_i)A_x(\boldsymbol{r}'_j)\right\rangle + \int dx_i\int dy'_j\left\langle A_x(\boldsymbol{r}_i)A_y(\boldsymbol{r}'_j)\right\rangle\\
&+ \int dy_i\int dx'_j\left\langle A_y(\boldsymbol{r}_i)A_x(\boldsymbol{r}'_j)\right\rangle + \int dy_i\int dy'_j\left\langle A_y(\boldsymbol{r}_i)A_y(\boldsymbol{r}'_j)\right\rangle\\
\langle\phi_g^2\rangle &= \langle\phi_g^2\rangle_1 + \langle\phi_g^2\rangle_2 + \langle\phi_g^2\rangle_3 + \langle\phi_g^2\rangle_4
\end{aligned}$$

Let us work out explicitly one of these contributions. The other three can be calculated in a similar maner. First consider

$$\langle\phi_g^2\rangle_1 = \sum_{i,j=1}^{n+1}\int_{\bar{x}_{i-1}}^{\bar{x}_i} dx_i\int_{\bar{x}'_{j-1}}^{\bar{x}'_j} dx'_j\left\langle A_x(\boldsymbol{r}_i)A_x(\boldsymbol{r}'_j)\right\rangle, \quad \text{(D.9)}$$

with

$$\begin{aligned}
\left\langle A_x(\boldsymbol{r}_i)A_x(\boldsymbol{r}'_j)\right\rangle &= \left(\frac{\hbar\beta}{ea}\right)^2\left[\left\langle u_{xx}(\boldsymbol{r}_i)u_{xx}(\boldsymbol{r}'_j)\right\rangle - \left\langle u_{xx}(\boldsymbol{r}_i)u_{y'y'}(\boldsymbol{r}'_j)\right\rangle - \left\langle u_{yy}(\boldsymbol{r}_i)u_{x'x'}(\boldsymbol{r}'_j)\right\rangle\right.\\
&+ \left.\left\langle u_{yy}(\boldsymbol{r}_i)u_{y'y'}(\boldsymbol{r}'_j)\right\rangle\right]. \quad \text{(D.10)}
\end{aligned}$$

Using the correlation function given in section(D.2), one writes

$$\begin{aligned}
\langle\phi_g^2\rangle_1 &= \left(\frac{\hbar\beta}{ea}\right)^2\frac{\Delta^4}{2\lambda^8}\sum_{i=1}^{n+1}\int_{\bar{x}_{i-1}}^{\bar{x}_i} dx_i\int_{\bar{x}'_{i-1}}^{\bar{x}'_i} dx'_i[2\lambda^4 - 2\lambda^2(|x_i-x'_i|^2+|y_i-y'_i|^2)\\
&+ \left(|x_i-x'_i|^2-|y_i-y'_i|^2\right)^2]e^{-\frac{(\boldsymbol{r}_i-\boldsymbol{r}'_i)^2}{\lambda^2}}, \quad \text{(D.11)}
\end{aligned}$$

or

$$\langle\phi_g^2\rangle_1 = \left(\frac{\hbar\beta}{ea}\right)^2\frac{\Delta^4}{2\lambda^8}\sum_{i=1}^{n+1} I_i, \quad \text{(D.12)}$$

with

$$\begin{aligned}
I_i &= \int_{\bar{x}_{i-1}}^{\bar{x}_i} dx_i\int_{\bar{x}'_{i-1}}^{\bar{x}'_i} dx'_i[2\lambda^4 - 2\lambda^2(|x_i-x'_i|^2+|y_i-y'_i|^2) + \left(|x_i-x'_i|^2-|y_i-y'_i|^2\right)^2]e^{-\frac{(\boldsymbol{r}_i-\boldsymbol{r}'_i)^2}{\lambda^2}}\\
&= \frac{1}{2}\cos^2(\theta_i)\sqrt{\pi}\lambda^5\left[|\boldsymbol{r}_i-\boldsymbol{r}_{i-1}| + \frac{3}{4}\frac{1}{|\boldsymbol{r}_i-\boldsymbol{r}_{i-1}|^3}\left(|x_i-x_{i-1}|^2-|y_i-y_{i-1}|^2\right)^2\right]. \quad \text{(D.13)}
\end{aligned}$$

Then the result for the first part is

$$\langle\phi_g^2\rangle_1 = \left(\frac{\hbar\beta}{ea}\right)^2 \frac{\sqrt{\pi}\Delta^4}{4\lambda^3}\sum_{i=1}^{n+1}\left[\frac{|x_i-x_{i-1}|^2}{|\boldsymbol{r}_i-\boldsymbol{r}_{i-1}|}+\frac{3}{4}\frac{|x_i-x_{i-1}|^2}{|\boldsymbol{r}_i-\boldsymbol{r}_{i-1}|^5}\left(|x_i-x_{i-1}|^2-|y_i-y_{i-1}|^2\right)^2\right], \tag{D.14}$$

Where we have assumed that $|\boldsymbol{r}_i-\boldsymbol{r}_{i-1}|\gg\lambda$. This is justified in the short-range limit $|\boldsymbol{r}_i-\boldsymbol{r}_{i-1}|\sim l_e\gg\lambda$. We also used the following relation to parametrize the path of integration

$$\begin{aligned} x_i-\bar{x}_{i-1} &= s\cos(\theta_i) \\ y_i-\bar{y}_{i-1} &= s\sin(\theta_i) \\ \bar{x}_i-\bar{x}_{i-1} &= |\boldsymbol{r}_i-\boldsymbol{r}_{i-1}|\cos(\theta_i) \\ \bar{y}_i-\bar{y}_{i-1} &= |\boldsymbol{r}_i-\boldsymbol{r}_{i-1}|\sin(\theta_i) \end{aligned} \tag{D.15}$$

D.2 Correlations functions needed in this appendix

$$\begin{aligned} \langle u_{xx}(\boldsymbol{r}_i)u_{xx}(\boldsymbol{r}_i')\rangle &= \pi^2\lambda^4\Delta^4\Bigg\{\frac{1}{4\pi^2\lambda^8} \\ &+ \frac{1}{2\pi^2\lambda^{12}}\left(\lambda^2-|x_i-x_i'|^2\right)^2 e^{-\frac{(\boldsymbol{r}_i-\boldsymbol{r}_i')^2}{\lambda^2}}\Bigg\} \end{aligned} \tag{D.16}$$

$$\begin{aligned} \langle u_{yy}(\boldsymbol{r}_i)u_{yy}(\boldsymbol{r}_i')\rangle &= \pi^2\lambda^4\Delta^4\Bigg\{\frac{1}{4\pi^2\lambda^8} \\ &+ \frac{1}{2\pi^2\lambda^{12}}\left(\lambda^2-|y_i-y_i'|^2\right)^2 e^{-\frac{(\boldsymbol{r}_i-\boldsymbol{r}_i')^2}{\lambda^2}}\Bigg\} \end{aligned} \tag{D.17}$$

$$\begin{aligned} \langle u_{xx}(\boldsymbol{r}_i)u_{yy}(\boldsymbol{r}_i')\rangle &= \pi^2\lambda^4\Delta^4\Bigg\{\frac{1}{4\pi^2\lambda^8} \\ &+ \frac{1}{2\pi^2\lambda^{12}}(x_i-x_i')^2(y_i-y_i')^2 e^{-\frac{(\boldsymbol{r}_i-\boldsymbol{r}_i')^2}{\lambda^2}}\Bigg\} \end{aligned} \tag{D.18}$$

$$\begin{aligned} \langle u_{yy}(\boldsymbol{r}_i)u_{xx}(\boldsymbol{r}_i')\rangle &= \pi^2\lambda^4\Delta^4\Bigg\{\frac{1}{4\pi^2\lambda^8} \\ &+ \frac{1}{2\pi^2\lambda^{12}}(x_i-x_i')^2(y_i-y_i')^2 e^{-\frac{(\boldsymbol{r}_i-\boldsymbol{r}_i')^2}{\lambda^2}}\Bigg\} \end{aligned} \tag{D.19}$$

$$\langle u_{xy}(\boldsymbol{r}_i)u_{xx}(\boldsymbol{r}'_i)\rangle = \frac{\Delta^4}{2\lambda^8}(\lambda^2 - |x_i - x'_i|^2)|x_i - x'_i||y_i - y'_i|e^{-\frac{(\boldsymbol{r}_i - \boldsymbol{r}'_i)^2}{\lambda^2}} \quad \text{(D.20)}$$

$$\langle u_{xx}(\boldsymbol{r}_i)u_{xy}(\boldsymbol{r}'_i)\rangle = \frac{\Delta^4}{2\lambda^8}(\lambda^2 - |x_i - x'_i|^2)|x_i - x'_i||y_i - y'_i|e^{-\frac{(\boldsymbol{r}_i - \boldsymbol{r}'_i)^2}{\lambda^2}} \quad \text{(D.21)}$$

$$\langle u_{yy}(\boldsymbol{r}_i)u_{xy}(\boldsymbol{r}'_i)\rangle = \frac{\Delta^4}{2\lambda^8}(\lambda^2 - |y_i - y'_i|^2)|x_i - x'_i||y_i - y'_i|e^{-\frac{(\boldsymbol{r}_i - \boldsymbol{r}'_i)^2}{\lambda^2}} \quad \text{(D.22)}$$

$$\langle u_{xy}(\boldsymbol{r}_i)u_{yy}(\boldsymbol{r}'_i)\rangle = \frac{\Delta^4}{2\lambda^8}(\lambda^2 - |y_i - y'_i|^2)|x_i - x'_i||y_i - y'_i|e^{-\frac{(\boldsymbol{r}_i - \boldsymbol{r}'_i)^2}{\lambda^2}} \quad \text{(D.23)}$$

$$\begin{aligned}\langle u_{xy}(\boldsymbol{r}_i)u_{xy}(\boldsymbol{r}'_i)\rangle &= \frac{\Delta^4}{4\lambda^8}\Big\{(\lambda^2 - |x_i - x'_i|^2)(\lambda^2 - |y_i - y'_i|^2)e^{-\frac{(\boldsymbol{r}_i - \boldsymbol{r}'_i)^2}{\lambda^2}} \\ &+ |x_i - x'_i|^2|y_i - y'_i|^2 e^{-\frac{(\boldsymbol{r}_i - \boldsymbol{r}'_i)^2}{\lambda^2}}\Big\}, \quad \text{(D.24)}\end{aligned}$$

Δ represents the hight of the profile using to model disorder.

References

[1] Mark Wilson. Electrons in atomically thin carbon sheets behave like massless particles. *Physics Today*, 59(1):21–23, 2006.

[2] K. S. Novoselov, A. K. Geim, S.V. Morozov, D. Jiang, Y. Zhang, S. V. Dubonos, I. V. Grigorieva, and A. A. Firsov. Electric Field Effect in Atomically Thin Carbon Films. *Science*, 306(5696):666–669, 2004.

[3] A. K. Geim and K. S. Novoselov. The rise of graphene. *Nat. Mater.*, 6(3):183–191, 2007.

[4] Y. B. Zhang, Y. W. Tan, H. L. Stormer, and P. Kim. Experimental observation of the quantum Hall effect and Berry's phase in graphene. *Nature*, 438(7065):201–204, 2005.

[5] K S Novoselov, a K Geim, S V Morozov, D Jiang, M I Katsnelson, I V Grigorieva, S V Dubonos, and a a Firsov. Two-dimensional gas of massless Dirac fermions in graphene. *Nature*, 438(7065):197–200, nov 2005.

[6] D Weiss, K V Klitzing, K Ploog, and G Weimann. Magnetoresistance Oscillations in a Two-Dimensional Electron Gas Induced by a Submicrometer Periodic Potential. *EPL (Europhysics Letters)*, 8(2):179, 1989.

[7] Dieter Weiss. MAGNETOQUANTUM OSCILLATIONS IN LATERAL SUPERLATTICE. *Electronic properties of multilayers and low-Dimensional Semiconductors Structures*, page 133, 1990.

[8] Frank Schwierz. Graphene transistors. *Nature nanotechnology*, 5(7):487–96, July 2010.

[9] Wei Han, Roland K Kawakami, Martin Gmitra, and Jaroslav Fabian. Graphene spintronics. *Nature nanotechnology*, 9(10):794–807, October 2014.

[10] S Dai, Q Ma, M K Liu, T Andersen, Z Fei, M D Goldflam, M Wagner, K Watanabe, T Taniguchi, M Thiemens, F Keilmann, G C a M Janssen, S-E Zhu, P Jarillo-Herrero, M M Fogler, and D N Basov. Graphene on hexagonal boron nitride as a tunable hyperbolic metamaterial. *Nature nanotechnology*, 10(8):682–6, August 2015.

[11] Phaedon Avouris, Zhihong Chen, and Vasili Perebeinos. Carbon-based electronics. *Nature nanotechnology*, 2(10):605–15, October 2007.

[12] Gianluca Fiori, Francesco Bonaccorso, Giuseppe Iannaccone, Tomás Palacios, Daniel Neumaier, Alan Seabaugh, Sanjay K Banerjee, and Luigi Colombo. Electronics based on two-dimensional materials. *Nature nanotechnology*, 9(10):768–79, October 2014.

[13] Bich Ha Nguyen and Van Hieu Nguyen. Advances in graphene-based optoelectronics, plasmonics and photonics. *Advances in Natural Sciences: Nanoscience and Nanotechnology*, 7(1):013002, January 2016.

[14] Jianing Chen, Michela Badioli, Pablo Alonso-González, Sukosin Thongrattanasiri, Florian Huth, Johann Osmond, Marko Spasenović, Alba Centeno, Amaia Pesquera, Philippe Godignon, Amaia Zurutuza Elorza, Nicolas Camara, F Javier García de Abajo, Rainer Hillenbrand, and Frank H L Koppens. Optical nano-imaging of gate-tunable graphene plasmons. *Nature*, 487(7405):77–81, July 2012.

[15] Bruno Dlubak, Marie-Blandine Martin, Cyrile Deranlot, Bernard Servet, Stéphane Xavier, Richard Mattana, Mike Sprinkle, Claire Berger, Walt a. De Heer, Frédéric Petroff, Abdelmadjid Anane, Pierre Seneor, and Albert Fert. Highly efficient spin transport in epitaxial graphene on SiC. *Nature Physics*, 8(7):557–561, June 2012.

[16] Wei Han, K Pi, K M McCreary, Yan Li, Jared J I Wong, a G Swartz, and R K Kawakami. Tunneling spin injection into single layer graphene. *Physical review letters*, 105(16):167202, October 2010.

[17] Wei Han and R K Kawakami. Spin relaxation in single-layer and bilayer graphene. *Physical review letters*, 107(4):047207, July 2011.

[18] Nikolaos Tombros, Csaba Jozsa, Mihaita Popinciuc, Harry T Jonkman, and Bart J van Wees. Electronic spin transport and spin precession in single graphene layers at room temperature. *Nature*, 448(7153):571–4, August 2007.

[19] T-Y Yang, J Balakrishnan, F Volmer, a Avsar, M Jaiswal, J Samm, S R Ali, a Pachoud, M Zeng, M Popinciuc, G Güntherodt, B Beschoten, and B Özyilmaz. Observation of long spin-relaxation times in bilayer graphene at room temperature. *Physical review letters*, 107(4):047206, July 2011.

[20] P. J. Zomer, M. H. D. Guimarães, N. Tombros, and B. J. van Wees. Long-distance spin transport in high-mobility graphene on hexagonal boron nitride. *Physical Review B*, 86(16):161416, October 2012.

[21] E. R. Mucciolo and C. H. Lewenkopf. Disorder and electronic transport in graphene. *J. Phys. Condens. Matter*, 22:273201, 2010.

[22] Caio H. Lewenkopf and Eduardo R. Mucciolo. The recursive Greens function method for graphene. *J. Comput. Electron.*, 12:203, 2013.

[23] C. H. Lewenkopf, E. R. Mucciolo, and A. H. Castro Neto. Numerical studies of conductivity and Fano factor in disordered graphene. *Phys. Rev. B*, 77:081410(R), 2008.

[24] P. M. Ostrovsky, I. V. Gornyi, and a. D. Mirlin. Electron transport in disordered graphene. *Phys. Rev. B*, 74(23):235443, December 2006.

[25] N. H Shon and Tsuneya Ando. Shon(Ando)98-KuboSCB-JPSJ67-2421.pdf. *J. Phys. Soc. Japan*, 67:2421–2429, 1998.

[26] Shaffique Adam, E H Hwang, V M Galitski, and S Das Sarma. A self-consistent theory for graphene transport. *Proceedings of the National Academy of Sciences of the United States of America*, 104(47):18392–7, November 2007.

[27] E H Hwang, S Adam, and S Das Sarma. Carrier Transport in Two-Dimensional Graphene Layers. *Phys. Rev. Lett.*, 98(18):186806, 2007.

[28] Shaffique Adam, E.H. Hwang, and S. Das Sarma. Scattering mechanisms and boltzmann transport in graphene. *Physica E: Low-dimensional Systems and Nanostructures*, 40(5):1022 – 1025, 2008. 17th International Conference on Electronic Properties of Two-Dimensional Systems.

[29] S. Adam and S. Das Sarma. Transport in suspended graphene. *Solid State Communications*, 146(9–10):356 – 360, 2008.

[30] S. Adam, E.H. Hwang, E. Rossi, and S. Das Sarma. Theory of charged impurity scattering in two-dimensional graphene. *Solid State Communications*, 149(27–28):1072 – 1079, 2009. Recent Progress in Graphene Studies.

[31] M. I. Katsnelson and A. K. Geim. Electron scattering on microscopic corrugations in graphene. *Phil. Trans. R. Soc. A*, 366:195–204, January 2008.

[32] Nuno J. G. Couto, Davide Costanzo, Stephan Engels, Dong-Keun Ki, Kenji Watanabe, Takashi Taniguchi, Christoph Stampfer, Francisco Guinea, and Alberto F. Morpurgo. Random Strain Fluctuations as Dominant Disorder Source for High-Quality On-Substrate Graphene Devices. *Phys. Rev. X*, 4:041019, 2014.

[33] Rhonald Burgos, Jesus Warnes, Leandro R F Lima, and Caio Lewenkopf. Effects of a random gauge field on the conductivity of graphene sheets with disordered ripples. *Phys. Rev. B*, 91(11):115403, March 2015.

[34] T. O. Wehling, A. V. Balatsky, A. M. Tsvelik, M. I. Katsnelson, and A. I. Lichtenstein. Midgap states in corrugated graphene: Ab initio calculations and effective field theory. *EPL (Europhysics Letters)*, 84(1):17003, 2008.

[35] Daqing Liu, Xin Ye, Shuyue Chen, Shengli Zhang, and Ning Ma. Low-energy quantum scattering induced by graphene ripples. *Physics Letters A*, 379(47–48):3141 – 3145, 2015.

[36] F. Guinea, Baruch Horovitz, and P. Le Doussal. Gauge field induced by ripples in graphene. *Phys. Rev. B*, 77(20):205421, May 2008.

[37] M A H Vozmediano, M I Katsnelson, and F Guinea. Gauge fields in graphene. *Phys. Rep.*, 496:109, 2010.

[38] Yasuhiro Tokura. Two-dimensional electron transport with anisotropic scattering potentials. *Phys. Rev. B*, 58(11):7151–7161, September 1998.

[39] J. M. Ziman. *Principles of the Theory of Solids*. Cambridge University Press, Cambridge, 1972.

[40] A. H. Castro Neto, F. Guinea, N. M. R. Peres, K. S. Novoselov, and A. K. Geim. The electronic properties of graphene. *Rev. Mod. Phys.*, 81(1):109–162, jan 2009.

[41] Mark Lundeberg and Joshua Folk. Rippled Graphene in an In-Plane Magnetic Field: Effects of a Random Vector Potential. *Phys. Rev. Lett.*, 105(14):146804, September 2010.

[42] F. Guinea, Baruch Horovitz, and P. Le Doussal. Gauge field induced by ripples in graphene. *Phys. Rev. B*, 77(20):205421, may 2008.

[43] Vitor M. Pereira, A. H. Castro Neto, and N. M. R. Peres. Tight-binding approach to uniaxial strain in graphene. *Phys. Rev. B*, 80:045401, Jul 2009.

[44] A. H. Castro Neto, F. Guinea, N. M. R. Peres, K. S. Novoselov, and A. K. Geim. The electronic properties of graphene. *Rev. Mod. Phys.*, 81(1):109, January 2009.

[45] M Ishigami, J H Chen, W G Cullen, M S Fuhrer, and E D Williams. Atomic structure of graphene on SiO2. *Nano Lett.*, 7:1643, 2007.

[46] V Geringer, M Liebmann, T Echtermeyer, S Runte, M Schmidt, R Rckamp, M C Lemme, and M Morgenstern. Intrinsic and extrinsic corrugation of monolayer graphene deposited on SiO2. *Phys. Rev. Lett.*, 102:76102, 2009.

[47] A Deshpande, W Bao, F Miao, C N Lau, and B J LeRoy. Spatially resolved spectroscopy of monolayer graphene on SiO2. *Phys. Rev. B*, 79:205411, 2009.

[48] W G Cullen, M Yamamoto, K M Burson, J H Chen, C Jang, L Li, M S Fuhrer, and E D Williams. High-Fidelity Conformation of Graphene to SiO2 Topographic Features. *Phys. Rev. Lett.*, 105:215504, 2010.

[49] P M Mensz and R G Wheeler. Magnetoconductance due to parallel fileds in silicon inversion layers. *Phys. Rev. B*, 35:2844, 1987.

[50] Warren R Anderson, D R Lombardi, R G Wheeler, and Tso-Ping Ma. Determination of Si/SiO, Interface Roughness Using Weak Localization. *IEEE Electron Device Lett.*, 14:351, 1993.

[51] D M Zumbühl, J B Miller, C M Marcus, V I Fal'ko, T Jungwirth, and J. S. Harris Jr. Orbital effects of in-plane magnetic fields probed by mesoscopic conductance fluctuations. *Phys. Rev. B*, 69:121305, 2004.

[52] Hidekatsu Suzuura and Tsuneya Ando. Phonons and electron-phonon scattering in carbon nanotubes. *Phys. Rev. B*, 65(23):235412, May 2002.

[53] J L Mañes. Symmetry-based approach to electron-phonon interactions in graphene. *Phys. Rev. B*, 76(4):45430, July 2007.

[54] A Cortijo, F Guinea, and M A H Vozmediano. Geometrical and topological aspects of graphene and related materials. *J. Phys. A*, 45(38):383001, 2012.

[55] S Das Sarma, Shaffique Adam, E H Hwang, and Enrico Rossi. Electronic transport in two-dimensional graphene. *Rev. Mod. Phys.*, 83:407, 2011.

[56] E. McCann, K. Kechedzhi, V. I. Fal'ko, H. Suzuura, T. Ando, B. L. Altshuler, and H Suzuura H. Weak-localization magnetoresistance and valley symmetry in graphene. *Phys. Rev. Lett.*, 97:109, 2006.

[57] K. Kechedzhi, E. McCann, V. I. Fal'ko, H. Suzuura, T. Ando, and B. L. Altshuler. Weak localization in monolayer and bilayer graphene. *Eur. Phys. J. Spec. Top.*, 148(1):39–54, September 2007.

[58] Aleksander P. Hinz, Stefan Kettemann, and Eduardo R. Mucciolo. Quantum corrections to thermopower and conductivity in graphene. *Phys. Rev. B*, 89(7):075411, February 2014.

[59] J. W. Kos and I. V. Zozoulenko. Effect of short- and long-range scattering on the conductivity of graphene: Boltzmann approach vs tight-binding calculations. *Phys. Rev. B*, 82(8):081414, August 2010.

[60] C. Kittel. *Quantum Theory of Solids*. Wiley, New York, 2nd revise edition, 1987.

[61] P. Hedegard and A. Smith. Solution of the Boltzmann equation in a random magnetic field. *Phys. Rev. B*, 51:10869, 1995.

[62] R. R. Brandão and L. Moriconi. arXiv:1410.6706. *arXiv:1410.6706*, 2014.

[63] C. Herring and E. Vogt. Transport and deformation-potential theory for many-valley semicondictors with anisotropic scattering. *Phys. Rev.*, 101:944, 1956.

[64] E. H. Sondheimer. The Boltzmann equation for anisotropic metals. *Proc. R. Soc. Lond. A*, 268:100, 1962.

[65] Kazuyuki Genma and Makoto Katori. Height correlation of rippled graphene and Lundeberg-Folk formula for magnetoresistance. *arXiv:1211.2046*, November 2012.

[66] A. W. Rushforth, B. L. Gallagher, P. C. Main, A. C. Neumann, M. Henini, C. H. Marrows, and B. J. Hickey. Anisotropic magnetoresistance in a two-dimensional electron gas in a quasirandom magnetic field. *Phys. Rev. B*, 70(19):193313, November 2004.

[67] Zhenbing Tan, Changling Tan, Li Ma, G T Liu, L Lu, and C L Yang. Shubnikov-de Haas oscillations of a single layer graphene under dc current bias. *Phys. Rev. B*, 84(11):115429, 2011.

[68] M Monteverde, C Ojeda-Aristizabal, R Weil, K Bennaceur, M Ferrier, S Guéron, C Glattli, H Bouchiat, J N Fuchs, and D L Maslov. Transport and Elastic Scattering Times as Probes of the Nature of Impurity Scattering in Single-Layer and Bilayer Graphene. *Phys. Rev. Lett.*, 104(12):126801, 2010.

[69] R W Winkler, J P Kotthaus, and K Ploog. Landau-Band Conductivity in a two-Dimensional Electron System Modulated by an Artificial One-Dimensional Superlattice Potential. *Phys. Rev. Lett.*, 62(10):1177–1180, 1989.

[70] R R Gerhardts, D Weiss, and K v. Klitzing. Novel magnetoresistance oscillations in a periodically modulated two-dimensional electron gas. *Phys. Rev. Lett.*, 62(10):1173–1176, mar 1989.

[71] P Vasilopoulos and F M Peeters. Quantum Magnetotransport of a Periodically Modulated Two-Dimensional Electron Gas. *Phys. Rev. Lett.*, 63(19):2120–2123, 1989.

[72] F M Peeters and P Vasilopoulos. Electrical and thermal properties of a two-dimensional electron gas in a one-dimensional periodic potential. *Phys. Rev. B*, 46(8):4667–4680, 1992.

[73] Chao Zhang and Rolf R Gerhardts. Theory of magnetotransport in two-dimensional electron systems with unidirectional periodic modulation. *Phys. Rev. B*, 41(18):12850–12861, 1990.

[74] C .W. J. Beenakker. Resonance in a Periodically Modulated Two-Dimensional. *Phys. Rev. Lett.*, 62(17):2020–2023, 1989.

[75] A D Mirlin and P Wölfle. Weiss oscillations in the presence of small-angle impurity scattering. *Phys. Rev. B*, 58(19):12986–12992, nov 1998.

[76] M. O. Goerbig. Electronic properties of graphene in a strong magnetic field. *Rev. Mod. Phys.*, 83(December):1193–1243, nov 2011.

[77] Hidekatsu Suzuura and Tsuneya Ando. Crossover from symplectic to orthogonal class in a two-dimensional honeycomb lattice. *Phys. Rev. Lett.*, 89(26):266603, December 2002.

[78] Felix von Oppen, Francisco Guinea, and Eros Mariani. Synthetic electric fields and phonon damping in carbon nanotubes and graphene. *Phys. Rev. B*, 80:075420, Aug 2009.

[79] Daniel Midtvedt, Caio H Lewenkopf, and Alexander Croy. Strain–displacement relations for strain engineering in single-layer 2d materials. *2D Materials*, 3(1):011005, 2016.

[80] F. Guinea, A. K. Geim, M. I. Katsnelson, and K. S. Novoselov. Generating quantizing pseudomagnetic fields by bending graphene ribbons. *Phys. Rev. B*, 81:035408, Jan 2010.

[81] M Mucha-Kruczynski and V.I Fal'ko. Pseudo-magnetic field distribution and pseudo-landau levels in suspended graphene flakes. *Solid State Commun.*, 152(15):1442 – 1445, 2012.

[82] E H Hwang and S Das Sarma. Dielectric function, screening, and plasmons in two-dimensional graphene. *Phys. Rev. B*, 75(20):205418, 2007.

[83] M Tahir and K Sabeeh. Quantum transport of Dirac electrons in graphene in the presence of a spatially modulated magnetic field. *Phys. Rev. B*, 77(19):195421, may 2008.

[84] A Matulis and F M Peeters. Appearance of enhanced Weiss oscillations in graphene: Theory. *Phys. Rev. B*, 75(12):125429, mar 2007.

[85] J. W. McClure. Diamagnetism of graphite. *Phys. Rev.*, 104:666–671, Nov 1956.

[86] Yisong Zheng and Tsuneya Ando. Hall conductivity of a two-dimensional graphite system. *Phys. Rev. B*, 65:245420, Jun 2002.

[87] M Charbonneau, K M van Vliet, and P Vasilopoulos. *J. Math. Phys.*, 23(2):318, 1982.

[88] Thiti Taychatanapat, Kenji Watanabe, Takashi Taniguchi, and Pablo Jarillo-Herrero. Electrically tunable transverse magnetic focusing in graphene. *Nat. Phys.*, 9(4):225–229, 2013.

[89] V. E. Calado, Shou-En Zhu, S. Goswami, Q. Xu, K. Watanabe, T. Taniguchi, G. C. A. M. Janssen, and L. M. K. Vandersypen. Ballistic transport in graphene grown by chemical vapor deposition. *Appl. Phys. Lett.*, 104(2):023103, 2014.

[90] Andreas Sandner, Tobias Preis, Christian Schell, Paula Giudici, Kenji Watanabe, Takashi Taniguchi, Dieter Weiss, and Jonathan Eroms. Ballistic Transport in Graphene Antidot Lattices. *Nano Lett.*, 15(12):8402–8406, 2015.

[91] H Mathur and Harold U Baranger. Random Berry phase magnetoresistance as a probe of interface roughness in Si MOSFET?s. *Phys. Rev. B*, 64:235325, 2001.

[92] Quirin Hummel, Juan Diego Urbina, and Klaus Richter. The Weyl expansion for systems of independent identical particles. *Journal of Physics A: Mathematical and Theoretical*, 47(1):15101, 2014.

[93] Belen Paredes, Artur Widera, Valentin Murg, Olaf Mandel, Simon Folling, Ignacio Cirac, Gora V Shlyapnikov, Theodor W Hansch, and Immanuel Bloch. Tonks-Girardeau gas of ultracold atoms in an optical lattice. *Nature*, 429(6989):277–281, may 2004.

[94] Toshiya Kinoshita, Trevor Wenger, and David S Weiss. Observation of a One-Dimensional Tonks-Girardeau Gas. *Science*, 305(5687):1125–1128, 2004.

[95] Elmar Haller, Mattias Gustavsson, Manfred J Mark, Johann G Danzl, Russell Hart, Guido Pupillo, and Hanns-Christoph Nägerl. Realization of an Excited, Strongly Correlated Quantum Gas Phase. *Science*, 325(5945):1224–1227, 2009.

[96] Elliott H Lieb and Werner Liniger. Exact Analysis of an Interacting Bose Gas. I. The General Solution and the Ground State. *Phys. Rev.*, 130(4):1605–1616, 1963.